MgF_2-coated gold nanostructures as a plasmonic substrate for analytical applications

D i s s e r t a t i o n

zur Erlangung des akademischen Grades

d o c t o r r e r u m n a t u r a l i u m

(Dr. rer. nat.)

im Fach Chemie

eingereicht an der

Mathematisch-NaturwissenschaftlicheFakultät

der Humboldt-Universität zu Berlin

von

Dorota Bartkowiak, M.Sc. Chemie

Präsidentin der Humboldt-Universität zu Berlin

Prof. Dr.-Ing. Dr. Sabine Kunst

Dekan der Mathematisch-Naturwissenschaftlichen Fakultät

Prof. Dr. Elmar Kulke

Gutachter/in: 1. Prof. Dr. Erhard Kemnitz

2. Prof. Dr. Janina Kneipp

Tag der mündlichen Prüfung: 16 Juli 2018.

Selbstständigkeitserklärung

Hiermit erkläre ich an Eides statt, dass die vorliegende Arbeit selbstständig und nur unter Nutzung der angegebenen Hilfsmittel angefertigt wurde.

Berlin, den 01.05.2018 Dorota Bartkowiak

Acknowledgements

I would like to express my sincere gratitude to my supervisors Prof. Dr. Erhard Kemnitz and Prof. Dr. Janina Kneipp. Thank you for giving me the opportunity to join your teams and to work in the interesting, multidisciplinary project. Without your valuable guidance, encouragement and continuous support writing this thesis would have been extremely challenging. Thank you for sharing with me your knowledge and for being a source of inspiration. I am heartily thankful for your understanding and supporting me thought the hard moments.

I would like to acknowledge Prof. Dr. Nicola Pinna, Dr. Guylhaine Clavel, Dr. Gianvito Caputo for the help with transmission electron microscopy measurements. I would like to express my gratitude to Dr. Virginia Merk and to Fani Madzharova for sharing with me their knowledge about surface enhanced Raman scattering measurements. I am very thankful to Valentin Reiter-Scherer for scanning force microscopy measurements. Finally, I would like to acknowledge Mr. Ulrich Gernert for his encouragement in performing, very challenging, scanning electron microscopy measurements, Dr. Steffi Rades for the energy dispersive X-ray spectroscopy measurements and Dr. Kai Nörthemann for performing the vapor coating experiments.

I am eternally grateful to my colleagues from Humboldt-Universität zu Berlin and from School of Analytical Sciences Adlershof for creating the amazing atmosphere during the time of my doctoral studies. I would like to express my special appreciation to Stefan Mahn for his constructive feedback and the huge amount of patience.

I would like to express my sincere gratitude to the School of Analytical Sciences Adlershof organizing team for your continuous support. Funding by DFG GSD1013 SALSA in gratefully acknowledged.

Finally, my heartfelt thanks to those, who have always supported me most: my family, especially my parents and my sister, Bartek and my friends.

Abstract

Plasmonic substrates can be a powerful tool for analytical applications. In order to broaden the spectrum of their applications and to push the detection limits of analytical spectroscopy, new plasmonic substrates are constantly developed. The motivation of this work was to coat plasmonic nanostructures with magnesium fluoride. Coatings of magnesium fluoride are porous but exhibit high mechanical stability and extraordinary optical properties that include a low refractive index and a wide optical window. Combining these properties with the beneficial properties of plasmonic nanostructures can lead to advanced plasmonic substrates for analytical applications.

Two different approaches for coating of the plasmonic nanostructures are proposed in this work: (i) a core-shell nanoparticles fabrication containing a plasmonic core and (ii) coating of plasmonic nanostructures immobilized on glass.

Although the fabrication of Au@MgF_2 core-shell nanoparticles is very promising, it turned out to be an extremely challenging approach. Metal@metal fluorides core-shell nanoparticles have not been reported in the literature yet. Therefore, an approach based on knowledge of metal@metal oxides and metal fluorides@metal fluorides core-shell nanoparticles synthesis was undertaken. Different magnesium precursors, solvents, stabilizing agents of gold nanoparticles, as well as different reaction conditions were investigated. The obtained structures were characterized using electron microscopy methods. Due to the numerous difficulties in the synthesis and characterization of those materials this way of coating plasmonic nanostructures with magnesium fluoride was not further processed.

The second investigated approach was based on immobilization of gold nanoparticles on glass and coating them with magnesium fluoride using a dip-coating method. This way of fabrication provides plasmonic substrates that are characterized by a high nanoscopic homogeneity of the gold nanoparticles distribution, a high mechanical stability and interesting optical properties. Moreover, enhancement factors of optical signals that allow for real analytical applications were obtained. Nanoscopic, plasmonic and mechanical properties of the substrates were characterized using SEM, SFM, UV-Vis and SERS. In conclusion, the coating of gold nanoparticles immobilized on the glass with magnesium fluoride results in very promising substrate that can be used for sensing and other applications in the future.

Keywords: magnesium fluoride, plasmonics, plasmonic substrate, gold nanoparticles, magnesium fluoride coating

Kurzfassung

Plasmonische Substrate (plasmonic substrates) stellen ein leistungsstarkes Werkzeug für analytische Anwendungen dar. Neue plasmonische Substrate werden ständig entwickelt, um das Spektrum ihrer Anwendungen und die Nachweisgrenzen der analytischen Spektroskopie zu erweitern. Diese Arbeit setzte sich zum Ziel, plasmonische Nanostrukturen mit Magnesiumfluorid zu beschichten. Magnesiumfluoridbeschichtungen sind zwar porös, weisen aber eine hohe mechanische Stabilität und außergewöhnliche optische Eigenschaften auf, einschließlich eines niedrigen Brechungsindexes und eines großen optischen Fensters. Die Kombination dieser Eigenschaften mit den positiven Eigenschaften von plasmonischen Nanostrukturen kann zu fortschrittlichen plasmonischen Substraten für analytische Anwendungen führen.

Diese Arbeit bietet zwei verschiedene Ansätze für die Beschichtung der plasmonischen Nanostrukturen an:

(i) die Core-Shell-Nanopartikelherstellung, die einen plasmonischen Core enthält, und (ii) die Beschichtung von auf Glas immobilisierten plasmonischen Nanostrukturen.

Obwohl die Herstellung von Au@MgF_2 Core-Shell-Nanopartikeln sehr vielversprechend ist, stellte sie sich als äußerst anspruchsvoller Ansatz heraus. Über Metal@metal Fluoride Core-Shell-Nanopartikel wurde in der Literatur noch nichts berichtet. Daher wurde ein Ansatz verfolgt, der auf dem Wissen über Metall-@Metalloxide und Metallfluoride@Metallfluoride basiert und die Synthese von Core-Shell-Nanopartikeln ermöglicht. Verschiedene Magnesiumvorläufer, Lösungsmittel, Stabilisierungsmittel von Goldnanopartikeln sowie unterschiedliche Reaktionsbedingungen wurden untersucht. Die erhaltenen Strukturen wurden mit elektronenmikroskopischen Methoden charakterisiert. Aufgrund der zahlreichen Schwierigkeiten bei der Synthese und Charakterisierung dieser Materialien wurde diese Art der Beschichtung plasmonischer Nanostrukturen mit Magnesiumfluorid nicht weiterverarbeitet.

Der zweite untersuchte Ansatz bestand in der Immobilisierung von Goldnanopartikeln auf Glas und deren Beschichtung mit Magnesiumfluorid durch Tauchbeschichtung. Diese Fertigungsart verleiht eine hohe mechanische Stabilität und wissenswerte optische Eigenschaften an plasmonischen Substraten, die sich durch eine hohe nanoskopische Homogenität der Goldnanopartikelverteilung auszeichnen. Darüber hinaus wurden Verstärkungsfaktoren optischer Signale, die echte analytische Anwendungen ermöglichen, ermittelt. Die Eigenschaften der nanoskopischen, plasmonischen und mechanischen Eigenschaften der Substrate wurden mit REM, SFM, UV-Vis und SERS charakterisiert. Zusammenfassend lässt sich sagen, dass die Beschichtung von auf Glas mit Magnesiumfluorid immobilisierten Goldnanopartikeln zu einem sehr vielversprechenden Substrat führt, das in Zukunft für Sensorik und andere Anwendungen verwendet werden kann.

Schlagwörter: Magnesiumfluorid, Plasmonik, Plasmonische Substrate, Goldnanopartikeln, Magnesiumfluoridbeschichtungen

Table of content

List of tables

List of figures

1. Introduction

1.1. The role of plasmonic nanomaterials

Plasmonic nanomaterials exhibit extraordinary optical properties, since they have a wide spectrum of applications, for example art conversation,[1] biosensing[2] including medical diagnostics,[3] photovoltaics,[4] and characterization of catalysis reactions.[5] Their extraordinary properties are mostly based on specific light-metal surface interactions. A whole field of research, plasmonics, has emerged, based on localized surface plasmon resonance (LSPR). Localized surface plasmon resonances arise from the coherent oscillations of conducting electrons on the surface of metal nanostructures excited by incident light at a metal-dielectric interface.[6] Changes of LSPR can be caused by binding of molecules on the metal surface, thus many analytical and sensing methods based on LSPR were developed.[2, 5, 7-15] Due to their versatility, plasmonic nanomaterials are applied as substrates for spectroanalytical optical methods based on LSPR for example Surface Enhanced Raman Scattering (SERS), Metal Enhanced Fluorescence (MEF) and Enhanced Plasmonic Circular Dichroism.[6, 16-18] The advantage of LSPR based spectroscopies over other methods is the nondestructive and ultrasensitive detection,[19, 20] thus they can be applied in art preservation e. g. pigment identification[1], cell investigations[21] and medical diagnostics.[3] Recently noninvasive SERS experiments on living animals have been reported.[2, 10] The huge advantage of LSPR based methods is a strong enhancement of analytical signals, which allows even single molecule detection.[13, 22] The increasing importance of plasmon enhanced analytics is strongly connected with the development of nanofabrication technologies.[23, 24] Plasmonic substrates cover the whole range of nanostructures with precisely controlled sizes, shapes and surface modifications. The most common substrates for optical applications are gold and silver nanoparticles, less common copper nanoparticles[20]. The need for selective detection caused a boost of novel approaches based on their surface modifications. The most common approach is coating of a gold or silver core by a dielectric shell susceptible to further modification, for example silica [3, 9, 10, 15, 18, 19, 21, 25-35] or titania.[7, 36] Many examples in literature show that a coating of plasmonic nanoparticles not only allows an easy modification of the surface,[3, 21] but also tunes the plasmonic properties of nanoparticles,[3, 21, 33, 37] regulates the distance between plasmonic nanoparticles and analyte molecules,[28, 38, 39] decreases toxicity,[15, 32] increases stability[3, 30, 32] and biocompatibility.[15, 21, 30]

The enhancement of signals is strongly dependent on the applied plasmonic substrate.[40] Powerful analytical tools that include combinations of different plasmonic sensing approaches require continuous improvements of the plasmonic substrates, enabling selectivity, stability of the nanostructures and of the optical signals, biocompatibility, easy and reproducible fabrication, and microscopic homogeneity.[40] Initially, plasmonic substrates were roughened metals surfaces;[41] however, significant advances in nanotechnology during the last years led to fabrication of plasmonic nanoparticles with well-defined morphologies. In order to maximize the enhancement factor and to improve reproducibility of sensing, different nanostructures, e.g. nanostars,[42] nanoprisms,[43] nanocubes,[44] nanosheets,[45] nanowires,[46] nanorods,[47] hollow nanostructures[48], core-shell nanoparticles,[34] preassembled plasmonic dimers and trimers[49] were investigated. This wide range of nanostructures can be applied in aqueous or organic solvents,[3, 31] as well as immobilized on solid substrates.[5, 30, 50-52] The most common methods of nanoparticles fabrication are the bottom-up approaches, however, top-down methods such as laser ablation or lithography can be also employed in order to prepare uniform, well defined morphology nanoparticles. Bottom-up based methods of fabrication of spherical nanoparticles are fast, simple and cost-effective; therefore this approach

dominates over other methods.[53, 54] Unfortunately, in many cases, colloidal solutions of nanoparticles are not stable enough to provide a good reproducibility of measurements, in particular in the presence of analyte molecules. Changes of the pH or the ionic strength of the solutions can lead to aggregation of nanoparticles, which results in significant changes of plasmon based enhancement.[30] In order to improve the stability and optical properties of plasmonic nanoparticles, numerous approaches of coating them by dielectric shells were developed.[34, 35, 55] A dielectric shell around the plasmonic core not only prevents the core material from aggregation and increases versatility of the plasmonic material by facilitating surface modifications, but also allows tuning the plasmonic properties of nanoparticles, as the LSPR strongly depends on the refractive index of the molecule surrounding the nanostructure.[6, 27, 56] The ability to control the shell thickness is important in order to control the distance between plasmonic surface and the analyte molecules. As an example this distance is a key factor for plasmon enhanced fluorescence experiments, where both the enhancement and quenching of fluorescence are distance dependent.[38, 39] In contrast in SERS the highest enhancement is reached very close to the surface of plasmonic nanoparticles, and it declines by increasing the distance.[38, 39] Because the strong electromagnetic fields through the shell material decays very fast, the shell should be very thin (1-5nm).[19] For this purpose, silica coating is very convenient, as the thickness of silica shell can be easily controlled by changing the pH value, temperature, reaction time and concentration.[19, 34, 35] However, to avoid problems related to very thin coatings, porous materials of greater thicknesses can allow analyte molecules access to the plasmonic nanoparticles[29]. Metal fluorides beside their extraordinary optical properties exhibit high porosity and therefore could be very beneficial for the coating plasmonic nanomaterials.

An important step in plasmonic substrate development was the immobilization of plasmonic nanoparticles on solid substrates.[51, 57] Similar to coating, this approach results in increasing the substrate stability and gives additional benefits like modified optical properties. This phenomenon is caused by coupling of the plasmon resonances of adjacent nanoparticles[58, 59] and allows the creation of highly active SERS nanoparticle arrays.[52, 60]

An initial method of nanoparticles immobilization was based on applying thin films of chromium or titanium on glass substrates in order to promote the adhesion of gold or silver nanoparticles on the surface[12, 61]. Because of the unfavorable influence of these metal layers on LSPR resulting in a deceasing of intensity and broadening of bands, organic amino-[7, 30, 50, 51] or mercapto-terminated silanes[51, 62, 63] were introduced in gold or silver nanoparticles to immobilize them on the glass or silica surfaces. Such systems provide a homogeneous distribution of immobilized nanoparticles, thus they are considered as very promising SERS sensors for quantitative analysis.[8, 11, 14] Density and morphology of immobilized particles on the surface can be regulated by the type of applied linker and solvent.[51, 60] A very popular linker is 3-aminopropyltriethoxysysilane (APTES). Gold and silver nanoparticles immobilized by APTES show a high level of enhancement concerning homogeneity and stability.[50]

The benefits of immobilization and coating can be combined in order to create stable and selective systems.[30] In this thesis, magnesium fluoride, a porous material with very beneficial optical and mechanical properties will be used for coating plasmonic nanostructures.

1.2. Core-shell nanoparticles

The term core-shell nanoparticles has been used in the early 1990s referring to concentric multilayer semiconductor nanoparticles.[64-66] However, novel properties of composite and sandwich colloidal semiconductors were reported already in the late 1980s.[67-69] In 1987 H. W. Lubomir Spanhel and Arnim

Henglein described illumination processes of colloidal solutions containing CdS and TiO_2 or ZnO particles.[70] One year later in 1988, B. Hyeong-Chan Youn, and Janos H. Fendler reported CdS crystals coated with ZnS for photoreduction of water.[71] Nowadays, core-shell nanoparticles have become an important group of nanoparticles with different morphologies and many applications, including functions in biomedicine and electronics. Abundant examples can, for example, be found in a review written by R. G. Chaudhuri and S. Paria.[53] The combination of core and shell materials leads to new properties of the nanomaterial, often different than properties of separated core or shell material itself. Moreover, the presence of the shell increases the stability of colloids and allows an easier surface modification. By changing size or shape of the core and the shell material and/or its thickness, properties of core-shell nanoparticles can be easily tuned. In principle, several criteria to classify core-shell nanoparticles exist, example shape, size, morphology or chemical composition. The physical properties of core-shell nanoparticles are mostly determined by the composition of core and shell material. Different classes of core-shell particles can be distinguished, that have very distinct properties:[53]

- Inorganic@inorganic core-shell NPs
- Inorganic@organic core-shell NPs
- Organic@inorganic core-shell NPs
- Organic@organic core-shell NPs

Some properties like catalytic activity and selectivity, electrical properties, optical properties, plasmonic properties, melting point are size and shape dependent.[53] The most common type of core-shell NPs are spherical nanoparticles (spherical core and spherical shell); however advances in nanotechnology allow to synthesize different shaped core-shell nanoparticles. Different shapes of core-shell nanoparticles were reported in the literature, for example Au@Pt rod core-rod shell[72], Ag@Au prism core-prism shell,[73] Ag@SiO_2 prism core-triangular shell,[74] Cu_2O@Au cubic core-flowery shell[75] etc.. Nanostructures with different morphologies for example multishell nanoparticles called nanomatryushka,[76] multiple core coated by a single shell[77] and hollow nanoparticles[78, 79] are also very interesting and promising materials.

In case of the investigations performed inside this thesis metal@nano-metal fluorides core-shell nanoparticles are of interest. These materials belong to the inorganic@inorganic core-shell nanoparticles group, therefore only this group will be described in details. This type of core-shell nanoparticles is the most popular class of core-shell nanoparticles.[53] Since nano-metal fluorides became available just recently, most of literature is related to nano-metal oxides. Therefore, in this chapter a rough overview about inorganic@inorganic core-shell nanoparticles will be focused mostly on metal@metal oxides core-shell nanoparticles. Synthesis and properties of metal fluorides will be discussed in the chapter 1.3.

Within inorganic@inorganic core-shell nanoparticles silica coated nanoparticles are a large subgroup. Coating with silica is very beneficial: due to high optical transparency, low refractive index and chemical inertness of silica (core protection), reducing bulk conductivity and increasing stability of suspension of core particles. Moreover, it is easy to control the thickness of the silica shell by controlling the concentration of reactants, and reaction time.[53] A combination of silica shell and gold or silver core are commonly used, however, different core materials, e.g. Ni[80], Fe[81, 82], Co[83, 84] are also applied.

A breakthrough in the field of silica coating was made by L. M. Liz-Marzán, M. Giersig and P. Mulvaney,[34] who developed an effective method for producing Au@SiO_2 core-shell nanoparticles in 1996. Previously reported in the literature silica coating procedures were limited to surfaces with a strong chemical or electrostatic affinity to silica.[34] Coating of gold nanoparticles with silica is much more challenging due to very little affinity between them and the presence of stabilizing agents preventing aggregation of nanoparticles (carboxylic acids or organic anions) which additionally decrease affinity of the gold surface to silica. To solve this problem, Liz-Marzán et al. proposed to increase gold affinity to silica by modifying the gold surface with a silane coupling agent, like 3-aminopropyltriethoxysilane and using active silica (SiO_3^{2-}).[34] Under carefully selected reaction conditions (pH, concentration of reagents and number of steps) the synthesis of a complete, uniform shell with controlled thickness was successfully achieved. [34]

Another subgroup of inorganic/inorganic core-shell NPs are different metals and metal oxides applications mostly in the field of catalysis, solar energy conversion or with magnetic properties .[53] Interesting examples of nonsilica inorganic/inorganic core-shell nanoparticles are MgO or CaO coated by a Fe_2O_3 shell used for adsorption of toxic gases like SO_2 and H_2S. [85, 86] MgO@Fe_2O_3 and CaO@Fe_2O_3 exhibit even better adsorption capacities than pure MgO or CaO. [85, 86]

Many different methods can be used in order to synthesize core-shell nanoparticles. Two major approaches can be distinguished: bottom-up and top-down synthesis.[53] The bottom-up approach is less precise than top-down, however, it is cheaper and allows to synthesize smaller particles. It includes many different approaches such as chemical synthesis, vapor deposition, laser-induced assembly, film deposition, self-assembly and colloidal aggregation etc.[87-89] The top-down approaches based on cutting, milling and shaping involve mostly lithography techniques such as electron or ion beam, scanning probe, optical near field[90, 91] and other methods for example laser-beam processing[92] or mechanical techniques as machining, grinding, polishing.[93-95]

The synthesis of core-shell NPs contains two steps: synthesis of the core nanoparticles and formation of the shell. The most challenging points for a successful synthesis are: preventing aggregation of particles in the reaction media, formation of the shell, rather than separate shell material, controlling the thickness of the shell and creating a uniform shell (full coverage of core particles). The most common methods of shell synthesis include: precipitation,[79, 96] sol-gel condensation,[97, 98] microemulsion,[99-101] polymerization[102-104] and layer by layer deposition methods.[105, 106] Synthesis of the core can be achieved by using many different methods like salt reduction with different reducing agents (e.g. sodium borohydride,[107] hydrazine,[108] sodium citrate,[109-111]), transmetalation, thermal decomposition of organic compounds and many others.[53] In Table 1 are some chosen methods characterized in short.

Table 1: Overview of selected methods of core nanoparticles synthesis.

Method	**Characteristic**
Sodium borohydride reduction[107]	• High reducing potential • Suitable for aqueous and non-aqueous reaction media • Successful in any pH, reduction mechanism depends on pH

Method	Characteristic
Hydrazine reduction[53, 108]	• Easy to control the reaction (pH and temperature determine reducing ability) • Application limited to metals with reduction potential higher than hydrazine • Performed mainly in alkaline media (maximum of reduction efficiency pH>11) • Weaker reducing agent than $NaBH_4$ • Suitable for Ni, Ag, Cu, Pt NPs and bimetallic compounds (e.g. Pd/Pt, Pt/Ru)
Sodium citrate reduction[109-111]	• Sodium citrate is simultaneously: reducing and stabilizing agent, pH buffer • Reaction require precisely controlled temperature • Performed in aqueous media
Reduction-transmetalation[53, 112-115]	• Additional reducing agent is not required • Shell formation occurs spontaneously • Self-nucleation of shell material is excluded • Shell growth is homogeneous • Limited only for systems, where shell metal has higher reduction potential than core material (eg. Ni@Au, Co@Pt, Ni@Ag, Co@Au, Co@Pd, Co@Cu, Ag@Au)
Thermal decomposition of organic compounds[53, 115-119]	• Obtained nanoparticles require surfactants, stabilizing agents and neutral atmosphere in order to prevent oxidation (e.g. Cu, Co, Au, Ni) • Suitable for fabrication metal@metal oxide systems (oxidation occurs spontaneously due to the oxygen and water in the atmosphere) e.g. $Cu@Cu_2O$ • Process requires high temperature
Wire electrical explosion[53, 80, 120-123]	• Extremely fast method (thermal expansion occurs within several tens of microseconds) • Expensive method (high voltage, inert gas atmosphere, high pressure are required) • Suitable only for highly conductive metals available in the wire form • Obtained NPs exhibit inhomogeneous size and have to be kept under neutral conditions to prevent oxidation • Suitable for synthesis of core NPs such as Ni, Al, Cu and core-shell e.g. Cu@Zn, Ti@Ni

All methods presented in Table 1 are very useful, however, each of them has its advantages and disadvantages. That is why the method of core synthesis has to be carefully considered and individually selected for the desired structure.

In case of this thesis gold nanoparticles were synthesized by a sodium citrate reduction approach. Sodium citrate reduction method was initially developed by Turkevich et al.[109] and further improved by many researchers. It is known as a very good method to synthesize gold nanoparticles. The protocol established by Bastús et al. allows a synthesis of stable, monodispersed, uniform, spherical particles of sizes from 10 to 180 nm in a high concentration of $3.0x10^{12}$ NPs/ml for particles in the size of 8.4±1.0 nm in diameter and $5.0x10^{9}$ NP/ml for the particles in the size of 180.5±10.7 nm in diameter.[110] Moreover no other reactants are needed, because sodium citrate acts as reducing agent, stabilizing agent and a pH buffer.

Since the shell formation is a complex problem, crucial to achieve the goal of this project and it depends on desired shell, only formation of metal fluorides will be discussed in this work (chapter 1.3.1).

1.3. Metal fluorides

In the previous chapters many examples of metal-metal oxides core-shell nanoparticles were described. Due to extraordinary optical properties, applying metal fluorides can be more beneficial than metal oxides including silica. Metal fluorides exhibit the lowest refractive indexes of all known inorganic materials[124] and show almost 100% optical transparency.[125] A low refractive index can be provided by high porosity of the material; however, a high porosity usually decreases it's mechanical stability[125]. Magnesium fluoride shows a refractive index of $n_{589\ nm}$ 1.38[124] and a surprisingly high mechanical stability (even against steel wool).[126] By applying organic copolymers, the porosity of magnesium fluoride can be significantly increased, which results in a decreasing refractive index even up to 1.11.[125] With the extraordinary low refractive index ($n_{589\ nm}$ = 1.38[124]) and its high mechanical stability approve magnesium fluoride is a much more promising material for optics and plasmonics than silica ($n_{589\ nm}$ = 1.46[124]).

Out of many synthetic routes described in the literature, the sol-gel route seems to be the best for synthesis of metal fluorides for the objective of this work. The trifluoroacetic acid method developed by Fujihara et al. produces a lot of toxic gases (CF_3COF, COF_2 and HF), moreover, the final MgF_2 sol is contaminated by residual carbon and oxygen (OH^- and COO^-)[127-129]. MgF_2 obtained by a liquid-phase method in water[130] and polyol-mediated approach[131] is not suitable for antireflective coating due to a high refractive indices or too low viscosity of the obtained sols.[132]

1.3.1. Sol-gel synthesis

Solution-gelation (sol-gel) synthesis was developed in mid- 1800s by Ebelman and Graham during their studies on silica gel and became a popular method for inorganic ceramic and glass materials processing.[133] Nowadays the sol-gel synthesis is a powerful, versatile method of fabrication porous materials including a lot of metal oxides nanoparticles. The sol-gel method provides a way to obtain materials offering a wide range of different sizes, shapes and applications.[134, 135] The classical sol-gel process consists of two steps: hydrolysis (1) and condensation (2a,2b) of metal alkoxides dissolved in mixture of alcohol and water as following[136]:

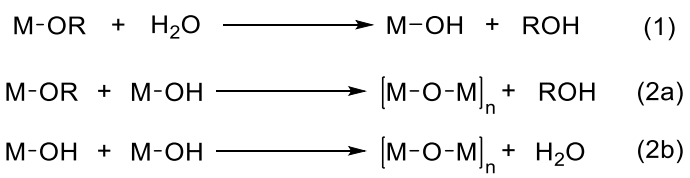

Usually condensation reactions are incomplete, therefore a post-calcination process is required in order to release organic contaminations (e.g. alcoholate groups) from the obtained material. For preparation of organic free metal oxide phases a calcination temperature up to 450 °C is required.

As mentioned in the previous chapter, most of known methods of MgF_2 synthesis are performed in water or with water containing magnesium precursors or aqueous HF solutions. Water is known from its unfavorable effects on the sol: promoting gelation processes and the formation of MgO or MgO_xF_y during the thermal treatment[132]. Therefore the non-aqueous fluorolytic sol-gel synthesis was developed, to obtain pure and transparent sols for a homogeneous coating.[137-139] In this method a metal alkoxide diluted in a low boiling organic solvent reacts with anhydrous HF as following:

$$M\text{-}OR + H\text{-}F \longrightarrow M\text{-}F + ROH \qquad (3)$$

In the case of metal fluorides, the formation of metal-fluoride-metal bridges occurs without condensation in contrast to metal oxides formation presented above (equation 2b). Similarly to metal oxides obtained on classical sol-gel route, metal fluorides synthesized via fluorolytic sol-gel process, also require a post-fluorination step: calcination (the reaction is usually incomplete). In opposite to metal oxides, calcination of metal fluorides can be performed under soft conditions (100-250 °C), however, a high temperature is preferable for anti-reflective coating purposes.[136] In the case of metal fluorides coating (e.g. glass coating) calcination brings additional benefits. During the calcination process, densification of the metal fluorides structure occurs, which results in increasing mechanical stability of the metal fluoride layer.

For the synthesis of metal fluorides via sol-gel process different reaction parameters can be applied, including different metal precursors, solvents, concentrations and temperature. The most significant impact on the sol-gel process has chosen metal precursor. Metal acetates,[140, 141] metal alkoxides[142] and inorganic[126, 143] metal precursors can be used for metal fluorides synthesis. The advantage of metal acetates is their high solubility in alcohols. However, their hydrated metal acetates can form hardly soluble solvated metal acetates in ethanol due to re-solvation process.[140] Therefore, in order to obtain clear, transparent metal fluorides sols, metal acetates have to be dried prior the synthesis.[140] The reaction of prior the synthesis dried acetates with HF leads to the formation of acetic acid, which can react with ethanol and form equimolar amounts of water.[140] Unlikely to the metal acetates, employing metal alkoxides does not lead to water formation; after the reaction with HF only the respective alcohol is formed.[142] Magnesium methoxide is a suitable precursor for magnesium fluoride synthesis. Unfortunately, commercially available magnesium methoxide does not react properly, therefore it has to be prepared prior the synthesis by the reaction of magnesium with dried methanol. This method has two significant drawbacks: release of large amount of hydrogen and employing a toxic solvent.[136] Alternatively, magnesium ethoxide can be used for magnesium fluoride sol-gel synthesis. Magnesium ethoxide can be dissolved in ethanol only the CO_2 is introduced.[144] An approach based on the fluorination of water-free metal chlorides leads to immediate clarification of the obtained sols. Such sols are characterized by long-time stability. As for the purposes of this work, only low concentrated magnesium fluorides sols will be used, the remain parameters do not have a significant impact.

Metal fluorides obtained via the fluorolytic sol-gel route are well dispersed, highly disordered, non-aggregated and their particles size varies between 5 to 10 nm. In comparison with metal fluorides obtained on the conventional routes, metal fluorides prepared by sol-gel method exhibit very high surface area and significantly increased Lewis acidity.[145] Therefore they can be successfully applied in the field of heterogeneous catalysis.[146 147]

Thin films of metal fluorides synthesized via the fluorolytic sol-gel process are homogeneous and exhibit a low refractive index after coating. [132] Such properties are beneficial for antireflective coatings.[126, 148, 149] Due to high thermal, mechanical and chemical stability combined with high transparency from UV to IR spectral range, nanoscopic metal fluorides are applied also in optics.[150] Rare earth metasl-doped calcium fluoride is an example of metal fluorides applications for up- and downconversion materials.[151]

1.3.2. Anti-reflective coating

The aim of anti-reflective coating is to reduce reflection in order to increase efficiency of optical materials like glasses (including windows), optical lenses and solar panels. Typical transparent glasses with refractive index about 1.5, reflect bout 4.3% of incident light (of the visible range).[125] For optical glass a zero reflection can be reached by coating it with a material with refractive index of 1.23 and a thickness of one-quarter of the incident light's wavelength (refractive index of the coating material matches the square root of the substrate's refractive index).[125] Unluckily, materials with such low reflective index do not exist in nature. The most suitable material is magnesium fluoride with a refractive index of 1.38. As mentioned before, increased porosity results also in a decreased refractive index. It was reported that applying organic copolymers, the porosity of magnesium fluoride increases and so the refractive index reaches even up to 1.11.[125] An extraordinary low refractive index, high transparency, mechanical stability and wide optical range turn out magnesium fluoride as a perfect material for anti-reflective coating. Coating techniques are based on two main approaches: vacuum-based methods and chemical processing ones. Vacuum based technologies (physical vapor deposition or chemical vapor deposition) are not suitable for preparing homogeneous, large areas films with controlled porosity,[152] thus they will not be discussed in this work. Wet chemical processes involve deposition of colloidal solutions, for example: spraying, spin coating or dip-coating.[152] Dip-coating has many advantages over other methods such as: less equipment is required, costs are lower, it is suitable for coating large areas and allows to tailored microstructure of deposited films.[153] In principle sol-gel dip-coating consists of two steps: withdrawing a substrate from a sol when gravitational draining occurs simultaneously with solvent evaporation and condensation reactions, resulting in the deposition of a solid film.[153] The structure of the film is influenced by different factors like: size, structure and reactivity of particles, stability of the sol, relative rates of condensation and evaporation liquid surface tension and dipping speed. The dip-coating process is described by Landau-Levich's equation,

$$h = 0.94 \cdot \frac{(\eta \cdot \upsilon)^{\frac{2}{3}}}{\gamma^{\frac{1}{6}} \cdot (\rho \cdot g)^{\frac{1}{2}}} \qquad (4)$$

where h = thickness of the thin layer, η=viscosity of the coating solution, υ= constant linear speed of withdrawal of the substrate from the coating solution, γ= liquid-vapor surface tension, ρ= density of the coating solution, g= acceleration due to gravity. [154] Viscosity, liquid-vapor surface tension and density of the coating solution depend on its concentration. For the purposes of experimental work it can be simplified that the thickness of deposited layer depends on the concentration of the coating solution and the speed of windrowing the substrate. Because of many advantages and simplicity of the dip-coating method, it was chosen as a coating method in this work.

2. Aim and scope of the presented work

The main objective of this work was to create a plasmonic substrate which meets the following criteria: exhibits microscopic homogeneity, stability of the nanostructures and the optical signals, selectivity and biocompatibility and can be obtained in a simple, cost effective and reproducible way. In order to achieve this aim the excellent plasmonic properties of gold nanoparticles were combined with the extraordinary optical properties of magnesium fluoride. Different methods of gold nanoparticles synthesis allow to control their size and shape in order to tune their plasmonic properties. Magnesium fluoride can be an excellent compound for the coating of plasmonic substrates in view of its biocompatibility, low refractive index and high porosity combined with high mechanical stability.

In order to obtain plasmonic substrates containing of gold nanoparticles coated by magnesium fluoride, two different approaches are proposed here. The first approach was based on the formation of Au@MgF_2 core-shell nanoparticles. Many studies on gold nanoparticles as a core material coated with different shell materials are reported in the literature. To the best of our present knowledge, Au@MgF_2 core-shell nanoparticles neither other metal nanoparticles coated with magnesium fluoride shell have been not reported yet. Using existing knowledge on metal oxides coating, as a strategy for coating with metal fluorides was proposed. Because of the benefits of using magnesium fluoride as a shell material are tremendous, the proposed approach was undertaken in spite of several differences between metal fluorides and metal oxides. Metal fluoride and oxides are characterized by different electron configurations, oxidation states, electronegativity and covalent radii, which result in different chemical properties. As will be discussed here many different possibilities for the synthesis of such core-shell structures will remain extremely challenging and cannot be considered as a possible route to magnesium fluoride coated nanoparticles.

The second investigated approach was the fabrication of porous magnesium fluoride-over-gold nanoparticles (MON). It includes immobilization of the gold nanoparticles on a glass substrate and coating it with magnesium fluoride using a dip-coating method. As will be shown immobilization of gold nanoparticles, provides high stability of the plasmonic substrate and additionally results in unusual optical properties caused by coupling of the plasmon resonances of adjacent nanoparticles. In order to provide high microscopic homogeneity and high SERS efficiency gold nanoparticles in different sizes were applied for the MON fabrication. Obtained MON were characterized by Scanning Electron Microscopy (SEM), Scanning Force Microscopy (SFM), UV-Vis spectroscopy and Surface Enhanced Raman Scattering (SERS). In order to compare SERS efficiency of different kinds of MON, the experimental enhancement factors were estimated.

3. Results and discussion

3.1 Synthesis and characterization of Au@MgF_2 core-shell nanoparticles

All experimental procedures discussed in this chapter are described in details in the experimental section. Numbers of the procedure mentioned in the text below correspond to the numbers of chapters in the experimental section for example procedure 4.1 refers to the chapter 4.1

A general approach of Au@MgF_2 core-shell nanoparticles synthesis based on formation of MgF_2 nanoparticles in the presence of gold nanoparticles. Due to unique optical properties of metal fluorides obtained via sol-gel synthesis, only this method was investigated in this work. In order to find the best conditions for the core-shell nanoparticles formation different magnesium precursors (e.g. $Mg(OAc)_2x4H_2O$, $MgCl_2x6H_2O$, $Mg(OEt)_2$) were attempted. The molar ratio of gold to magnesium precursors was varied from 1:2 to 1:10 in order to obtain shells of different thickness. Ethanolic or seldom methanolic solution of HF was always used in the stoichiometric ratios to the magnesium precursors. Gold nanoparticles in the size of 18 nm in diameter were fabricated by reduction of tetrachloroauric acid with sodium citrate according to the procedure proposed by Bastús et al (procedure 4.1).[110] The final concentration of gold in each sample was fixed as 0.1 mM.

Different modifications of this approach including changing the sequence of adding regents, using different magnesium precursors and different solvents, applying different stabilizing agents and/or linkers (PVP, 16-MHDA, magnesium citrate) were performed.

Attempts of synthesis Au@SrF_2 and Au@ZrF_2 based on the same approach (formation of metal fluoride in presence of gold nanoparticles) were taken in order to eventually facilitate TEM investigations because of their higher molar mass regarding to magnesium fluoride.

3.1.1 Fabrication and characterization of the gold nanoparticles

For the research on the synthesis of Au@MgF_2 core-shell nanoparticles presented in this work, spherical gold nanoparticles of a diameter of 18 nm were chosen due to their easy fabrication and predictable optical and plasmonic properties. For the fabrication of MgF_2-coated gold nanoparticles arrays described in the second part of this thesis (chapter 3.2.3), gold nanoparticles in the size of 26, 36 and 47 nm in diameter were applied. Synthesis of gold nanoparticles in all chosen sizes will be discussed together in this chapter.

Physicochemical properties of gold nanoparticles strongly depend on their size and shape; therefore in the chapter 3.2.3 spherical gold nanoparticles in different sizes were applied for SERS sensors. In order to compare gold nanoparticles in different sizes, they should be fabricated by the same procedure, thus the sodium citrate reduction procedure described by Bastús, Comenge and Puntes[110] was chosen. This approach allows to synthesize spherical gold nanoparticles in different sizes by repeating parts of the procedure. The sodium citrate reduction method is based on single-phase aqueous reductions of tetrachloroauric acid with sodium citrate reported in 1951 by Turkevich et al.[109] and was refined 22 years later by Frens[155]. Frens et al. were able to synthesize gold nanoparticles in the size from 5 to 150 nm by varying pH of the solution, sodium citrate to gold ratio and solvent, however, the obtained particles showed a very wide size and shape distribution. An approach proposed by Bastús at al. provides a highly concentrated ($3x10^{12}$ NPs/ml for gold seeds in the size of 8.4 ± 1.0 nm in diameter up to $5x10^9$ NPs/ml for the AuNPs in the size of 180.5 ± 10.7 nm in diameter), highly monodispersed gold nanoparticles characterized by uniform shape and narrow size distribution.

Such particles were fabricated by suppression of secondary nucleation. When the secondary nucleation does not occur, particles are allowed to enlarge their size via surface-catalyzed reduction of Au^{3+} by sodium citrate. The kinetic of the growth process on the gold nanoparticles is controlled by adjusting temperature and pH of the solution, as well as the seeds concentration. Applying sodium citrate reduction for gold nanoparticles synthesis has also other advantages. Sodium citrate acts as reducing agent, stabilizing agent and pH buffer simultaneously; therefore, applying additional components is not required (less contaminations in the solution). Moreover, sodium citrate can be easily replaced by other stabilizing molecules, especially functionalized thiols, which are very beneficial for bio and medical applications.[34, 156-158]

The crucial point of the successful synthesis of the monodispersed gold nanoparticles of narrow size and shape distribution is to maintain a required temperature (100 °C for synthesis of Au seeds and then 90 °C for seeds growth), a pH around 7 and to control the amount of gold precursor. Gold seeds formation occurs at 100 °C, therefore an aqueous solution of tetrachloroauric acid has to be injected to the boiling aqueous solution of sodium citrate. When the transparent, colorless mixture reaches a red-wine color, the temperature has to be decreased to 90 °C for the seeds growth process in order to prevent a secondary nucleation. Sequential injections of sodium citrate and tetrachloroauric acid (with a time delay of 2 min) every 30 min provide homogeneous growth of the nanoparticles. Each addition of tetrachloroauric acid results in decreasing pH, what leads to the protonation of carboxylic group of the citrate molecules. Protonated carboxylic groups are not capable to stabilize gold nanoparticles anymore, thus addition of the pH buffer (sodium citrate) is required for every step. Experimental details of the gold nanoparticles fabrication are described by the procedure 4.1. According to Bastús et al. repeating sequential injections of sodium citrate and tetrachloroauric acid up to 14 generations results in fabrication of gold nanoparticles with a size of 30.5 ± 3.9 nm in diameter. [110] In order to produce particles bigger than 30 nm in diameter (up to 180 nm in diameter) the solution has to be diluted after two growing steps. [110] Although this procedure was not applied for the purposes of this work, particles in the size 47 nm in diameter were produced. That can be possibly caused by the difficulties in maintaining the required temperature during growing nanoparticles (required temperature is 90 °C, actual temperature during the synthesis was varied between 80 and 95 °C). Therefore, each batch of gold nanoparticles synthesized by citrate reduction (procedure 4.1) was characterized using transmission electron microscopy (TEM) and ultraviolet-visible spectroscopy (UV-Vis) in order to define their size, shape and aggregation state. Figure 1 shows TEM images of 3 representative batches of gold nanoparticles in the size of 26 ± 3 nm (Fig 1a), 36± 4 nm (Fig 2b) and 46± 5 nm (fig 1c). The size of gold nanoparticles was estimated from TEM images using ImageJ software. For each batch, the size of 150 to 200 nanoparticles was measured and then a averaged value was calculated. Obtained particles are mostly spherical (only a few triangular and oval nanoparticles were observed) and characterized by narrow size distribution. Larger nanoparticles show a higher size distribution than the smaller ones, which is in accordance with the data presented by Bastús et al.[110] Figure 2 shows UV-Vis spectra of synthesized gold nanoparticles. Maximum of absorbance for 26, 36 and 47 nm gold nanoparticles appears as single, symmetric and sharp band at wavelength of 524, 527 and 531 respectively and no absorbance is observed at higher wavelengths. This indicates a high monodispersity of nanoparticles in accordance with presented TEM images (figure 1). The red shift observed on the spectra is characteristic for increasing the size of gold nanoparticles.[110] Although the required temperature for the nanoparticles growth was not maintained, the obtained particles are spherical, monodispersed and characterized by only slightly wider size distribution than

expected (e.g. obtained nanoparticles 36± 4 nm in diameter, expected nanoparticles 36±2 nm in diameter).

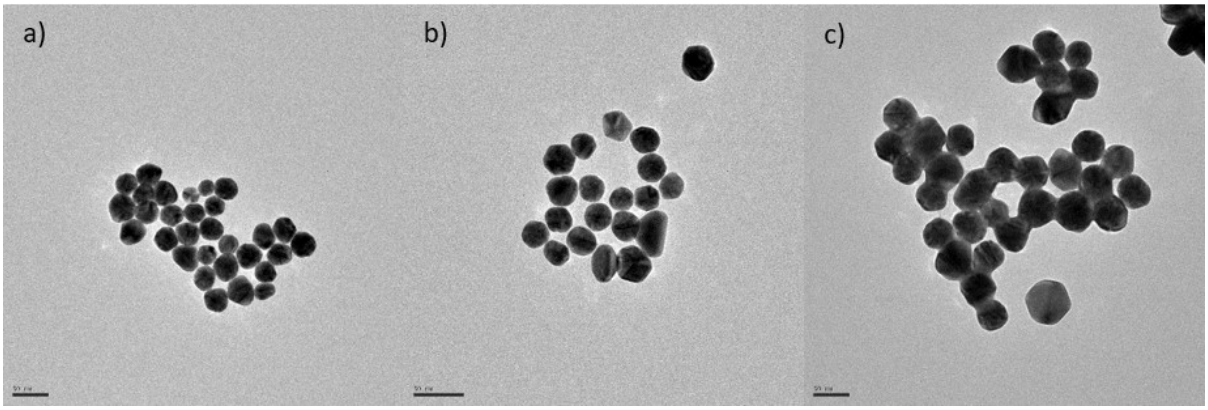

Figure 1: Transmission electron micrographs of the gold nanoparticles with an average diameter of a) 26±3 nm, b) 36±4 nm and c) 47±5 nm. Scale bar 50 nm.

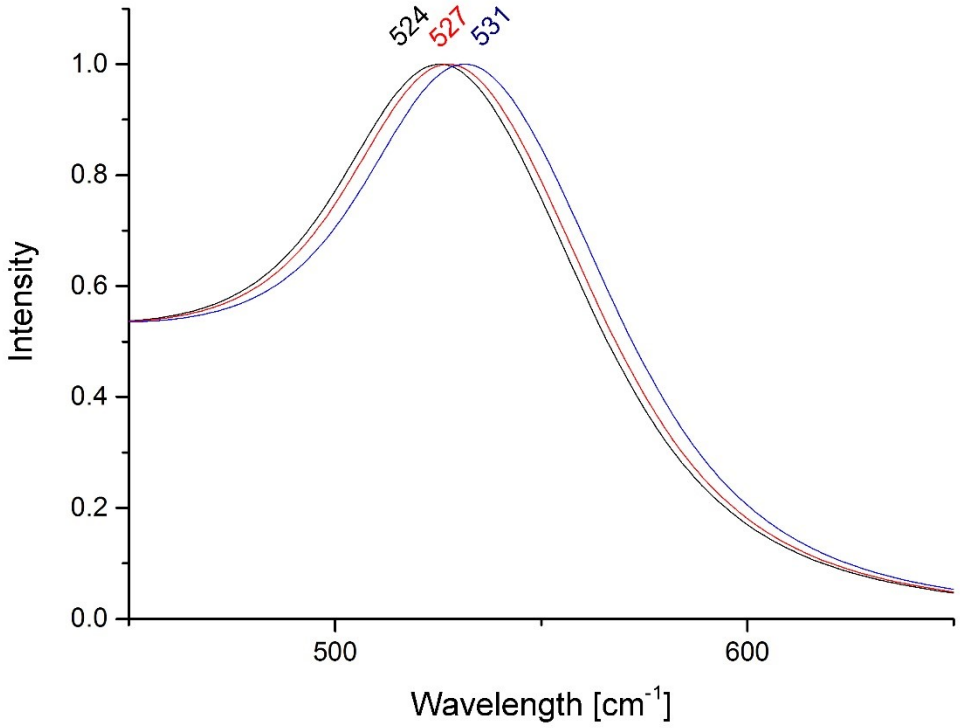

Figure 2: UV-Vis spectra of freshly synthesized gold nanoparticles in the size of 26 nm (black line), 36 nm (red line) and 47 nm (blue line).

3.1.2 Synthesis and characterization of Au@MgF_2 using $Mg(OAc)_2x4H_2O$ and $MgCl_2x6H_2O$ as a magnesium precursor

A primary approach to the synthesis of gold-magnesium fluoride core-shell nanoparticles was a simple formation of magnesium fluoride via sol-gel synthesis in the presence of citrate stabilized gold nanoparticles. Due to opposite zeta potentials of magnesium fluoride (around -40 mV)[159] and gold nanoparticles (around +40 mV),[160] electrostatic interactions between core and shell materials were

taken into consideration. Magnesium fluoride obtained via sol gel synthesis has slightly different properties depending on applied magnesium precursor, therefore several precursors of different character were used.[161, 162] Moreover, different precursors can interact with the gold surface differently.

In the first synthetic experiment (procedure 4.2) $Mg(OAc)_2x4H_2O$ (organic magnesium precursor) and $MgCl_2x6H_2O$ (inorganic magnesium precursor) were used. In all experiments, described in this part of my thesis, aqueous stock solution of gold nanoparticles and hydrated magnesium precursors were used (example $Mg(OAc)_2x4H_2O$, $MgCl_2x6H_2O$. As mentioned in the introduction, the fluorolytic sol-gel synthesis should be carried out under anhydrous conditions, however, in the described system a little amount of water is still acceptable. HF is a stronger reagent compared to water. Therefore, the presence of water in the system leads to formation of a few insignificant impurities (e.g. MgO or MgO_xF_y)[132]. For the purpose of Au@MgF_2 core-shell nanoparticles fabrication a little amount of water in the system is acceptable, however, for the fabrication of MgF_2-coated gold nanoparticles arrays, described in the second part of this thesis, magnesium fluoride will to be synthesized on the classical fluorolytic sol-gel route.

Right before the synthesis of Au@MgF_2 50 mM ethanolic solutions of magnesium precursors (magnesium acetate and magnesium chloride respectively) were prepared (precursor solutions have to be prepared prior the synthesis).[140] To each of 6 plastic containers, 400 µL of 2,5 mM aqueous stock solution of citrate stabilized gold nanoparticles was transferred and then diluted with ethanol according to Table 2. As mentioned above such a small amount of water is negligible; therefore the solution will be further considered as an ethanolic solution. In the next step 50 mM ethanolic solution of magnesium acetate and magnesium chloride were added under magnetic stirring to the gold nanoparticles solution according to Table 2 in the experimental part. Molar ratio of Au:Mg was fixed as 1:2 for samples 2.1 and 2.4, 1:5 for samples 2.2 and 2.5, and 1:10 for samples 2.3 and 2.6. After 5 min of magnetic stirring, stoichiometric amount of 50 mM ethanolic solution of HF was added to each sample. The final concentration of gold in each sample was fixed as 0.1 mM. After synthesis a few droplets of the obtained sols were placed on TEM grids and dried before the measurements.

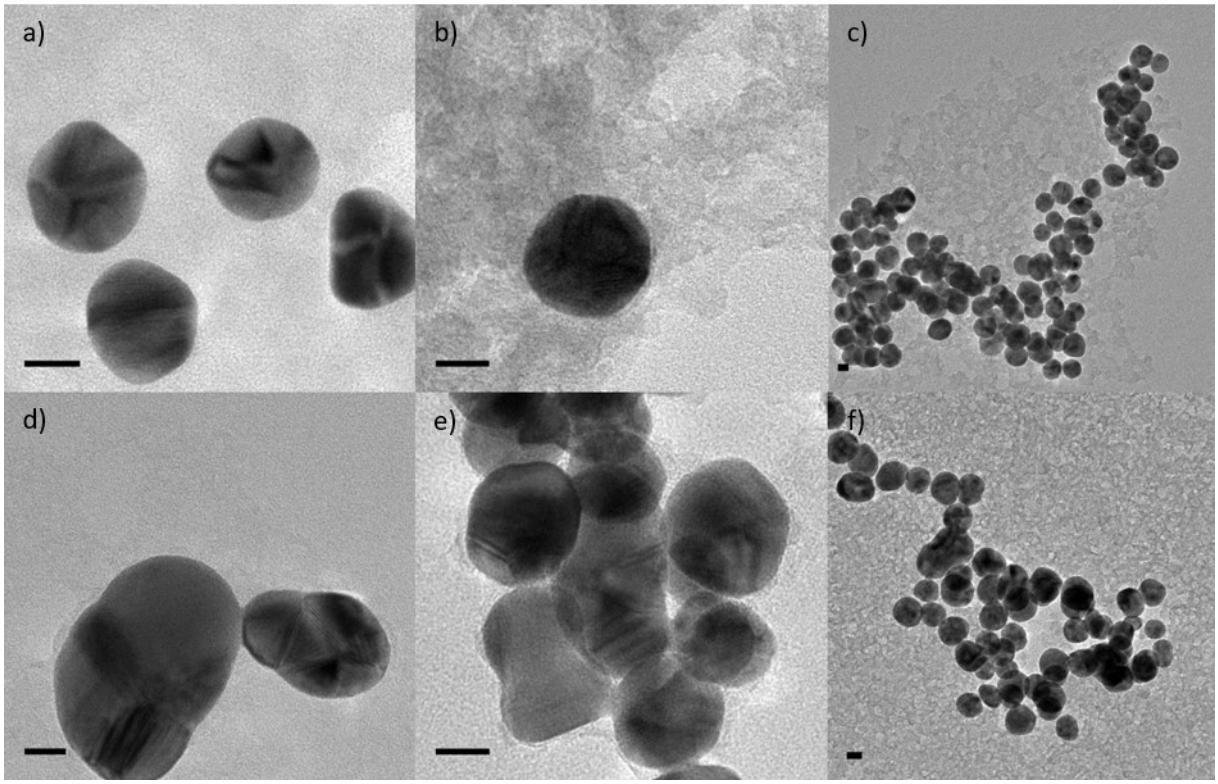

Figure 3: TEM images of samples 2.1-2.6 prepared by mixing ethanolic gold nanoparticles solution with magnesium acetate (a-c, samples 2.1-2.3) and magnesium chloride (d-e, samples 2.4-2.6) and fluorinated afterwards. Gold to magnesium molar ratios are fixed as 1:2 for samples 2.1 and 2.3 (a, d) 1:5 for samples 2.2 and 2.4 (b, e) and 1:10 for samples 2.3 and 2.6 (c, f). Scale bar 10 nm.

From the obtained TEM images (figure 3) can be concluded that the magnesium fluoride shell formation was not successful. However, on the images 3d-e very thin, irregular layer of a very low contrast, surrounding gold nanoparticles can be observed. It indicates presence of organic material (like sodium citrate) or measurements artefacts, rather than formation of magnesium fluoride shell. At this point, it has to be emphasized that magnesium fluoride is a very difficult material for TEM investigations. Magnesium fluoride synthesized via sol-gel synthesis exhibits a very low refractive index and low molar mass (M=62,3 g/mol); therefore, it has a very low contrast on the carbon grids. Moreover, magnesium fluoride is a beam sensitive material, thus taken images can be eventually changed due to interaction of the investigated material by the electron beam. Interpretation of such images is a very challenging process.

Most of core-shell nanoparticles reported in the literature have clearly visible and easy to distinguish core and shell. Magnesium fluoride is not a common material for the core-shell nanoparticles synthesis; however, Nandiyanto, Ogi and Okuyama [78]published recently very good TEM images of polystyrene-magnesium fluoride core-shell nanoparticles. Their magnesium fluoride shell, obtained via hydrothermal method, is complete, homogeneous and easy to recognized. All presented core-shell structures are well dispersed and do not form agglomerates. Based on the work of Nandiyanto et al., clearly visible core-shell nanoparticles were expected. However, the system investigated in this work differs from the literature example; therefore, significant differences can be observed on TEM images. Thus, additional, reference TEM images of a mixture of gold nanoparticles and magnesium fluoride (0.1 mM AuNPs, 0.5 mM MgF_2) were taken (figure 4). Gold nanoparticles solution and magnesium fluoride were synthesized separately and mixed afterwards prior the TEM investigations. The

formation of core-shell nanoparticles was not expected. Figure 4 shows different areas of the TEM grid containing the same reference sample. Figure 4a clearly shows that the magnesium fluoride shell was not formed around gold nanoparticles. Black spheres corresponding to gold nanoparticles are not coated by magnesium fluoride (darker grey, irregular areas on the image). Smooth bright-grey areas correspond to the uncoated TEM grid. In contrast to figure 4a, during accurate analysis of figures 4b-c can be concluded that some particles are surrounded by thick, irregular layer like it was observed at the figure 3. The origin of this "quasi-shell" is unknown. It can possibly be an organic sodium citrate layer or overlapping of gold nanoparticles and magnesium fluoride layer. Gold nanoparticles can be located on the surface or underneath magnesium fluoride layers or trapped inside a magnesium fluoride matrix. Such structures can be formed on the TEM grid during solvent evaporation while sample preparation. Other unidentified measurement artefacts should be also taken into consideration.

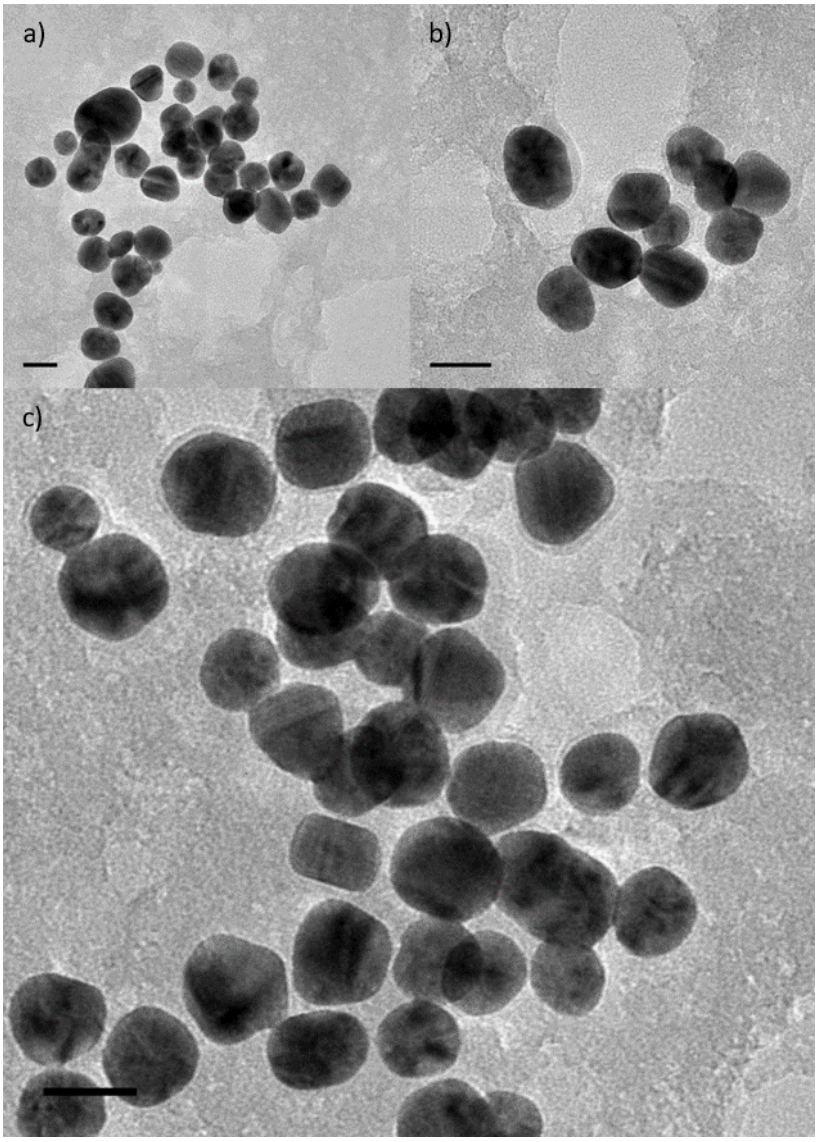

Figure 4: Figure 4. TEM images of different areas (a-c) of the TEM grid coated with mixture of gold nanoparticles [0.1 mM] and magnesium fluoride [0.5 mM] solutions. Scale bar 20 nm.

Based on comparison of TEM images of samples 2.1-2.6 and reference sample it was concluded, that the magnesium fluoride shell was not formed successfully. Core-shell nanoparticles containing metal

fluorides are not well known yet. In this work, some assumptions were made on the basis of knowledge from metal oxides, however, metal fluorides are significantly different than metal oxides. Therefore it can be only speculated that formation of magnesium fluoride aggregates might be energetically privileged over shell formation. A similar problem was faced by Mathias Karg, who was trying to increase the size of obtained magnesium fluoride nanoparticles. He also speculates that probably the formation of magnesium fluorides nanoparticles is preferable over growth of existing particles.[163] Too weak interaction between gold nanoparticles and magnesium fluoride precursors can be another presumable reason of failure in the Au@MgF_2 core-shell nanoparticles formation, therefore numerus modifications of the applied procedure will be examined. It was observed that addition of magnesium salts to the gold nanoparticles ethanolic solution leads to the aggregation of gold nanoparticles (addition of magnesium salts leads to increase in the ionic strength of the solution which results in aggregation of gold nanoparticles); therefore, for next experiments (procedure 4.3), the sequence of adding reagents will be reversed. Further, different strategies include an applying of different magnesium precursors and solvents or exchanging the gold nanoparticles stabilizing agent were taken into consideration.

As mentioned above procedure 4.3 applies the same regents as procedure 4.2, however, the sequence of adding them is reversed in order to avoid an aggregation of gold nanoparticles . First, an ethanolic solution of HF was mixed with an ethanolic gold nanoparticles solution and then magnesium precursors ($Mg(OAc)_2x4H_2O$, $MgCl_2x6H_2O$) were added (in the procedure 4.2 gold nanoparticles solution was mixed first with magnesium salts, then HF was added). The molar ratio of Au:Mg was fixed as 1:2 for samples 3.1 and 3.4, 1:5 for samples 3.2 and 3.5, and 1:10 for samples 3.3 and 3.6. The final concentration of gold in each sample was fixed as 0.1 mM. Ethanolic HF solution was added in the stoichiometric amounts. Experimental details are described in the chapter experimental procedure by procedure 4.3. Figure 5 presents results of TEM investigations of samples 3.1-3.6. In this case shell formation was also not observed. The reason for being not successful can be the same as in experiments done before: too fast magnesium fluoride formation or lack of interactions between gold nanoparticles and magnesium fluoride precursors.

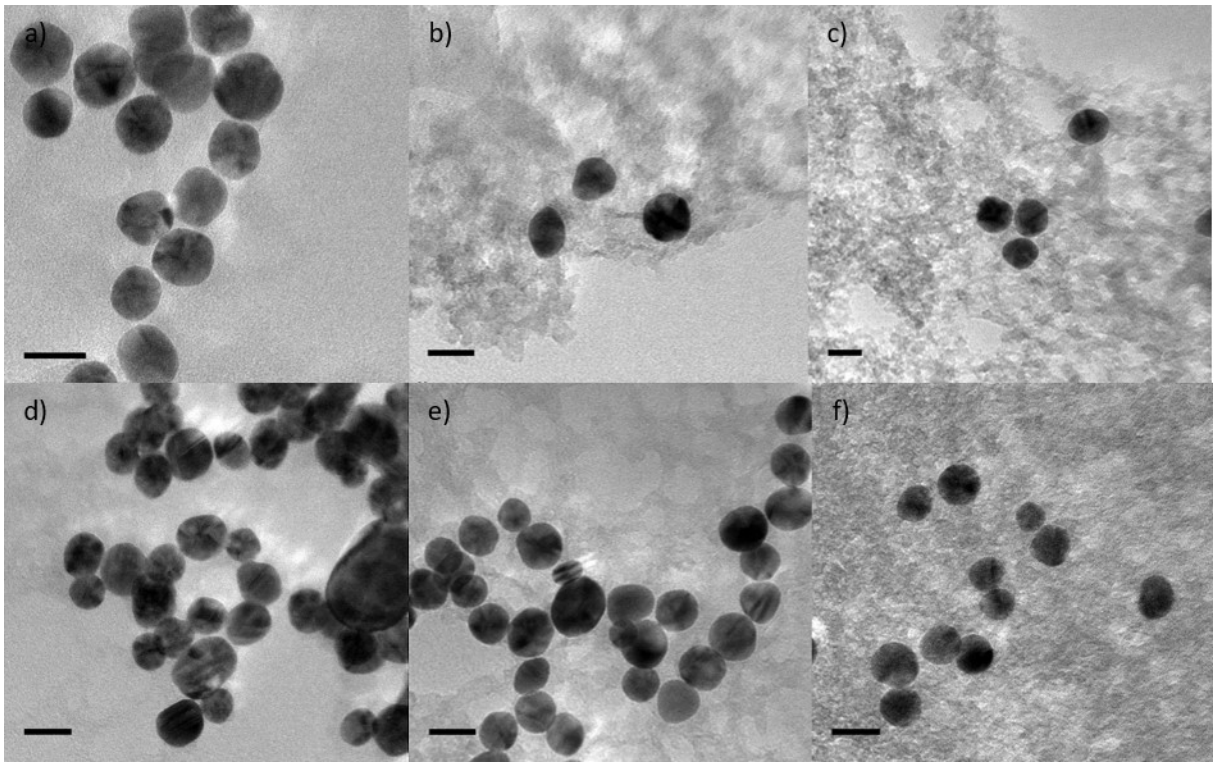

Figure 5: TEM images of samples 3.1-3.6 prepared by mixing ethanolic gold nanoparticles solution with HF solution and afterwards magnesium acetate (a-c, samples 3.1-3.3) and magnesium chloride (d-e, samples 3.4-3.6). Gold to magnesium molar ratios are fixed as 1:2 for samples 3.1 and 3.4 (a, d), 1:5 for samples 3.2 and 3.5 (b, e) and 1:10 for samples 3.3 and 3.6 (c, f). Scale bar 20 nm.

3.1.3 Synthesis and characterization of Au@MgF_2 using $Mg(OEt)_2$ as a magnesium precursor

Before applying more sophisticated experimental procedures an additional precursor of magnesium, magnesium ethoxide, was used. Applying magnesium ethoxide does not lead to esterification reactions and water formation after the fluorination. However, solubility of magnesium ethoxide in ethanol is very limited. Procedures 4.4 and 4.5 employing magnesium ethoxide as a magnesium precursor are based on procedure 4.2 and 4.3 described above. Due to very limited solubility of magnesium ethoxide in ethanol, magnesium ethoxide powder was mixed with ethanol and magnetically stirred and heated to 35 °C for 3h. An obtained white, turbid solution was used for the synthesis. Ethanolic solutions of gold nanoparticles were prepared as previously by diluting their aqueous solution with ethanol according to the Table 4 and Table 5 in the experimental section (procedures 4.4 and 4.5). The ethanolic solution of magnesium ethoxide was added to the ethanolic solution of gold nanoparticles and fluorinated according to the procedure 4.4. The same as before, Au:Mg ratio was fixed as 1:2, 1:5 and 1:10 respectively, the amount of applied HF was stoichiometric to the amount of magnesium. Procedure 4.5 based on employing the same reagents as procedure 4.4, however, in different sequence: HF solution was added to the ethanolic gold nanoparticles solutions before the addition of magnesium methoxide solution. Figure 6 shows TEM images of samples 4.1-4.3 and 5.1-5.3. The presence of core-shell nanoparticles was not observed. It can be speculated that applying magnesium precursors with very limited solubility results in increasing reaction speed because of huge excess of fluorinating agent and very limited amount of magnesium precursor. Therefore, magnesium ethoxide will not be further investigated.

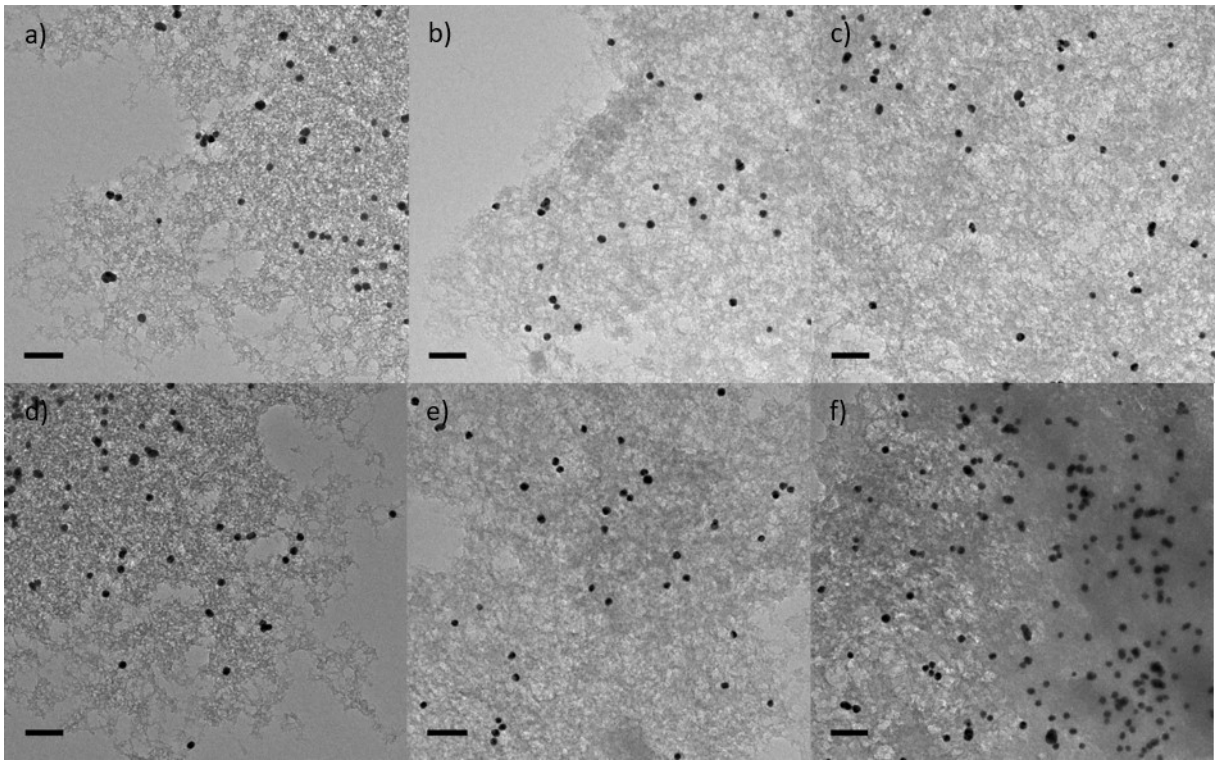

Figure 6:TEM images of samples 4.1-4.3 obtained by mixing ethanolic solution of gold nanoparticles with magnesium ethoxide solution and fluorinated afterwards (a-c) and samples 5.1-5.3 obtained by mixing ethanolic solution of gold nanoparticles with HF solution and magnesium methoxide afterwards (d-f). Gold to magnesium molar ratios are fixed as 1:2 for samples 4.1 and 5.1 (a, d), 1:5 for samples 4.2 and 5.2 (b, e) and 1:10 for samples 4.3 and 5.3 (c, f). Scale bar 100 nm.

Based on TEM investigations it was concluded that attempts based on formation of magnesium fluoride in the presence of citrate stabilized gold nanoparticles using different magnesium precursors (procedures 4.2-4.5) are not suitable for a Au@MgF_2 core-shell nanoparticles synthesis. For all performed synthesis routes core-shell nanoparticles were not observed on TEM images. Although figure 4c-d may suggest presence of very thin, irregular layer around some gold nanoparticles, the same phenomenon was observed for the reference sample (figure 4c), were core-shell formation was not expected. Presence of this thin, nonhomogeneous and non-complete shell is considered to be a measurement artefact, organic layer (e. g. sodium citrate from gold nanoparticles solution) or an effect of overlapping of gold nanoparticles and magnesium fluoride film, rather than a magnesium fluoride shell. Difficulties in TEM investigations of metal@metal fluorides and metal fluorides@metal fluorides core-shell nanoparticles will be further discussed in the end of this chapter.

3.1.4 Dropwise synthesis of Au@MgF_2 and their characterization

Many difficulties on the way of a successful gold-magnesium fluoride core-shell nanoparticles synthesis have been considered; therefore, different synthetically approaches were investigated. Procedures 4.6 and 4.7 were developed to address a lack of interaction or too weak interactions between gold nanoparticles and magnesium precursors or HF respectively and too fast magnesium fluoride formation. In both procedures (4.6 and 4.7) a reaction vessel was placed in the ice bath and reagents were added dropwise in order to slow down magnesium fluoride formation. A close distance between gold nanoparticles and magnesium precursors (procedure 4.6) and gold nanoparticles and HF

(procedure 4.7) was provided by preparation high concentrated solutions of regents corresponding to the Table 6 and Table 7 respectively.

According to the procedure 4.6, required amounts (Table 6) of 50 mM ethanolic magnesium precursors solutions (magnesium acetate and magnesium chloride) added to 400 µL of aqueous stock solution of gold nanoparticles (M=2.5 mM) (solution A, Table 6).The gold to magnesium ratio was fixed as 1:2 and 1:5. Applying a higher ratio (1:10) in such high concentrated solution leads to strong aggregation of gold nanoparticles and their sedimentation, therefore, only lower ratios (1:2 and 1:5) were further investigated. Under gentle magnetic stirring, very diluted ethanolic solution of HF (solution B, Table 6) was added dropwise (40 droplets per 1 min) to the mixture of gold nanoparticles and magnesium precursors (solution A, Table 6) placed in the ice bath. The aim was to decrease the distance between gold nanoparticles and magnesium precursors and to slow down magnesium fluoride formation, in order to increase the probability of shell formation, by additions of small amounts of diluted HF to highly concentrated mixture of gold nanoparticles and magnesium precursor. Figure 7 shows that magnesium fluoride was formed in the close neighborhood of gold nanoparticles as expected, however, core-shell nanoparticles were not formed. As expected for both magnesium precursors for the higher Au:Mg ratio (1:5) showed a very strong aggregation of old nanoparticles(figure 8 c, d, g, h). For the lower Au:Mg ratio (1:2) both aggregated and not aggregated gold nanoparticles can be found on the TEM images (figure 8 a, b, e, f). Especially interesting is figure 8b where gold nanoparticles seem to be incorporated in magnesium fluoride network.

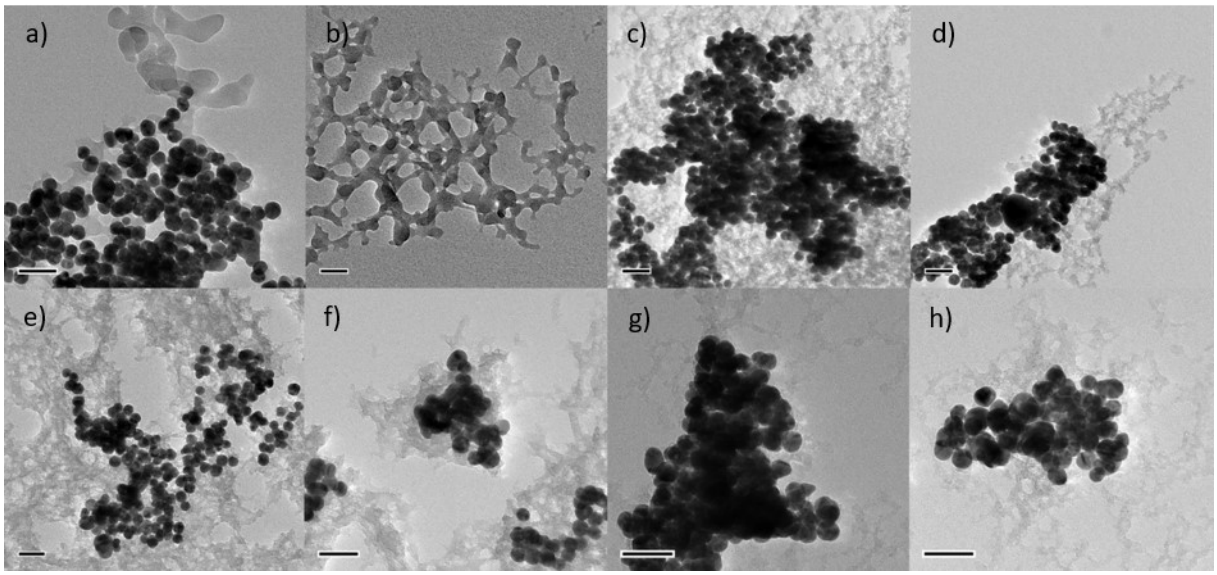

Figure 7: TEM images of samples 6.1-6.4 obtained by dropwise addition of diluted ethanolic HF solution to the mixture of high concentrated aqueous solution of gold nanoparticles and ethanolic solution of magnesium acetate (a-d) or magnesium chloride (e-h). Au:Mg ratio 1:2 samples 6.1 (a-b) and 6.3 (e-f), 1:5 for samples 6.2 (c-d) and 6.4 (g-h). Scale bar 50 nm.

In order to prevent aggregation of gold nanoparticles procedure 4.6 was modified. According to procedure 4.7 concentrated water-ethanolic solutions of gold nanoparticles and HF (H_2O:EtOH V/V= 1:1.45) were dripped to the diluted ethanolic solution of magnesium acetate and magnesium chloride respectively (details in procedure 4.7 and Table 7). Figure 8 presents non aggregated gold nanoparticles embedded in a magnesium fluoride matrix. Unluckily to the previous experiment, magnesium fluoride distribution is not correlated with the distribution of gold nanoparticles. The formation of a magnesium fluoride network with trapped gold nanoparticles inside was not noticed.

Although, for the low Au:Mg ratio magnesium fluoride (1:2) a network structure was formed (samples 7.1 and 7.3, figure 8 a, c), gold nanoparticles seemed to be not incorporated into it. It can be concluded, that procedure 4.7 is more effective than procedure 4.8, even though aggregation of gold nanoparticles was observed. Fabrication of gold nanoparticles incorporated in a magnesium fluoride network is a progress in comparison with the previous results; however, it is not the desirable core-shell structure, therefore other approaches will be investigated.

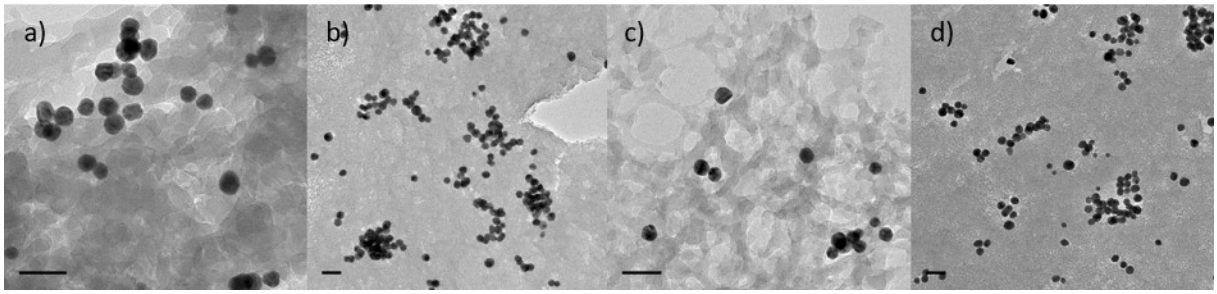

Figure 8: TEM images of samples 7.1-7.4 obtained by dropwise addition of mixture of high concentrated aqueous-ethanolic solution of gold nanoparticles and HF to diluted ethanolic solution of magnesium acetate (a-b) or magnesium chloride (c-d). Au:Mg ratio 1:2 for samples 7.1 (a) and 7.3 (c), 1:5 for samples 7.2 (b) and 7.4 (d). Scale bar 50 nm.

3.1.5 Synthesis and characterization of Au@MgF_2 synthesized in ethylene glycol using magnesium acetate and magnesium chloride as a magnesium precursors

Recently a very promising method to obtain core-shell metal fluorides nanoparticles via fluorolytic sol-gel synthesis was developed in our group by B. Ritter, P. Haida, T. Krahl, G. Scholz and E. Kemnitz.[164] Unlikely to previously described experiments this approach requires ethylene glycol as a solvent. Ritter et al. successfully obtained core–shell structures of the compositions SrF_2@CaF_2/SrF_2/CaF_2 (core@shell/shell/shell) and CaF_2@SrF_2/CaF_2/SrF_2 doped with a chosen rare earth metals. The formation of core-shell nanoparticles was demonstrated by TEM, DLS, NMR and photoluminescence experiments (photoluminescence measurements were possible due to addition of Tb^{3+} and Eu^{3+}). TEM images presented by Ritter et al. do not clearly show differences between core and shell material, however, increasing the size of the particles was observed. TEM observations were in good agreement with DLS measurements, where an increasing the size of particles after shell synthesis was observed. Moreover, NMR and photoluminescence data confirmed formation of core-shell nanoparticles. A huge advantage of Ritter's approach is no need of centrifugation, filtration, thermal treatment or other further reprocessing after the synthesis. [164]

Based on the procedure described by Ritter et al.,[164] the attempt of synthesizing gold-magnesium fluoride core-shell nanoparticles in ethylene glycol was adapted (procedure 4.8). Prior the synthesis 50 mM solutions of magnesium acetate and magnesium chloride in ethylene glycol were prepared. Stock solution of gold nanoparticles was diluted with ethylene glycol. Required amounts of magnesium acetate and magnesium chloride were added to the gold nanoparticles solution according procedure 4.8 (Table 8). In the last step a stoichiometric amount of methanolic solution of HF was added to each sample. As usual, the Au:Mg ratio was fixed as 1:2, 1:5 and 1:10. TEM investigations (figure 9) were in this case hindered by ethylene glycol covering the TEM grid. Due to the high boiling temperature of ethylene glycol TEM grids were dried for two days. But still the ethylene glycol layer present on the surface of the grid hindered focusing on the obtained nanoparticles (figure 9 g-h). This phenomenon is specially inconvenient in the case of light materials of low contrast to the carbon like metal fluorides.

After long investigations representative, ethylene glycol-free areas of each sample were found (figure 9a-f). The formation of core-shell nanoparticles was not observed. Unlikely to core-shell nanoparticles synthesized by Ritter et al., [164] potentially formed gold-magnesium fluoride core-shell nanoparticles cannot be investigated by using the same methods. The presence of gold nanoparticles in the system excludes NMR measurements, excess of magnesium fluoride excludes DLS, introducing luminescent cations for photoluminescence measurements would make this unknown system even more complicated, thus data interpretation would be extremely difficult and not reliable.

According to nonpublished data obtained by Ritter et al. their approach is suitable for many different metal fluorides core-shell nanoparticles except magnesium fluoride. The reason why magnesium fluoride is not suitable for core-shell nanoparticles formation is, so far, unknown. According to Karg's investigation it can be speculated that formation of new particles of magnesium fluoride is preferable over growth of existing particles and shell formation.[163]

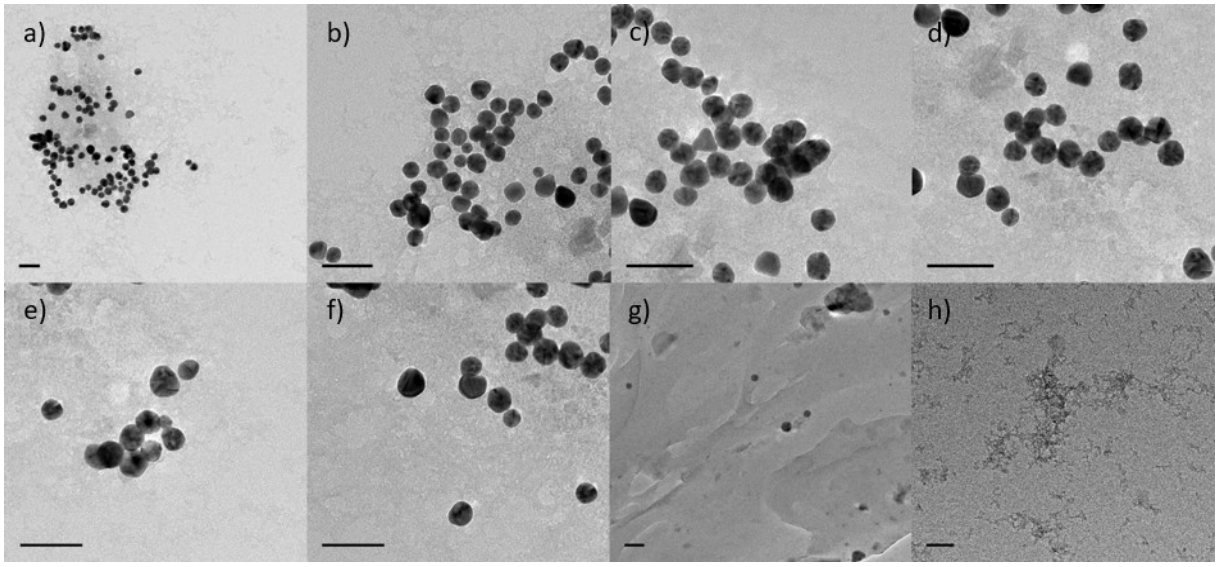

Figure 9: TEM images of samples 8.1-8.6 synthesized prepared in ethylene glycol by mixing gold nanoparticles solution with magnesium acetate (a-c) and magnesium chloride (d-f) and fluorinated afterwards. Au: Mg ratio 1:2 for samples 8.1 and 8.4 (a, d), 1:5 for samples 8.2 and 8.4 (b, e) and 1:10 for samples 8.3 and 8.6 (c, e). Ethylene glycol film covering samples and disturbing TEM measurements (g-h). Scale bar 50 nm.

3.1.6 Exchange of gold nanoparticles stabilizing agent

Many research performed over last years in our group on magnesium fluoride as a potential shell material show that this material is very difficult and, so far, nobody succeeded in core-shell (core@MgF_2) nanoparticles formation. Combination of citrate stabilized gold nanoparticles and magnesium fluoride is extremely challenging, not only due to magnesium fluoride itself, but also citrate stabilized gold nanoparticles. Described before, sodium citrate reduction of tetrachloroauric acid has many advantages, in particular for plasmonic applications. However, from the gold-metal oxides core-shell synthesis is known, that using sodium stabilized gold nanoparticles as the core material can possibly result in difficulties with shell formation.[34] Due to the lack of data about metal-metal fluorides systems it was decided to base on the knowledge gained from metal@metal oxides systems.

In respect of the two last described experiments, two approaches can be considered: using another metal fluoride instead of magnesium fluoride or surface modification of gold nanoparticles. Because

applying magnesium fluoride is the main focus of this work, therefore, surface modifications of citrate stabilized gold nanoparticles were investigated firstly.

Problems related to applying sodium stabilized gold nanoparticles as the core material were discussed by Liz-Marzan et al.[34] in their work "Synthesis of gold-silica core-shell particles". Gold nanoparticles do not form passivating oxide film on the surface, unlike to most other metals, what results in a lower affinity to commonly applied as a shell metal oxides (in this case silica). Additionally the presence of organic anions on the gold surface makes the surface vitreophobic, thereby a silica coating is not successful. In order to facilitate core-shell formation sodium citrate was exchanged for another ligand with high affinity to silica: 3-aminopropyltrimethoxysilane. Graf et al. proposed a post synthetic exchange of sodium citrate for polyvinylpyrrolidone (PVP).[157] PVP was successfully applied, not only for silica coated gold nanoparticles, but also silver nanoparticles, boehmite rods, gibbsite platelets, and positively or negatively charged polystyrene. Gold nanoparticles stabilizing agents with a high affinity to metal fluorides are unknown; therefore, the chosen stabilizing agents with high affinity to metal oxides will be investigated.

In order to avoid exchanging the gold nanoparticles stabilizing agents, they can be synthesized directly in the presence of these chosen stabilizing agent. An additional step is not necessary. However this approach usually does not provide such a good control of size and shape of the obtained nanoparticles as sodium citrate reduction does. Size and shape of gold nanoparticles in a plasmonic sensor have a significant impact for its properties and for sensing. [165, 166]Because sodium citrate can be easily exchanged for other ligands,[167] the synthesis of gold nanoparticles by sodium citrate reduction was chosen, followed by a post synthetic exchange of it. Among different known stabilizers (sulphur ligands (mostly thiols), phosphines, phosphine oxides, amides, carboxylate ligands)[156] polyvinylpyrrolidone (PVP) and 16-mercaptohexadecanoic acid (16-MHDA) were chosen. PVP was successfully employed in synthesis of many core-shell nanoparticles like: Ag@Fe_2O_3, Ag@TiO2, Au@SiO_2. [168-171] 16-MHDA is a molecule terminated with a thiol group with high affinity to gold surface and carboxyl group which can interact with magnesium fluoride. [158]

3.1.7 Synthesis of Au@MgF_2 using PVP-stabilized gold nanoparticles and their characterization

Due to the presence of nonpolar methylene and methane groups in the ring and the backbone and a highly polar amid group (in the pyrrolidone ring), PVP is a nonionic, amphiphilic polymer soluble in water, as well as in nonaqueous solvents, which can interact with many different surfaces.[157] Moreover, PVP stabilized gold nanoparticles are more stable in ethanol than citrate stabilized particles, thus they can be highly concentrated.[171] Average molar mass of PVP is an important factor for the shell formation process. It was reported that for the particles in the size of 7 nm in diameter, PVP with the molar mass M=10kg/mol is suitable. It prevents aggregation during the silica shell formation and allows the formation of a smooth and homogenous shell.[157] Gold nanoparticles used in all experiments before and described in this chapter have the dimension of 18 nm in diameter; therefore, PVP with higher average molar mass (40kg/mol) was employed. Gold nanoparticles in the size of 18 nm in diameter were synthesized by sodium citrate reduction of tetrachloroauric acid (procedure 4.1). According to the procedure 4.9 the aqueous solution of gold nanoparticles was diluted with water until a required volume (procedure 4.9), aqueous solution of PVP was then added and magnetically stirred for 36 h in order to ensure binding of PVP molecules on the gold surface.[157, 170] The ratio of gold nanoparticles to PVP was fixed as 1:10.[170] After 36 h of magnetic stirring, the mixture was centrifuged to remove the

excess of PVP. Remaining PVP-stabilized gold nanoparticles were redispersed in ethanol and used for further experiments. According to the procedure 4.9 magnesium acetate and magnesium chloride were dissolved in ethanolic solutions and added to the ethanolic solution of PVP-stabilized gold nanoparticles. The mixtures were prepared in the usual ratio of gold to magnesium 1:2, 1:5 and 1:10 and fluorinated afterwards (for detailed samples composition see Table 9 in the experimental section). In the next experiment described by procedure 4.10 the sequence of adding reagents was modified: ethanolic solution of HF was added to the ethanolic solution of PVP-stabilized gold nanoparticles solution in the first step, magnesium precursors (acetate and chloride) were added afterwards. The ratio of gold to magnesium was fixed as 1:2, 1:5 and 1:10. The amount of HF was stoichiometric to the amount of magnesium. Figures 10 and 11 show TEM images of samples 9.1-9.6, synthesized according to the procedure 4.9 and samples 10.1-10.6, synthesized according to the procedure 4.10. For any of the obtained samples the formation of core-shell nanoparticles was not determined. It indicates that PVP, a powerful stabilizing agent for metal-metal oxides core-shell nanoparticles is not suitable for a magnesium fluoride coating. Since metal fluorides and metal oxides differ significantly, it was taken into consideration that stabilizing agents working for oxides may not work for fluorides.

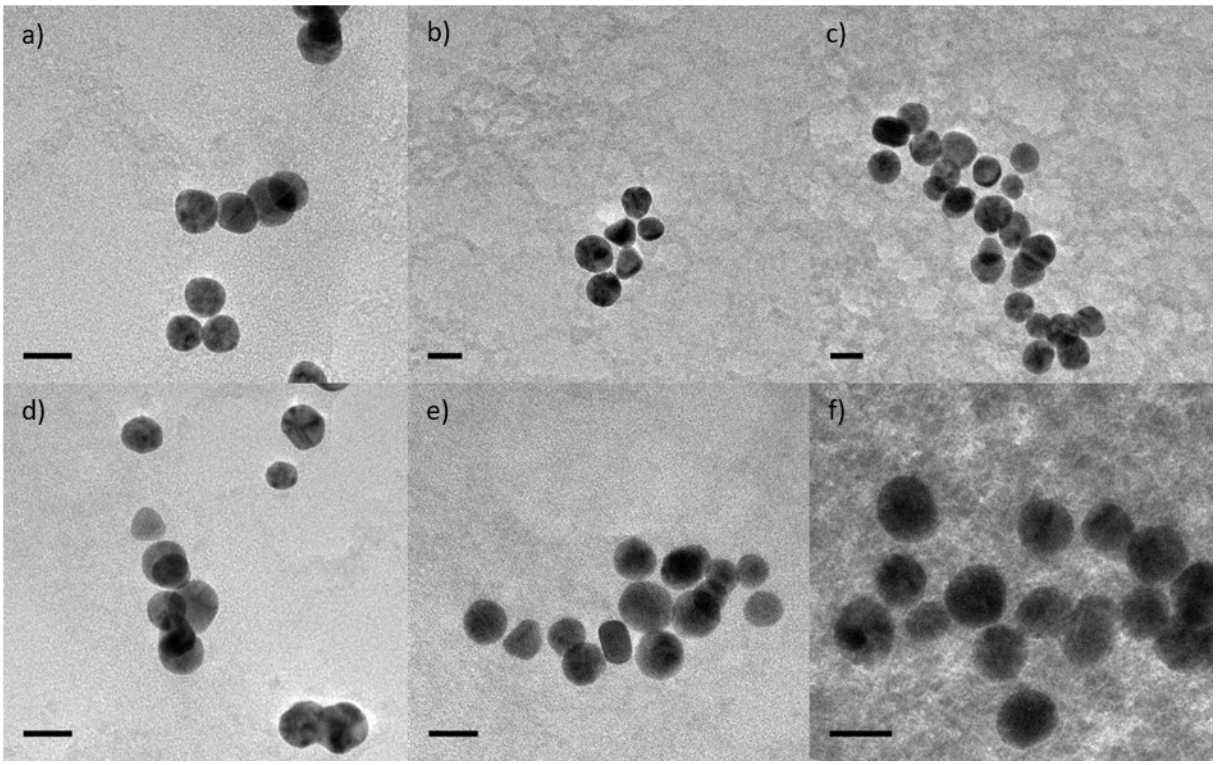

Figure 10: TEM images of samples 9.1-9.6 prepared by addition of magnesium acetate (a-c) and magnesium chloride (d-f) to ethanolic solution of PVP stabilized gold nanoparticles solution and fluorinated. The gold to magnesium fluoride ratio 1:2 for samples 9.1 and 9.4 (a, d), 1:5 for samples 9.2 and 9.5 (b, e) and 1:10 for samples 9.3 and 9.6 (c, f). Scale bar 20 nm.

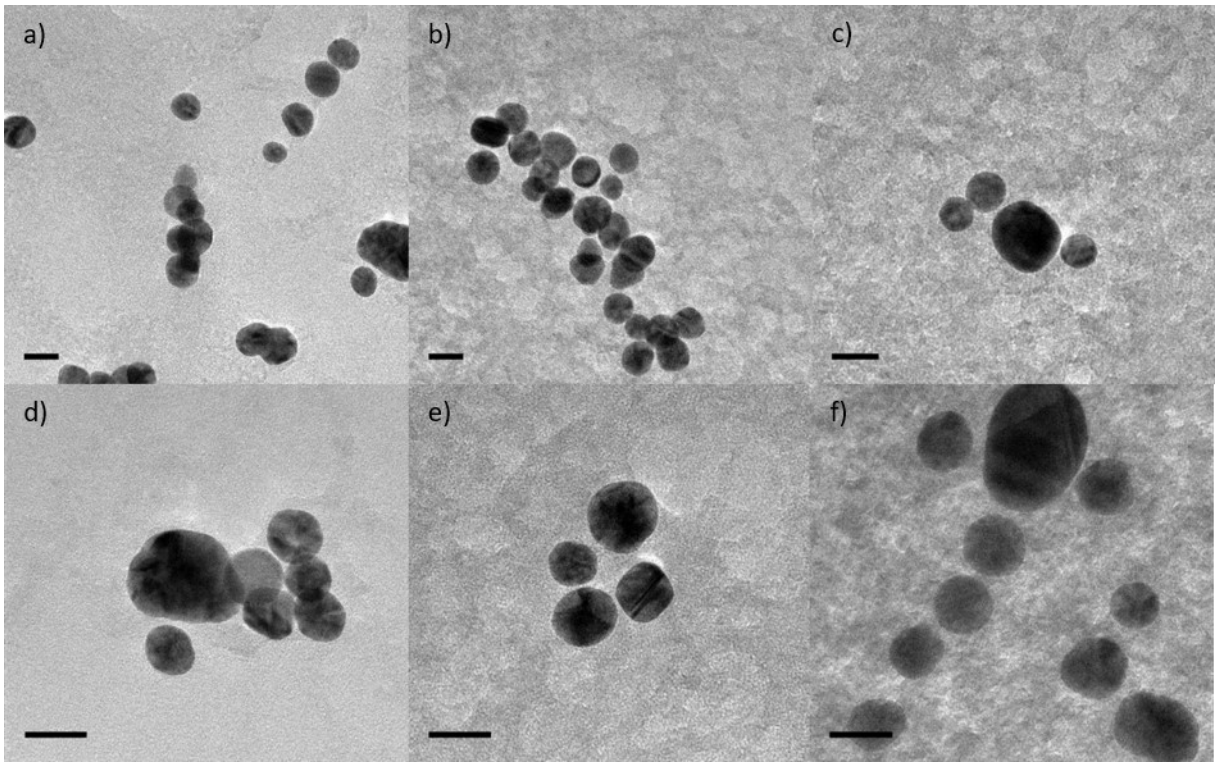

Figure 11: TEM images of samples 10.1-10.6 prepared by addition of magnesium acetate (a-c) and magnesium chloride (d-f) to ethanolic solution of PVP stabilized gold nanoparticles solution and fluorinated. The gold to magnesium fluoride ratio 1:2 for samples 10.1 and 10.4 (a, d), 1:5 for samples 20.1 and 10.4 (b, e) and 1:10 for samples 10.3 and 10.6 (c, f). Scale bar 20 nm.

3.1.8 Synthesis of Au@MgF_2 using 16-MHDA-stabilized gold nanoparticles and their characterization

An approach described by procedure 4.11 was inspired by the publication: "Tailoring the surface potential of gold nanoparticles with self-assembled monolayers with mixed functional groups" written by Lin, Yu, Lin, Lee, Kuo, Shyue.[158] They reported a successful synthesis of gold nanoparticles (reduction of tetrachloroauric acid with sodium borohydride) in the presence of two thiol-terminated ligands: 16-mercaptohexadecanoic acid and 8-amino-1-octanethiol. Changing the ratio of these two ligands (ratio of amino and carboxylic groups) allows to control the surface charge of particles. Such self-assembled monolayers are mostly used in order to immobilize and transport different molecules (including proteins and DNA) based on electrostatic interactions. Thanks to the possibility to control the surface charge of the nanoparticles, the self-assembled system described by Lin et al. [158] is interesting for the preparation of gold-magnesium fluoride core-shell nanoparticles. Thickness and morphology of the magnesium fluoride shell can possibly be tailored by changing the surface charge of gold nanoparticles. Lin et al. show that applying only 16-mercaptohexadecanoic during the gold nanoparticles synthesis would lead to fabrication of nanoparticles with a low zeta potential value (around -40 mV at neutral pH). [158] The zeta potential of magnesium fluoride is exactly the opposite (around +40 mV at neutral pH),[159] therefore electrostatic interactions between 16-MHDA-stabilized gold nanoparticles and magnesium fluoride are expected.

Gold nanoparticles synthesized by Lin et al. by reduction of $HAuCl_4$ with $NaBH_4$ in presence of 16-mercaptohexadecanoic acid and 8-amino-1-octanethiol are in the size 2-10 nm and characterized by high size distribution (2-10 nm) due to repulsion forces between negatively charged carboxylic acid

covered gold seeds and the presence of $AuCl_4^-$ precursors preventing the growth of particles. [158] As mentioned before, such particles are not suitable for a homogeneous plasmonic substrates fabrication, therefore gold nanoparticles obtained via citrate reduction were subjected to the post synthetic ligand exchange according to the procedure 4.11 based on ref. [157]

In order to facilitate a further separation of core-shell nanoparticles in excess of magnesium fluoride based on the sedimentation phenomenon, gold nanoparticles in the size of 30, 55 and 80 nm in diameter were used in this experiment. Such big particles were synthesized according to procedure 4.1 by multiply repeating addition of tetrachloroauric acid and sodium citrate and diluting the solution after three addition cycles (procedure 4.1.2). Right after the synthesis gold nanoparticles were diluted with ethanol and mixed with an ethanolic solution of 16-MHDA. The solution was magnetically stirred for 30 min in order to exchange the stabilizing agent. The ratio of gold to 16-MHDA was fixed with 3:1.[158] The samples were centrifuged, decanted and dispersed in ethanol in order to remove organic impurities from the system. Then magnesium fluoride was formed in the presence of 16-MHDA stabilized gold nanoparticles according to the procedure 4.11. The molar ratio of gold to magnesium fluoride for all sizes was fixed as 1:5. After the synthesis all samples were shaken and placed into long and narrow glass tube quipped with a tap of the bottom and left there for 10 min. Afterwards the tap was opened and ten fractions (1 ml each fraction) were collected dropwise into glass viols. Figure 12 shows a SEM image and EDX based elemental maps of fraction 1 of sample 11.5. For the synthesis of this sample magnesium acetate was used as magnesium precursor. On figure 12a gold nanoparticles appear as black spheres surrounded by a grey area corresponding to magnesium fluoride. This image suggests that magnesium fluoride is located mostly in the close neighborhood of gold nanoparticles, what indicates a successful purification. Images 12 b-d represent maps of distribution of respectively gold (figure 12 b), magnesium (figure 12 c) and fluorine (figure 12 d). The maps of distribution of each element show that magnesium fluoride is located mostly, but not only, around gold nanoparticles. A less significant amount of magnesium fluoride is uniformly distributed all over the measured area. Unfortunately the presented images and maps are not sufficient to state, weather core-shell nanoparticles were formed or not. As already mentioned reliable repeatable methods of imaging of low contrast, light materials with low refractive index are still not available.

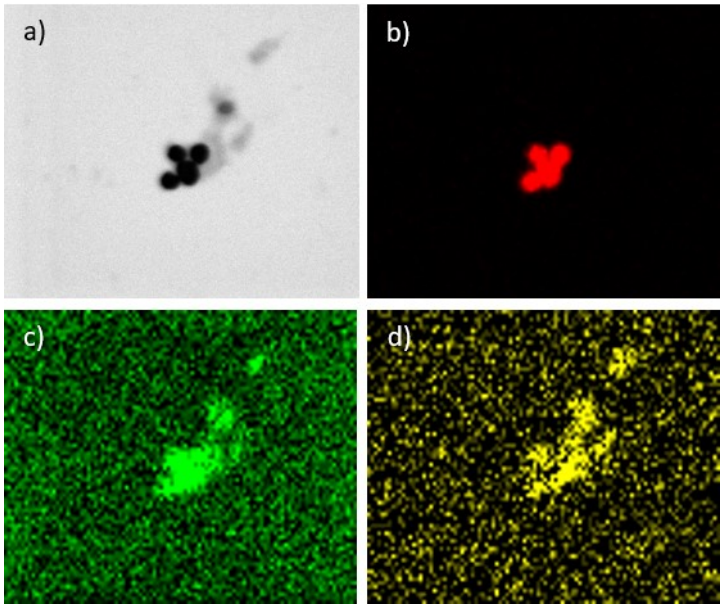

Figure 12: SEM image of the chosen for EDX investigation area of sample 11.5 (a); EDX maps of distribution of gold (b), fluorine (c) and magnesium (d).

Continuing the search for a prove of formation of core-shell nanoparticles another area of the sample containing a single gold nanoparticle was found and again examined by EDX. Instead of mapping the distribution of elements point measurements and scan lines were taken. Point measurements were performed in order to choose a single gold nanoparticles not surrounded by magnesium fluoride. Areas of points measurements appear on the figure 13 a as grey spots in the close neighborhood of single gold nanoparticles. Because the measurements had only auxiliary character, spectra are not shown. Based on them, a single gold nanoparticle marked on the figure 13 with a red line was chosen for scan lines measurements. The scan measurement was taken from the left to the right side as the yellow spearhead shows. The graph of intensities of gold, magnesium and fluorine from the distance is shown in figure 13 b. The increase in intensity of gold, magnesium and fluorine correspond to the single gold nanoparticle visible in figure 13 a. Zero intensity on the left and on the right side of the gold nanoparticle indicates that this nanoparticle is located on the magnesium fluoride-free area of the grid. It is in good agreement with preliminary point EDX measurements. A slight increasing in intensity of magnesium and fluorine signals corresponding to the gold nanoparticle surface, indicates that thin layers of magnesium fluoride are present of the gold surface. From EDX scan lines presented in figure 13 b it cannot be concluded weather the presented gold nanoparticle is really a core-shell nanoparticle. Although, many attempts of purification were undertaken, some excess of magnesium fluoride was still present in the measured samples. Also some gold nanoparticles were aggregated; therefore it was not possible to use another methods like XPS and DLS. The presence of gold nanoparticles exclude also the possibility of NMR measurements. Finding a single gold nanoparticle suitable for EDX scan lines measurements was very challenging and time consuming (particles were mostly aggregated and/or surrounded by magnesium fluoride matrix).

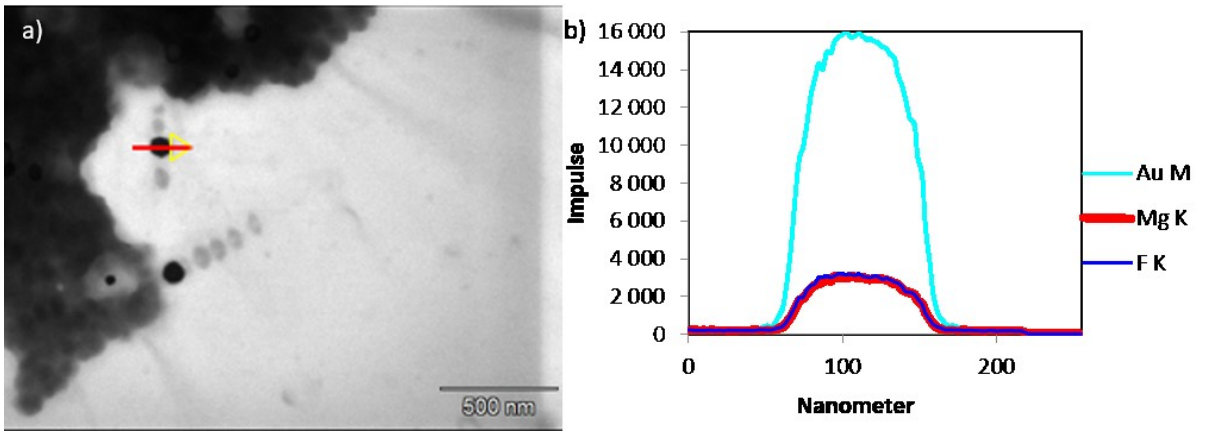

Figure 13: SEM image of the separated gold nanoparticles from the sample 11.5 chosen for further EDX exanimations (a); EDX scan lines of chosen separated gold nanoparticle (b).

3.1.9 Attempts to synthesize magnesium citrate stabilized gold nanoparticles for Au@MgF_2 synthesis

Conventional methods known for the synthesis of metal@metal oxides core-shell nanoparticles are not suitable for metal@metal fluorides core-shell nanoparticles fabrication due to significant differences between metal oxides and metal fluorides. Therefore, an unconventional approach based on using magnesium containing stabilizing agent for gold nanoparticles synthesis will be examined. Looking for already known ones from the literature working as stabilizing agent for gold nanoparticles synthesis was not successful. Therefore, sodium citrate in the procedure 4.1 was replaced by a equivalent amount of magnesium citrate. The synthesis was performed according to the procedure 4.1. Magnesium citrate was dissolved in MQ water and heated until the boiling point under magnetic stirring. Afterwards tetrachloroauric acid was added to the solution under intensive magnetic stirring and kept in the same conditions for 15 min. Within this time the solution became black. During cooling down the solution to 90 °C a black cloggy sediment was formed. The solution became transparent and no nanoparticles were found in it (UV-Vis measurements, not shown in this work). Due to the presence of a different cation, magnesium fluoride does not exhibit stabilizing properties unlikely to the magnesium citrate.

3.1.10 Synthesis of Au@SrF_2 and Au@ZrF_2 core-shell nanoparticles and their characterization

As mentioned above, problems with the core-shell formation can be connected to the citrate stabilized gold nanoparticles, as well as to magnesium fluoride properties. Ritter et al. successfully synthesized core-shell nanoparticles containing several metal fluorides[164] besides magnesium fluoride; therefore, attempts to synthesize Au@SrF_2 and Au@ZrF_2 were taken. Applying SrF_2 and ZrF_2 should be beneficial for TEM investigations, because of their, higher than MgF_2, molar masses (higher contrast on the TEM images is expected).

Both strontium and zirconium fluoride were synthesized in the presence of citrate stabilized gold nanoparticles. Strontium fluoride was synthesized from two different precursors: strontium acetate and strontium chloride (procedure 4.13). Both strontium precursors have limited solubility in ethanol and required special treatment. Strontium acetate was dissolved in mixture of denatured ethanol and TFA in order to clear up the sol and magnetically stirred for 30 min. Strontium chloride was dissolved in mixture of ethanol and acetic acid in the volume ratio 3:1.[172] Obtained solutions were transparent

and clear. Zirconium acetate is soluble in methanol; therefore, fabrication of $Au@ZrF_2$ nanoparticles was performed in methanol (procedure 4.13). [173]

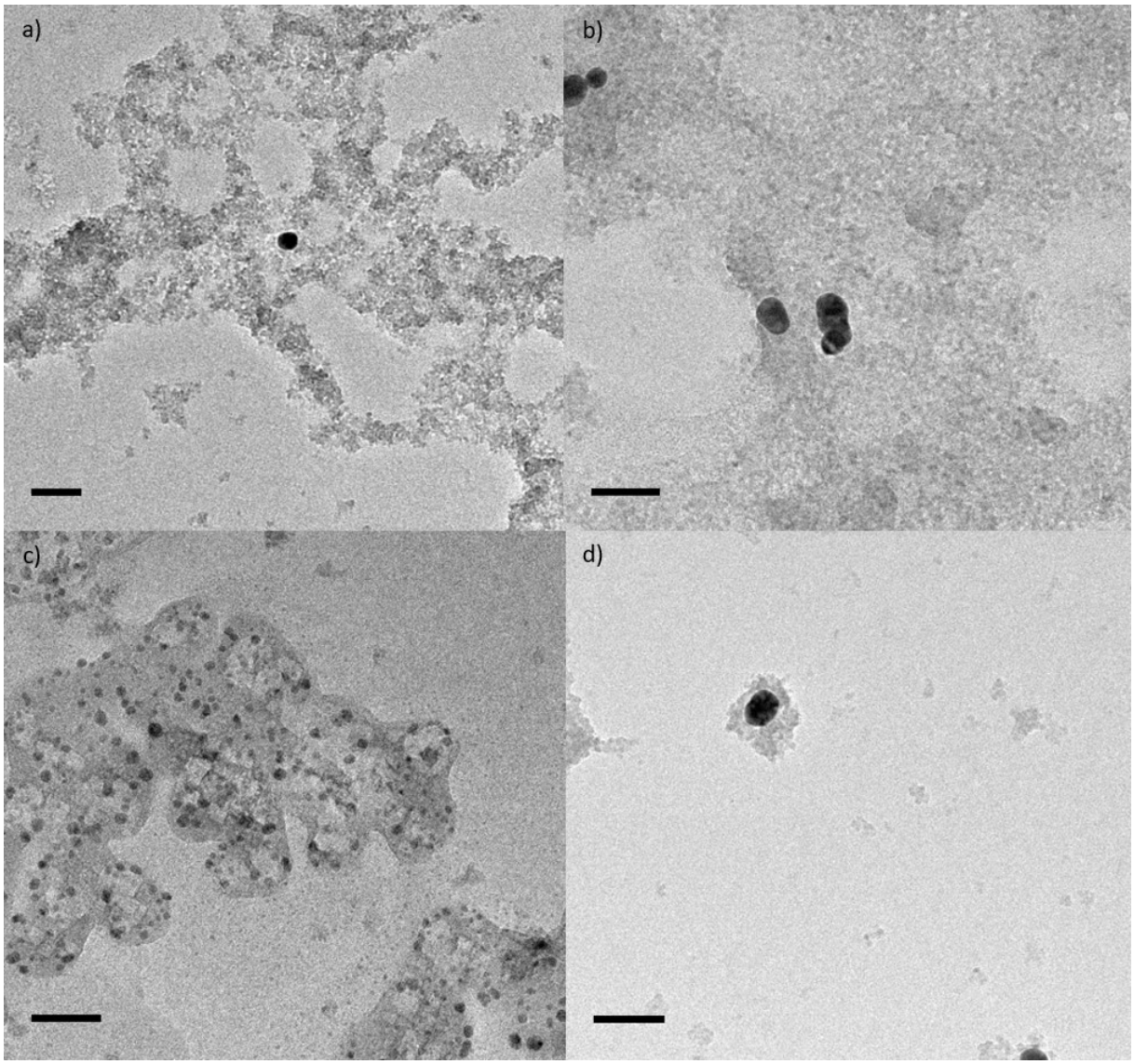

Figure 14: TEM images samples 12.1-21.2 prepared by addition of strontium acetate solution to gold nanoparticles ethanolic solution and fluorinated afterwards (a, b) and strontium chloride solution to gold nanoparticles ethanolic solution and fluorinated afterwards (c, d). The gold to strontium fluoride ratio was fixed as 1:5 for all samples. Scale bar 50 nm.

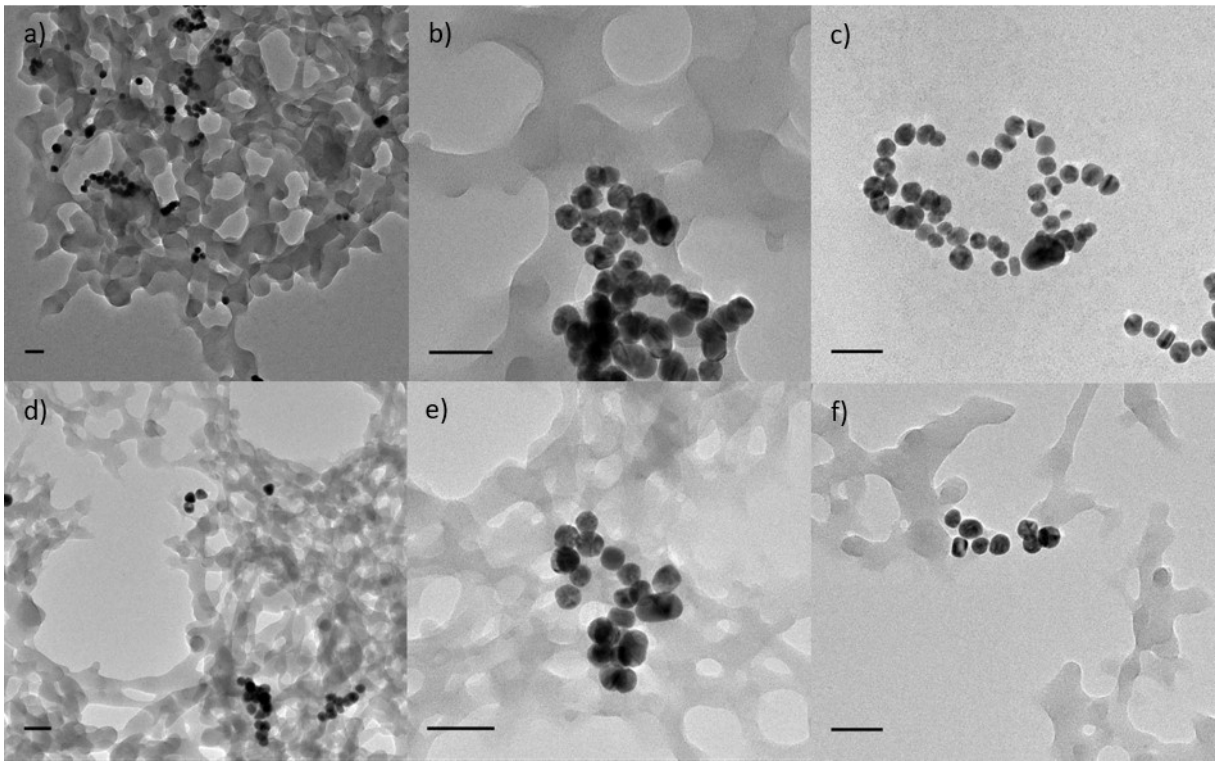

Figure 15: TEM images of samples 12.1 and 12.3 prepared by addition of zirconium acetate solution to the gold nanoparticles solution and fluorinated afterwards. The gold to zirconium fluoride ratio 1:2 for sample 12.1 (a-c) and 1:10 for sample 12.3 (d-e). Scale bar 50 nm.

As expected, figures 14 and 15 show that both strontium fluoride and zirconium fluoride exhibit a higher contrast, to the carbon coated TEM grids, than magnesium fluoride. Thus TEM investigations of the formed structures are significantly easier. Figures 14 a and b indicates that core-shell nanoparticles were not formed; gold nanoparticles are randomly distributed in strontium fluoride matrix. Figure 14c also show random distribution of gold nanoparticles in strontium fluoride matrix; however, at this sample a few core-shell looking particles were found (figure 14 d). Regarding to the previous TEM investigations described in this work, figure 14 d indicates rather location of the gold nanoparticles on the surface strontium fluoride, than core-shell nanoparticles formation. In contrast to the strontium fluoride, zirconium fluoride forms network structures. Some gold nanoparticles are embedded into this network (figures 15 a, b, d, e) and some are not (figures 15 c, f). A correlation between location of gold nanoparticles (inside or outside the zirconium fluoride matrix) and the zirconium fluoride concentration was not observed. Structures indicating a core-shell structure formation were not found. It indicates that sodium citrate stabilized gold nanoparticles are not suitable for core-shell nanoparticles synthesis containing metal fluorides shell. Experiments performed for magnesium fluoride suggest, that even exchanging the stabilizing agent for stabilizing agents known from a successful metal@metal oxides core-shell nanoparticles formation, does not allow core-shell nanoparticles formation in the case of metal fluorides.

3.1.11. Summary

Combination of the plasmonic properties of gold nanoparticles and the extraordinary optical properties of magnesium fluoride can be very beneficial for a desired plasmonic substrate. The approach of Au@MgF_2 core-shell nanoparticles synthesis, described in this chapter, turned out to be

extremely difficult. To the best of our knowledge, such structures has not been described is the literature. Therefore, undertaken attempts of Au@MgF_2 core-shell nanoparticles synthesis were based on the knowledge of metal@metal oxides and metal fluorides@metal fluorides doped with rare earth metals core-shell nanoparticles synthesis. Despite the use of different magnesium precursors, several gold nanoparticles stabilizing agents, different solvents and different reaction conditions, a suitable approach of Au@gF_2 was not developed. Moreover, nanoscopic characterization of obtained structures was very difficult due to the presence an excess of magnesium fluoride. The undertaken attempts to remove redundant magnesium fluoride were not successful. For such systems, obtaining a solid proof of core-shell nanoparticles formation using conventional analytical is very challenging. Excess of magnesium fluoride in the samples hinders TEM and EDX investigations of a separated gold nanoparticles (e. g. chapter 3.1.8). The excess of magnesium fluoride and in some cases aggregation of gold nanoparticles, exclude the possibility of DLS or XPS investigations. The presence of gold nanoparticles in the samples excludes NMR measurements. However, based on the obtained TEM and in some cases EDX data presented in this work, can be concluded that Au@MgF_2 nanoparticles were not formed. This is in line with conclusions made by Ritter et al. that magnesium fluoride does not form a shell even around metal fluoride cores.[164] Studies performed by Karg indicate that formation of new seeds of magnesium fluoride is preferable over increasing size of the existing MgF_2 nanoparticles or eventual shell formation.[163] The reason of a different than other metal fluorides behavior of magnesium fluoride can be only speculated. One potential reason can be its, different than other metal fluorides, crystalline structure of rutile. Another possible scenario is a lack of interactions between gold nanoparticles and metal fluorides (core-shell nanoparticles formation was also not observed for strontium fluoride and zirconium fluoride). Investigated in this work linkers (agents stabilizing the gold nanoparticles), suitable for metal oxides, turned out to be not suitable for metal fluorides.

Due to many difficulties during the synthesis and characterization of the core-shell nanoparticles, this approach is not considered as a suitable approach for coating of the plasmonic substrates with magnesium fluoride. Therefore, another approach, based on magnesium fluoride dip-coating of plasmonic nanoparticles immobilized on the glass substrate was proposed.

3.2. Porous magnesium fluoride-over-gold nanoparticles as plasmonic substrate for analytical applications

Parts of this chapter were published in: Porous MgF_2-over-gold nanoparticles (MON) as plasmonic substrate for analytical applications, D. Bartkowiak, V. Merk, V. Reiter-Scherer, U. Gernert, J. P. Rabe, J. Kneipp and E. Kemnitz, RSC Adv., 2016,6, 71557-71566

As concluded from the results discussed in the first part of this work, the synthesis of Au@MgF_2 core-shell nanoparticles is, so far, not well enough understood in order to successfully synthesize such materials according this route. However, since plasmonic sensors combining the plasmonic properties of the gold nanoparticles and the extraordinary optical properties of the magnesium fluoride are of high interest, another approach based on coating the gold nanoparticles immobilized on glass covered with magnesium fluoride was examined. The gold nanoparticles were firstly immobilized on the glass surface with 3-aminopropyltriethoxysilane (APTES) and then coated with magnesium fluoride via dip-coating. The immobilization of plasmonic nanoparticles on a solid substrate increases the stability of the plasmonic substrate and provides unusual optical properties caused by coupling of the plasmon resonances of the neighboring nanoparticles.[52, 56, 58-60] The obtained systems were characterized by SEM, AFM, UV-Vis and SERS. Numerous modifications of the preparation procedure and different experimental conditions applied in order to provide the best substrate homogeneity and SERS efficiency will be discussed in this chapter.

3.2.1 Fabrication of porous MgF_2-over-gold nanoparticles (MON)

Prior the plasmonic substrate preparation, gold nanoparticles in a desired size were synthesized according to procedure 4.1. For a research on MON fabrication gold nanoparticles in the size of 18nm were used. Synthesis and characterization of the gold nanoparticles were already discussed in the chapter 3.1.1. The magnesium fluoride sol was prepared according to the procedure 4.14 via fluorolytic sol-gel method.[174] Microscope glass slides in the size of 76 x 24 mm and a thickness of about 1 mm were used as a solid substrate for the MON fabrication. In order to immobilize gold nanoparticles on the glass surface 3-aminopropyltriethoxysilane (APTES) was used as a linker.[50] Figure 16 shows a schematic representation of the preparation of MgF_2-coated gold nanoparticle arrays. Prior to the fabrication of the plasmonic substrate, microscope glass slides were washed with piranha solution (mixture of sulfuric acid and 1 part of 30% hydrogen peroxide in the volume ratio 3:1) in order to remove impurities from the surface and to increase the amount of hydroxyl groups on the glass surface according to procedure 4.15.1 (figure 16a). Afterwards the glass slides were immersed in an aqueous APTES solution for 30 min, then washed with distilled water, dried (figure 16 b),immersed in the gold nanoparticles solution for 24 h and dried (figure 16 c) (details in procedure 4.15.1). Such plasmonic substrates are already known in the field of plasmonic sensing.[50] The procedure applied for their fabrication provides an uniform distribution of gold nanoparticles on the glass surface; however, the mechanical stability of such substrates is very poor. Gold nanoparticles are attached to the surface only by a weak, electrostatic interaction between the gold surface and amino groups of APTES molecules (figure 16 c). Therefore, in the next step, glass slides with immobilized gold nanoparticles on the surface were coated with a magnesium fluoride layer via the dip-coating method according to the procedure 4.15.2 (figure 16d). Magnesium fluoride films deposited on glass are known from their high mechanical stability.[126] Dip-coating parameters have a significant impact on the magnesium fluoride layer, therefore they will be discussed separately in the next chapter (chapter 3.2.2). The last step of fabrication of MON is a calcination process (figure 16d). The calcination is required in order to

remove organic impurities from the magnesium fluoride layer and to increase its mechanical stability (during the calcination process occurs a densification of the MgF_2 structure).

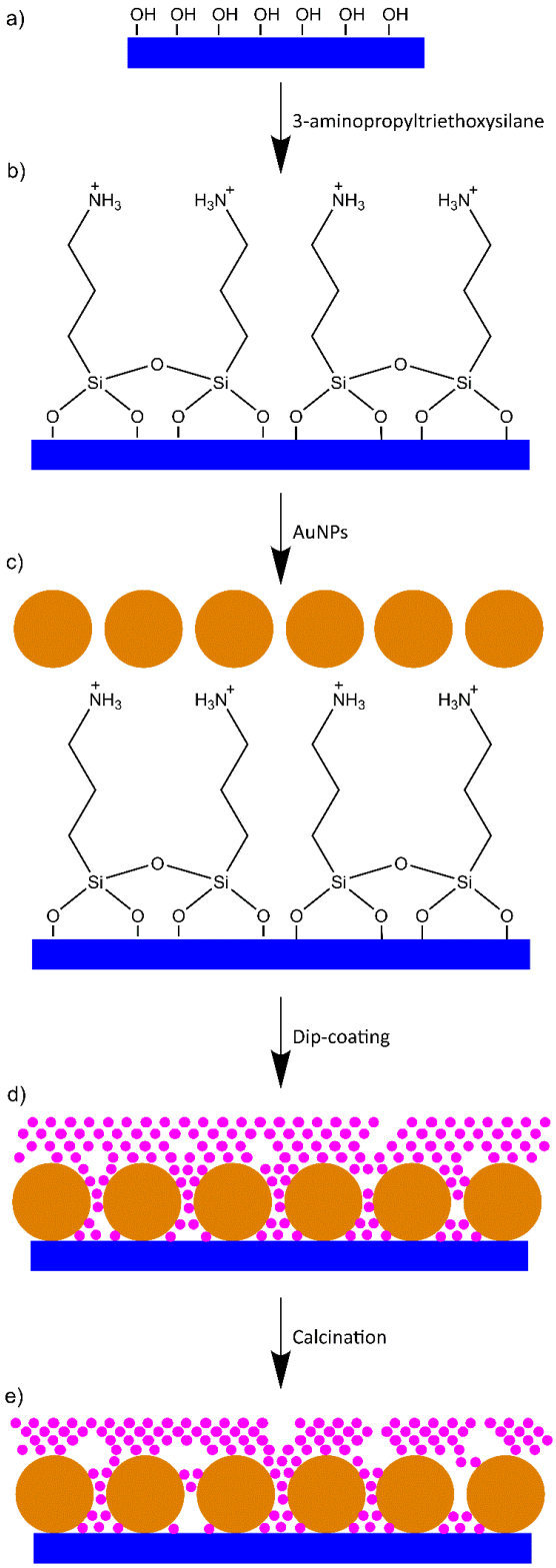

Figure 16: Schematic representation of MON preparation: glass slides washed with piranha solution (a); silanized glass slides (b); gold nanoparticles immobilized on the silanized glass surface (c); immobilized gold nanoparticles coated with magnesium fluoride (d); calcined substrate (f).

3.2.2 Adjusting parameters of dip-coating

The basics of the dip-coating process were already described in the chapter 1.3.2. From the Landau-Levich's equation follows, that the thickness of a thin layer deposited on a solid substrate depends on the viscosity of a coating solution, a constant linear speed of withdrawal of the substrate from the coating solution, the liquid-vapor surface tension and the density of the coating solution.[154] Practically, it means that the thickness of the magnesium fluoride layer on the glass substrate depends on the concentration of the magnesium fluoride sol and the speed of withdrawing the substrate from the sol. For the experiments of MON fabrication, magnesium fluoride in a concentration of 0.1 M was synthesized according to the procedure 4.14; the speed of withdrawing the glass substrate with immobilized gold nanoparticles on the surface was chosen to be 20 cm/min. In order to provide a reference sample for further measurements only half of the glass containing immobilized gold nanoparticles on the surface was coated with MgF_2. Before the windrowing process, the glass substrate with immobilized gold nanoparticles on the surface was immersed in the magnesium fluoride sol for 5 s. The outcome of the dip-coating process was assessed based on SEM measurements.

Plane view SEM images of the obtained MON are displayed in panel A of figure 17. Nonconductive materials, including glass, are not suitable substrates for electron microscopy investigations, therefore sputtering of the samples with conductive material (e. g. gold) is commonly applied. For SEM investigations of MON, sputtering can result in difficult interpretation of the images. Therefore, measurements were taken without sputtering, using a low acceleration voltage and a deceleration mode. As a result of measuring on the nonconductive substrate in some images (e. g. figure 17 panel A, left bottom image) black or white streaks/areas can be observed. They are caused by the charging of the surface. In order to minimalize charging effects the operating parameters were modified for each picture individually. Different blemishes (mostly cavities in the magnesium fluoride layer) were observed on the surface. Those artefacts were not only present close to the border between the coated and uncoated areas (figure 16, panel A, bottom images), but also in the central part of the coated area (figure 16, panel a, top images). Therefore, longer immersion times (30 s and 60 s) in magnesium fluoride sol were applied. Images presented on the figure 17 in panel B and C show, that the amount of blemishes is decreasing with an increasing of immersion time. A few blemishes were observed only close to the border between the coated and uncoated areas. It can be speculated, that due to a different roughness and adhesion comparing to the pure glass, glass slides coated with gold nanoparticles require a longer immersion time in order to form a homogenous layer of magnesium fluoride. Significant differences between the 30 s (figure 17, panel B) and 60 s immersion time (figure 17 panel B) were not observed. Therefore 30 s immersion time was fixed as the most suitable for further experiments.

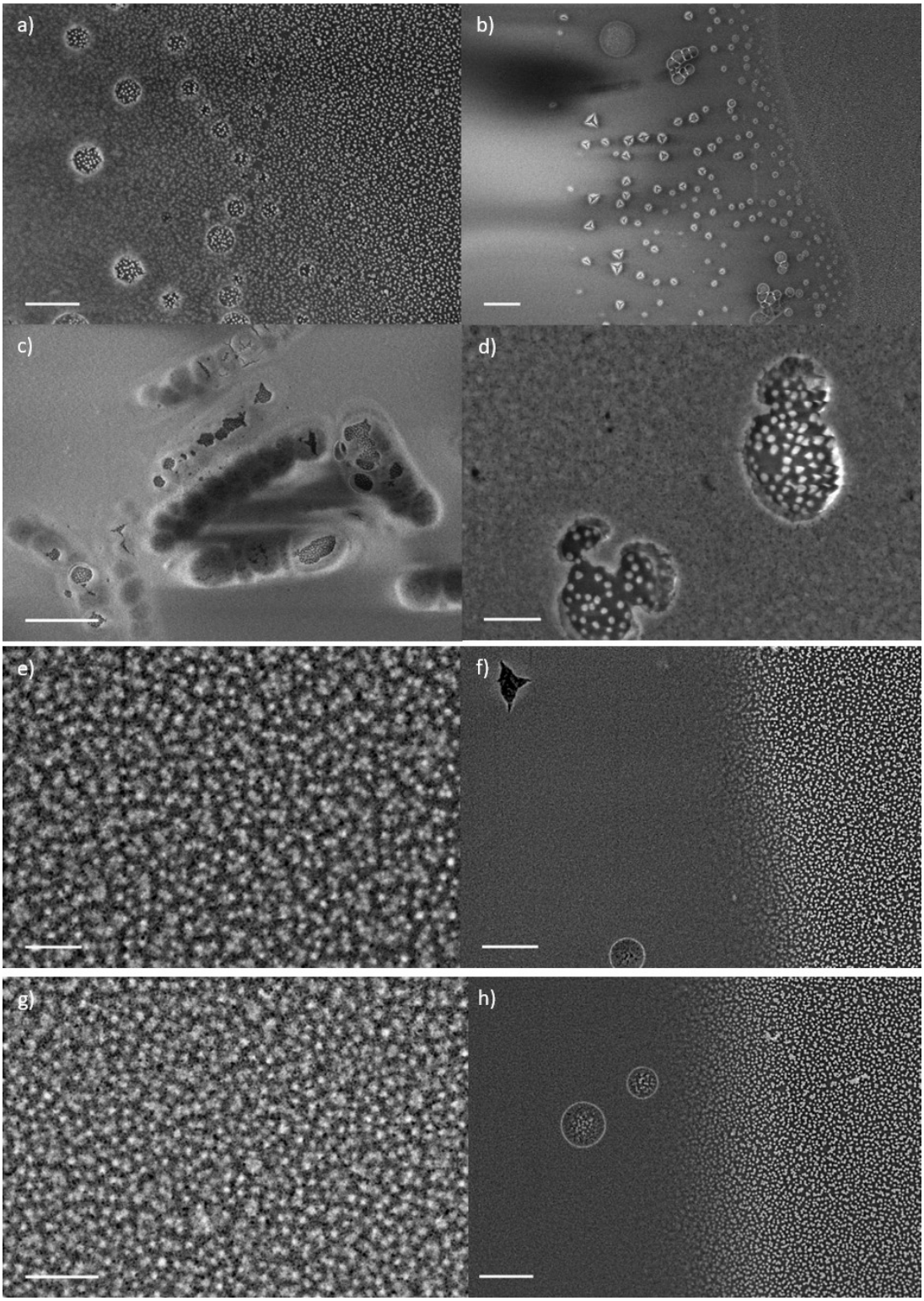

Figure 17: SEM images gold nanoparticles immobilized on the glass surface partly coated with magnesium fluoride; dip-coating parameters: withdrawing speed 20cm/min, concertation of MgF_2 sol 0.1 M, immersion time: a-d: 5 s; e-f: 30 ; g-h: 60 s. Scale bar: a, g, h: 500 nm; b: 2000 nm; c: 1000 nm; d, e, g: 200 nm.

Cross sectional SEM images (figure 18) indicate that the immersion time does not have an influence on the thickness of the magnesium fluoride layer. For all the applied immersion times (5 s, 30 s and 60 s) the thickness of the obtained magnesium fluoride layers was approximately 30 nm.

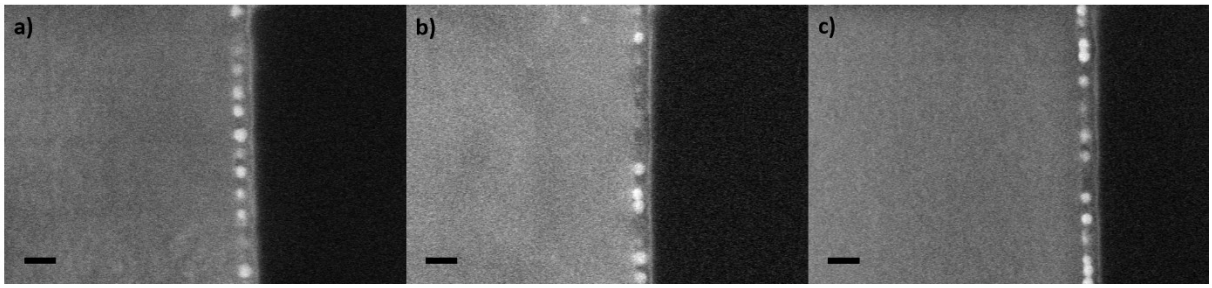

Figure 18: Cross section SEM images of gold nanoparticles immobilized of the glass coated with magnesium fluoride layer; dip-coating parameters: withdrawing speed 20 cm/min, concertation of MgF_2 sol: 0.1 M, immersion time: 5 s: panel A, 30 s panel and 60 s, panel C. Scale bar 50nm.

Dip-coating parameters chosen for the MON fabrication experiments (MgF_2 concentration 0.1 M, withdrawing speed 20 cm/min) and 30 s immersion time provide a homogeneous, 30 nm thick magnesium fluoride layer covering gold nanoparticles previously immobilized on the glass. Those parameters were fixed for fabrication MONs with different sized gold nanoparticles for further SERS experiments.

3.2.3 Assessing the influence of gold nanoparticles size and the presence of magnesium fluoride layer on morphology and plasmonic properties of the analytical substrate

The plasmonic properties of nanoparticles depend on their size, shape and refractive index of the surrounding material. For a research presented in this work it was decided to examine spherical gold nanoparticles synthesized according to the sodium citrate reduction (procedure 4.1).[110] In order to find conditions providing a maximum SERS efficiency, gold nanoparticles in the size of 26±3 nm, 36±4 nm and 47±5 nm were examined. For further applications gold nanoparticles in different shapes and sizes may be applied. Before the MON fabrication, freshly synthesized gold nanoparticles were characterized using transmission electron microscopy (TEM) and ultraviolet-visible spectroscopy (UV-Vis) in order to define their size, shape and aggregation state. Characterization of gold nanoparticles synthesized by sodium reduction method was already shown and discussed in the chapter 3.1.1 (figure 1, figure 2). Briefly: the obtained particles are spherical, monodisperse and characterized by a narrow size distribution. Such particles were immobilized on the glass slides according to the procedure 4.15.1. Afterwards, half of each glass slice with immobilized gold nanoparticles on the surface was coated with a magnesium fluoride layer according to the procedure 15.2. The dip-coating parameters adjusted in the previous chapter (0.1 mM MgF_2 sol and 20 cm/min withdrawing speed) were applied for preparation of all the samples. Figure 19 shows SEM images of the uncoated gold nanoparticles immobilized on the glass substrate (a, d) and the MgF_2-coated gold nanoparticles immobilized on the glass substrate (b-c, e-f) in the size of 26±3 nm (a-c) and 36±4 nm (d-f).

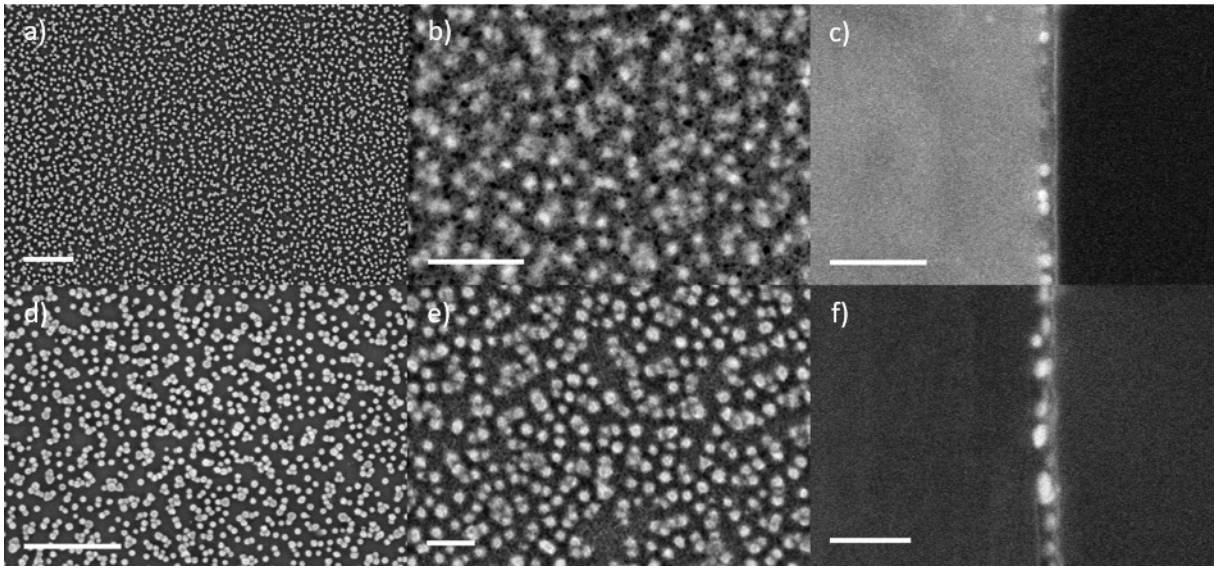

Figure 19: Scanning electron micrographs of 26 nm (a–c) and 36 nm (d–f) sized gold nanoparticles: (a and d) uncoated particles immobilized on glass, (b and e) immobilized particles coated with magnesium fluoride, (c and f) cross sectional image of immobilized and coated gold nanoparticles. Scale bar: a, d 500 nm; b-c, e-f 150 nm

Uncoated, immobilized gold nanoparticles appear as sharp and white spheres on the SEM images (figures 19 (a, d). MgF_2-coated immobilized gold nanoparticles can be still observed on SEM images; however, the picture does not have a high contrast due to the presence of MgF_2 layer. Cross sectional images (figures 19 c, f) were taken in order to estimate the thickness of the magnesium fluoride film. As it was already shown in figure 18 the thickness of MgF_2 layer approximates 30 nm. The same thickness was observed in the figures 19 c and f. Having that in mind there remains the question, if all gold nanoparticles are completely coated with the magnesium fluoride layer. The gold nanoparticles approximate a averaged size of 26 nm in diameter (figure 19 a-c) and 36 nm in diameter (figure 19 d-f), while the thickness of the magnesium fluoride layer was estimated to be around 30 nm in both cases. Figure 19 c clearly shows totally coated gold nanoparticles in the size of 26 nm by a magnesium fluoride layer. For the particles in the size of 36 nm in diameter it cannot be clearly stated from the SEM images. It seems, that the magnesium fluoride film is rougher and fully covers the gold nanoparticles, but it has to be proven by additional scanning force microscopy (SFM) measurements. Further SEM investigations on gold nanoparticles of the size of 47 nm in diameter, were not performed.

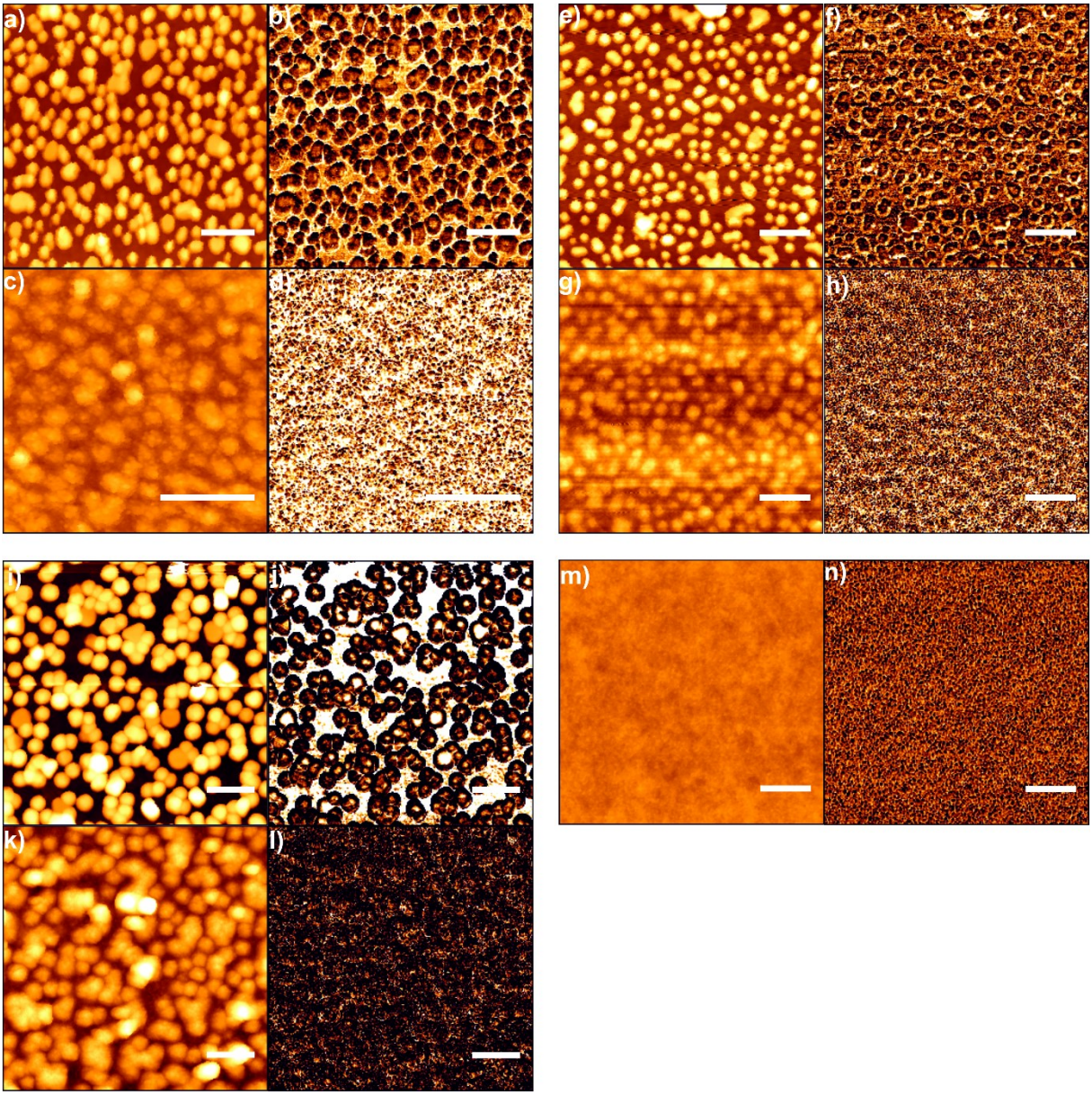

Figure 20: SFM images of the uncoated (a, b, e, f, i and j), MgF_2- coated (c, d, g, h, k and l) immobilized gold nanoparticles in the size of 26 nm (a–d), 36 nm (e–h), and 47 nm (i–l) and a control sample of silanized glass coated with magnesium fluoride (m and n). All panels in the left columns display the height images, all panels in the right columns show adhesion images. Scale bar 200 nm.

Figure 20 shows the SFM topography and adhesion images of uncoated and MgF_2-coated gold nanoparticles in the size of 26 nm, 36 nm and 47 nm in diameter immobilized on the glass substrate. The topography images were determined from measurements of force-distance curved measured for every point of the image by the extension of the piezo controlling the cantilever height when reaching a predefined setpoint. The adhesion refers to the pull-off force occurring when the cantilever is retracted from the sample.[175] The topography images are shown in the left column of each panel of figure 20; adhesion images are displayed in the right column. A silanized and coated with magnesium fluoride glass was investigated as a reference sample. The gold nanoparticles of all of three size classes appear on the topography images as bright spheres, while on the adhesion images as dark spheres. In agreement with the SEM images (figure 19), gold nanoparticles form a monolayer of single particles and small aggregates. It was observed that the amount of the aggregated particles increases by

increasing the size of the applied nanoparticles. Immobilized nanoparticles in size of 26 nm in diameter appear mostly as well dispersed particles; however only some small aggregates were observed (figure 19a, figure 20a). The gold nanoparticles with size of 36 nm in diameter show a tendency to form dimers, trimers and oligomers; however, single nanoparticles are also present (figure 19d, figure 20e). Gold nanoparticles in the size of 47 nm are therefore mostly aggregated; however, after a careful investigation, some single gold nanoparticles can be also found (figure 20i). Because gold nanoparticles used for immobilization were monodispersed in the solution (figure 1), it was concluded, that the aggregation process occurs during the immobilization of gold nanoparticles on glass surface.

Increasing the size of applied gold nanoparticles results not only in an increasing amount of aggregates on the surface, but also in dropping the number of immobilized particles. In the area of 1 μm^2 of the substrate 838 nanoparticles in the size of 26 nm, 345 nanoparticles in the size of 36 nm and 238 nanoparticles in the size of 47nm were found. Such diverse numbers of nanoparticles in different sizes correspond to similar surface areas of gold nanoparticles: $1.9x10^6$ nm^2/ 1 μm^2 of the substrate containing gold nanoparticles in the size of 26 nm, $1.4x10^6$ nm^2/ 1 μm^2 of the substrate containing gold nanoparticles in the size of 36 nm and $1.6x10^6$ nm^2/ 1 μm^2 of the substrate containing gold nanoparticles in the size of 47 nm in diameter (Table 2). The MgF_2-coated gold nanoparticles were not well distinctive on SEM, as well as on SFM images; therefore, it was assumed that the number of gold nanoparticles per 1 μm^2 is the same as the number of uncoated nanoparticles. Magnesium fluoride nanoparticles appear on the topography images as textured surface due to their small size in the range of a few nanometers. The topography of coated samples appears to be smother than compared to uncoated samples, therefore, height profiles corresponding to the figure 20e and 20g were performed (figure 21).

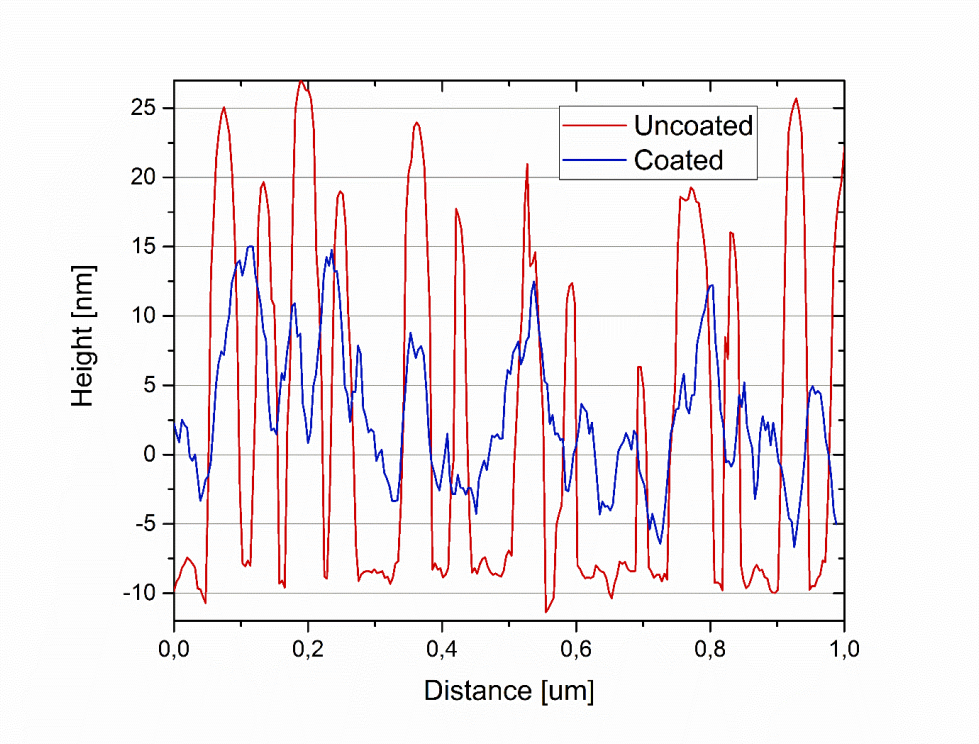

Figure 21: Height profiles of an MgF_2-coated (blue line) and an uncoated sample (red line) of gold nanoparticles with a nominal height of 36 nm.

The red line in the figure 21 shows a high profile of the uncoated immobilized gold nanoparticles in the size of 36nm, while the blue line corresponds to the coated gold nanoparticles in the same size. It is clearly shown that the coating by magnesium fluoride results in a reduction of height difference overall the surface.

The adhesion images (figure 20, right columns) show the maximum negative deflection of the cantilever due to adhesive forces between the tip and the sample, therefore different materials can be distinguish. Uncalibrated cantilevers were used for the adhesion measurement; therefore, images cannot be compared between each other's and only some general qualitative observations can be made. In all images of uncoated substrates (figure 20 a, b, e, f, i and j) gold nanoparticles and silanized glass can be clearly differentiated. Less adhesive spots (dark areas) correspond to gold nanoparticles, more adhesive, brighter areas correspond to silanized glass. Adhesion images of MgF_2- coated gold nanoparticles show uniform adhesion over the whole measured area. It indicates, that gold nanoparticles in all applied sizes (even 47nm in diameter) are completely coated with magnesium fluoride. Those data are in good agreement with the SEM images (figure 19). As expected based on the SEM cross sectional measurements, an increasing size of applied gold nanoparticles leads to an increased roughness of the surface. RMS roughness was calculated for each sample from the topography images (Table 2). Calculated RMS roughness approximates 9 nm for gold nanoparticles in the size of 26 nm in diameter, 11 nm for gold nanoparticles in the size of 36 nm in diameter and 18 nm for gold nanoparticles in the size of 47 nm in diameter. After coating of the applied gold nanoparticles with the magnesium fluoride, RSM roughness decreased to 3 nm for gold nanoparticles in the size of 26 nm in diameter, 4 nm for gold nanoparticles in the size of 36 nm in diameter and 10 nm for gold nanoparticles in the size of 47nm in diameter. It indicates that magnesium fluoride fills spaces and gaps around the gold nanoparticles like it was shown on the SEM cross section images (figure 20) and the SFM adhesion images (figure 21).

In order to characterize plasmonic properties of the obtained MONs containing gold nanoparticles in the size of 26 nm, 36 nm and 47 nm in diameter, UV-Vis and SERS measurements were performed. As mentioned in the introduction, optical and plasmonic properties are size dependent, therefore, three different sizes of gold nanoparticles were examined in order to provide a maximal SERS efficiency. Figure 22 shows changes of the localized surface plasmon resonance represented by the absorbance spectra of freshly synthesized gold nanoparticles, gold nanoparticles immobilized on the glass substrate and MgF_2-coated immobilized gold nanoparticles on the glass substrate. The spectra of freshly synthesized gold nanoparticles were broadly discussed in the chapter 3.1.1. Briefly: the sharp plasmon bands with a single absorbance maximum at 524 nm for gold nanoparticles in the size 26 nm in diameter, 527nm for gold nanoparticles in the size 46 nm in diameter and 531 nm for gold nanoparticles in the size 47 nm in diameter indicate high monodispersity of nanoparticles (black lines in figure 22). Spectra of the gold nanoparticles immobilized on the glass substrate (red spectra in the figure 22) are significantly different than spectra of particles in the solution (black spectra in figure 22). Additional bands at 611 nm and 686 nm for the gold nanoparticles in the size of 26 nm in diameter, 624 nm and 729 nm for the gold nanoparticles in the size of 36 nm in diameter and 627 nm and 742 nm for the gold nanoparticles in the size of 47 nm in diameter appear on the spectra. These bands are more intensive than bands at 524 nm, 527 nm and 531 nm respectively. It indicates the formation of different kinds of aggregates. This is in good agreement with SMF topography images, where distinct kinds of aggregates were also observed. The same phenomenon was reported by Joseph et al.[50]

After coating with magnesium fluoride additional bands are still present; however, their maxima are shifted to longer wavelengths (blue spectra in figure 22). This effect is especially pronounced for larger nanoparticles; the band is significantly wider than for small particles. As mentioned before, the large particles form more aggregates than small particles, therefore, it can be concluded that high absorbance values in the NIR range is connected to change pf properties of aggregated particles. This indicates that MgF_2-coated particles (especially in the size of 47 nm in diameter) form a larger variety of aggregates than uncoated particles. This cannot be shown in SEM or AFM images due to the layer of MgF_2 covering the gold nanoparticles. The MgF_2-coated gold nanoparticles in SEM images appear as blurred, unfocused irregular shapes; in SFM images as bigger, blurred and textured spheres, therefore in some cases it is not possible to distinguish adjacent particles and aggregated particles.

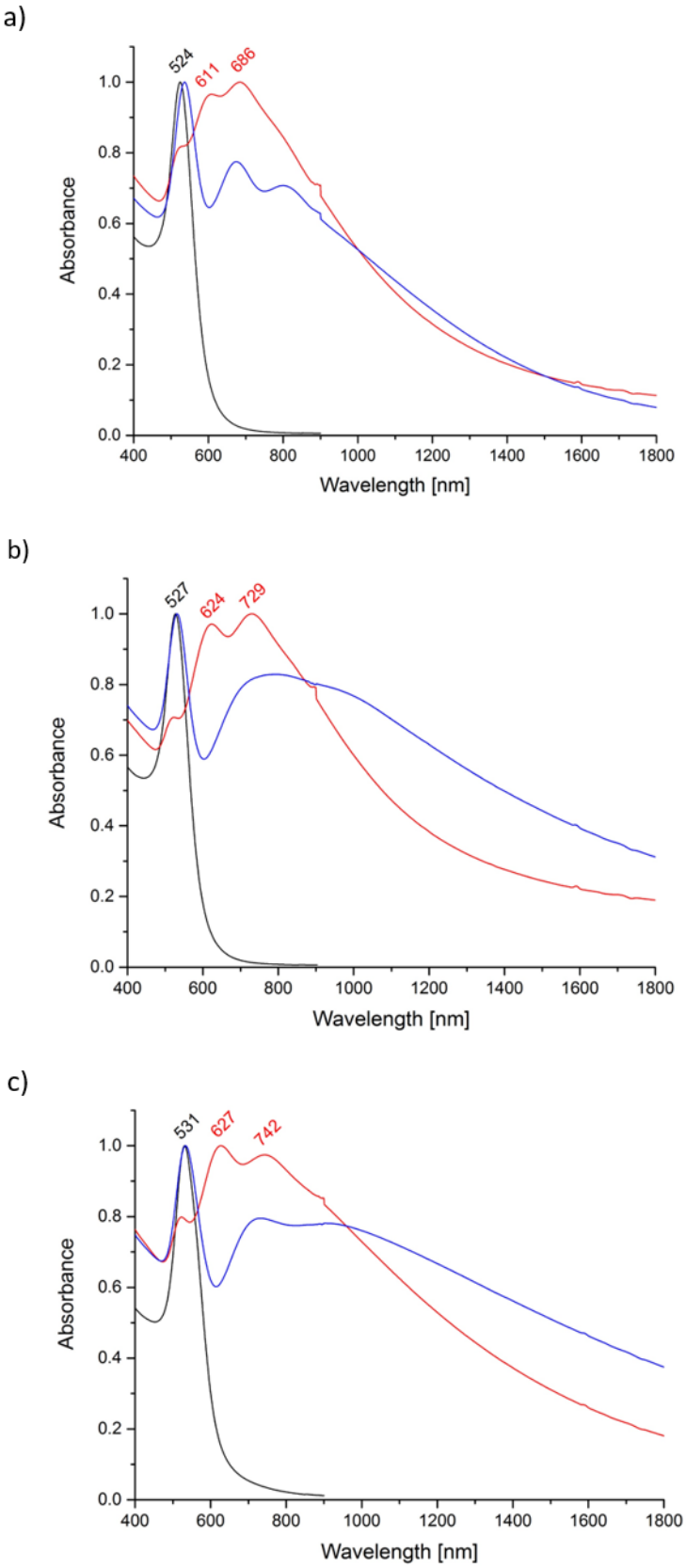

Figure 22: UV-Vis spectra of gold nanoparticles with size of (a) 26 nm, (b) 36 nm, and (c) 47 nm in solution (black lines), after immobilization on the glass surface (red lines) and after immobilization on the glass surface and coating with magnesium fluoride (blue lines).

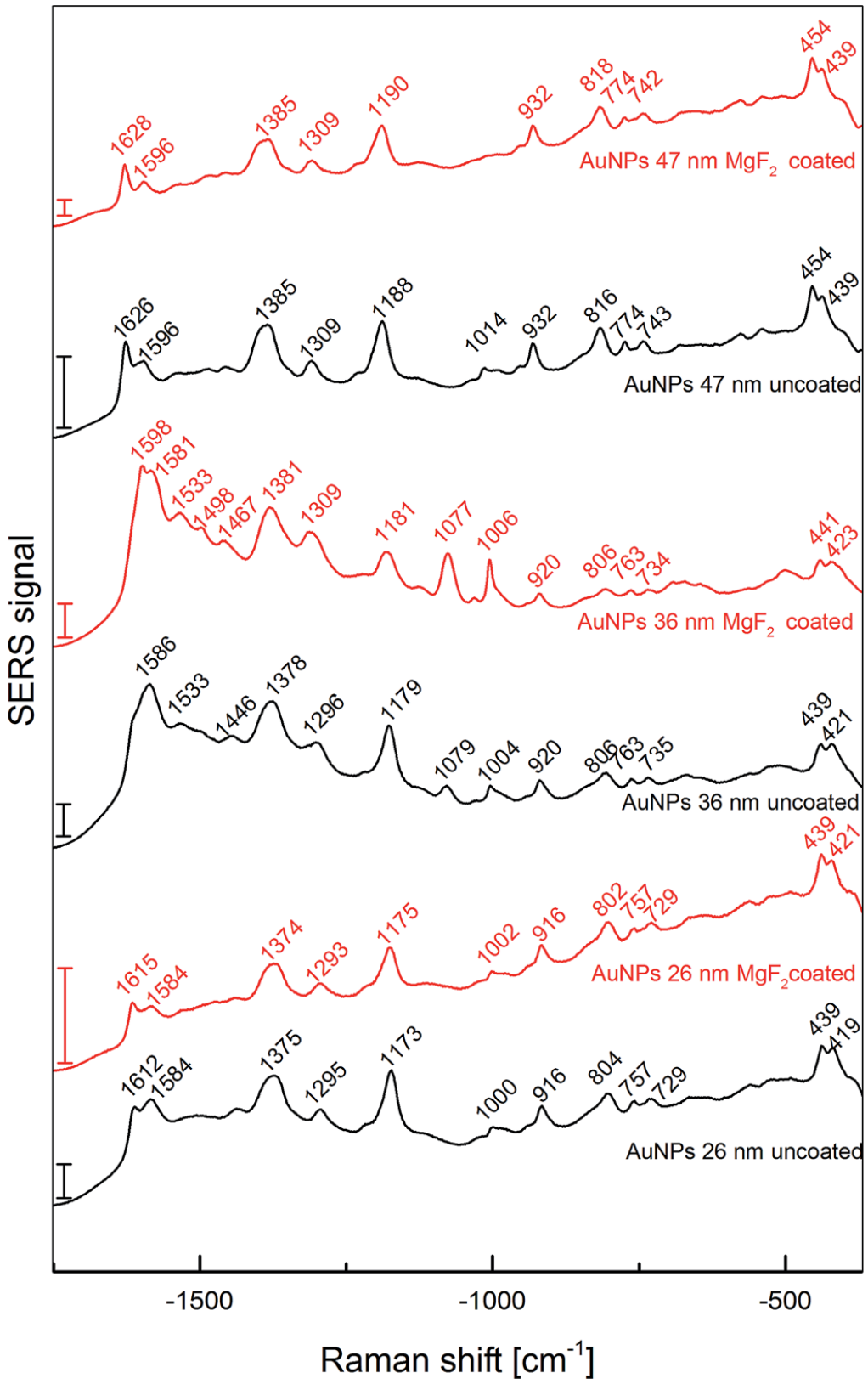

Figure 23: Surfaced enhanced Raman scattering (SERS) spectra of 1 x 10^{-6} M crystal violet solution on immobilized gold nanoparticles uncoated (black lines) and coated with magnesium fluoride (red lines) in the size of 26 nm, 36 nm, and 47 nm. Each spectrum is an average spectrum of 50–100 individual microspectra. Scale bar 2000 cps. Excitation wavelength: 633 nm, intensity: 1.2 x 10^{5} W cm^{-2}, accumulation time: 1 s.

In order to investigate the influence of magnesium fluoride on SERS properties, experiments on uncoated and MgF_2-coated subtracts were carried out using crystal violet (analyte molecule) at 633 nm excitation wavelength (figure 23). Black spectra in figure 23 correspond to the crystal violet spectra on uncoated gold nanoparticles in the size of 26 nm, 36 nm and 47 nm respectively. Red spectra (figure 23) correspond to crystal violet spectra on MgF_2-coated gold nanoparticles in the size of 26 nm, 36 nm and 47 nm. In order to provide a representative number of spectra, 50-100 spectra were measured in each of 2 to 4 different areas of each sample. Figure 23 shows the averaged spectra of all measured spectra. All presented spectra display signals characteristic for the crystal violet molecule. Tentative assignments are presented in Table 2. The crystal violet spectra measured on uncoated and coated gold nanoparticles of the same size were compared. Only some small changes were observed. Some bands in the spectrum of coated particles appear sharper and more pronounced than on the uncoated particles. This is especially pronounced for gold nanoparticles in the size of 36 nm in diameter where the ring breathing mode at 1006 cm^{-1}, or the band at 1598 cm^{-1}, assigned to a ring C–C stretching vibration band are significantly sharper and more pronounced for coated particles. This can be a result of slightly changed interactions between crystal violet and gold nanoparticles surface caused by the presence of magnesium fluoride. Taking the porosity of magnesium fluoride into account, analyte molecules are able to diffuse to the gold nanoparticles surface, however, the possibilities to access the gold surface can be different than for the uncoated gold nanoparticles. Therefore, some small changes were observed on the spectra. Differences observed for coated and uncoated gold nanoparticles in different sizes were much more pronounced than the differences described above. Although the number of gold nanoparticles immobilized on the glass substrate in each size differs significantly (Table 2), the surface area of gold nanoparticles is comparable for each size (details were discussed in the chapter 3.2.3).Therefore, it can be concluded that the qualitative differences of the spectra obtained by nanoparticles of different sizes are a result of different surface properties of gold nanoparticles on the respective substrates. It was already discussed in the chapter 3.2.3 that formation of different types of aggregates for different sizes of gold nanoparticles occurs during the immobilization process (figure 19 and figure 20). Therefore, it can be concluded that differences in the spectra are not connected to the concentration of crystal violet molecules, but to different interactions with gold nanoparticles and it is not caused by the magnesium fluoride coating.

In order to compare the SERS performance of the described substrates the enhancement factor was estimated. In order to do that, reference (pre-resonant) measurements were performed under identical conditions as SERS measurements (procedure 4.22).[176] Enhancement factors were estimated for each substrate according to the following equation:

$$E = \frac{I_{SERS}/N_{Surf}}{I_{RS}/N_{Vol}}$$

where I_{SERS} and I_{RS} are the intensities of the band at 1620 cm^{-1} in the spectra of the SERS and Raman experiment, respectively. N_{Vol} represents the number of molecules in the scattering volume of the reference Raman experiment and N_{Surf} the maximum number of molecules that would cover the gold surface in the scattering volume and hence would participate in the SERS enhancement. For the estimation of N_{Surf} the surface area taken by a crystal violet molecule on the gold surface was assumed as 4 nm^2.[177]

The values of the estimated enhancement factors for each substrate are presented in Table 2. The averaged enhancement factors values are varied from 1 x 10^4 for MgF_2-coated gold nanoparticles in

the size of 26 nm up to 7 x 10^5 for uncoated gold nanoparticles in the size of 47 nm in diameter. The enhancement factors estimated for MgF_2-coated gold nanoparticles in all sizes are only slightly lower than enhancement factors estimated for the uncoated substrates. Such a slight decrease of enhancement factors after coating with magnesium fluoride indicates, that porosity of magnesium fluoride provides almost free access of the analyte molecules to the gold surface.

Table 2: Nanoscopic properties of the samples containing uncoated and MgF_2-coated gold nanoparticles in the size of 26 nm, 36 nm and 47 nm in diameter and their enhancement factors in the SERS experiment

Sample	AuNPs 26 nm		Au NPs 36 nm		Au NPs 47 nm		MgF_2
	Uncoated	Coated	Uncoated	Coated	Uncoated	Coated	On glass
Number of AuNPs per surface area in mm^2	383	n. d.	345	n. d.	238	n. d.	-
AuNPs' surface in nm^2 per area in mm^2	1.9 x 10^6	n. d.	1.4 x 10^6	n. d.	1.6 x 10^6	n. d.	-
RMS roughness in nm	9	3	11	4	18	10	1.2
Average SERS enhancement	3.0 x 10^4	1.0 x 10^4	2.0 x 10^5	1.7 x 10^5	7.0 x 10^5	5.3 x 10^5	-
Maximum SERS enhancement	6.3 x 10^4	2.8 x 10^4	2.8 x 10^5	3.6 x 10^5	1.2 x 10^6	1.2 x 10^6	-

The highest maximum enhancement factor of 1.2 x 10^6 was reached for the largest gold nanoparticles; however, such high enhancement cannot be reached for the whole surface, therefore average enhancement is lower by one order of magnitude. It supports the conclusions based on SFM images, that the distribution of gold nanoparticles in the size of 47 nm is slightly uneven. The highest microscopic homogeneity was observed for the substrate containing gold nanoparticles in the size of 26 nm, however this substrate exhibits a low enhancement factor compared to the other substrates. For the substrate containing gold nanoparticles in the size of 36 nm in diameter, both, high homogeneity and high enhancement were achieved.

3D finite-difference time domain (FDTD) simulations were performed in order to obtain more information about the influence of the magnesium fluoride layer on the electric field distribution around the gold nanoparticles. An example geometry displayed in figure 24 was created based on SFM images of gold nanoparticles in the size of 26 nm in diameter immobilized on the glass substrate. Figures A and C show uncoated gold nanoparticles, while figures B and D show coated with a simulated,

30 nm thick layer of magnesium fluoride. For the simulation two wavelengths were used: 633 nm as in the performed SERS measurements (figures 24 A-B) and 1064 nm because of significant absorbance in the near infrared region (figures 24 C-D). In both cases it can be concluded that a coating with magnesium fluoride does not result in changes of the electric field intensity distribution. The electric field is enhanced by a factor of ~10^2. Assuming that the Raman scattered light is enhanced by the same factor, this would result in an enhancement factor of ~10^4 in the SERS experiment, which is in good agreement with experimental data (Table 2). Distribution of spots in high field enhancement differs for the 633 nm and 1064 nm excitation wavelength. Such nanoscopic differences are not relevant for the SERS measurements, because the usual spot sizes on such a substrate in a typical microscopic application will be best at an average of an area displayed in figure 24. SERS experiments at 1064 nm were not performed in this work, because further modifications of the substrate and its nanoscopic characterization were in in the main focus of this work.

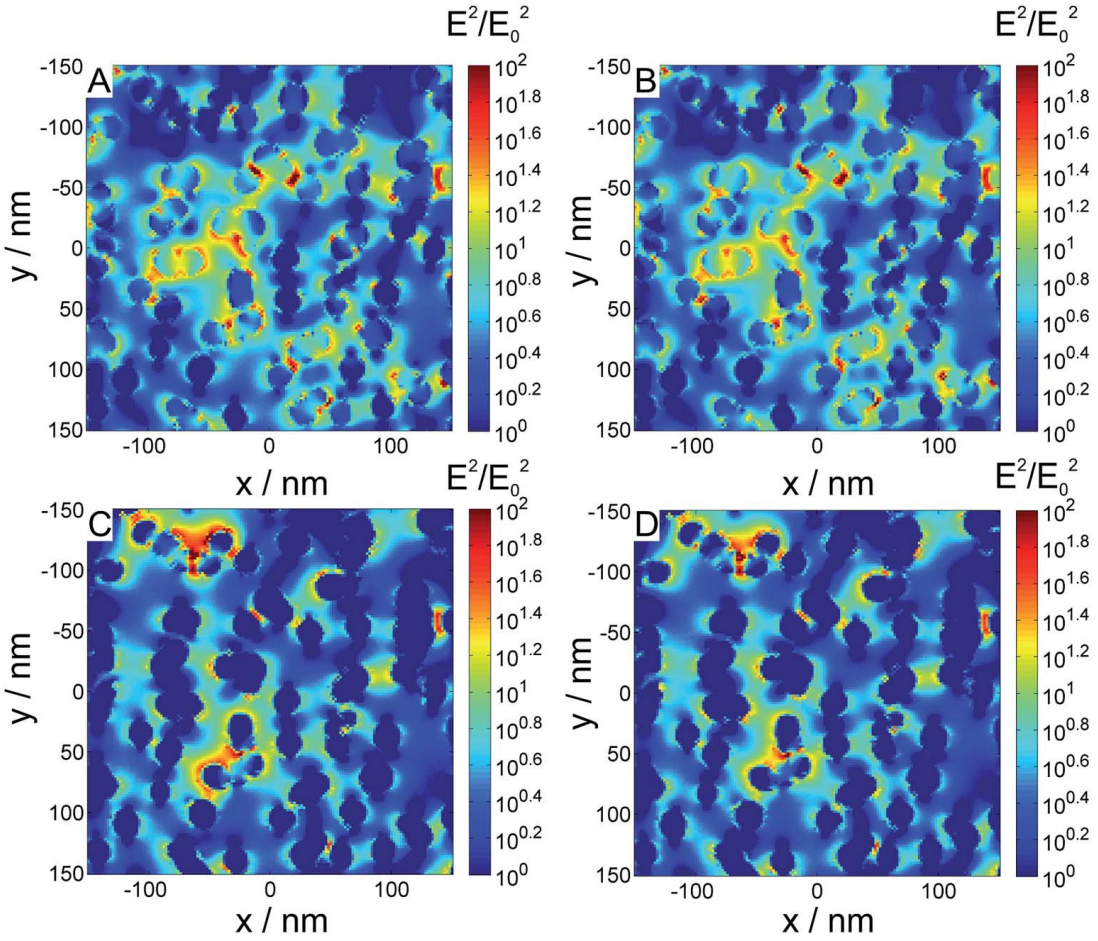

Figure 24: Simulated (3D-FDTD) electric field intensity distribution in the xy-plane. For one example of an experimentally observed surface with gold nanoparticles of 26 nm diameter, immobilized on a glass substrate without coating (A and C), and coated with a 30 nm thick magnesium fluoride layer (B and D). The field distribution is shown for an excitation wavelength of 633 nm (A and B) and of 1064 nm (C and D). The monitor was placed 13 nm above the glass substrate.

Table 3: Bands observed in the spectrum of crystal violet on immobilized gold nanoparticles 26 nm, 36 nm, and 47 nm in size and their tentative assignments based on ref.156, 157. Abbreviations: n, stretching (s, symmetric; as, asymmetric); d, bending; g, out-of-plane deformation (with respect to the benzene ring).

26 nm		**36 nm**		**47 nm**		**Tentative assignments**
Uncoated [cm^{-1}]	**Coated [cm^{-1}]**	**Uncoated [cm^{-1}]**	**Coated [cm^{-1}]**	**Uncoated [cm^{-1}]**	**Coated [cm^{-1}]**	
1612	1615	1611	1598	1626	1628	$\nu(C_{ring}C)$
1584	1584	1586	1581	1596	1596	$\nu(C_{ring}C)$
		1533	1533			$\nu(C_{ring}N)/\delta_s(CH_3)$
		1500	1498			$\delta_{as}(CH_3)$
1438		1446	1467			$\delta_{as}(CH_3)$
1375	1374	1378	1381	1385	1385	$\delta(CH)/\delta_s(CH_3)/\delta(CCC)_{ring}$
1295	1293	1296	1309	1309	1309	$\nu_{as}(CC_{center}C)/\delta(CCC)_{ring}/\delta($ CH)
1173	1175	1179	1181	1188	1190	$\nu_{as}(CC_{center}C)$
		1079	1077			$\delta(CC_{center}C)/\nu CN)$
1000	1002	1004	1006	1014		$\delta(CCC)$
916	916	920	920	932	932	$\delta(CC_{center}C)$
804	802	806	806	816	818	$^{\nu}(C_{ring}H)$
757	757	763	763	774	774	$\nu s(CC_{center}C)/\nu(CN)$
729	729	735	734	743	742	$\nu(CN)$
439	439	439	441	454	454	$\delta(CNC)$
419	421	421	423	439	439	$\delta(CNC)/\delta(CC_{center}C)$

The size of gold nanoparticles immobilized on the glass determines nanoscopic and plasmonic properties of the obtained MON. Depending on the size of applied gold nanoparticles a different number of single particles, dimers, trimers or small planar aggregates were formed, what results in slightly different plasmonic properties. For gold nanoparticles in all applied sizes complete coverage of gold nanoparticles was shown; magnesium fluoride was found in between the particles as well as on their surface. The magnesium fluoride layer has almost no influence on the enhancement nor on the qualitative properties of the spectra, that indicate a direct interaction of the analyte molecules with the gold surfaces.

3.2.4 Mechanical stability of MON

The SFM scratch experiments were performed in order to investigate the influence of the magnesium fluoride layer on the mechanical stability of gold nanoparticles immobilized on the glass (figure 25). In this purpose topography images in quantitative mode of uncoated and coated nanoparticles were taken, then a small area was scratched by using contact mode with the feedback controlling the SFM cantilever height reduced to a minimum. The applied force was fixed for each single measurement. Many measurements were performed on the MgF_2-coated samples and the force was gradually increased from 5 nN up to 100 nN. After each scratch, topography images in quantitative mode were taken in order to assess possible damages of the surface. Figure 25 shows uncoated gold nanoparticles before (figure 25 a) and after scratching with a force of 5 nN (figure 25 b). The scratching area is marked with a white frame. Uncoated gold nanoparticles immobilized on the glass surface using 3-aminopropyltriethoxysilane are attached to the glass surface only by weak electrostatic interactions; therefore, an applied force of 5 nN was sufficient to remove uncoated gold nanoparticles from the surface and push them to the rim of the scratched area (figure 25 b). In contrast to the uncoated immobilized gold nanoparticles, applying 5 nN force on MgF_2-coated immobilized gold nanoparticles did not cause any damages of the surface (figure 25 d). The first significant changes on the surface were observed by applying 100 nN force (figure 25 f). Gold nanoparticles seem to be still attached to the surface; however, some big structures are present on the rim of the scratched area (very bright

areas inside the white frame in figure 25 f). It can be concluded that these structures are formed by magnesium fluoride removed from the surface and pushed to the rim.

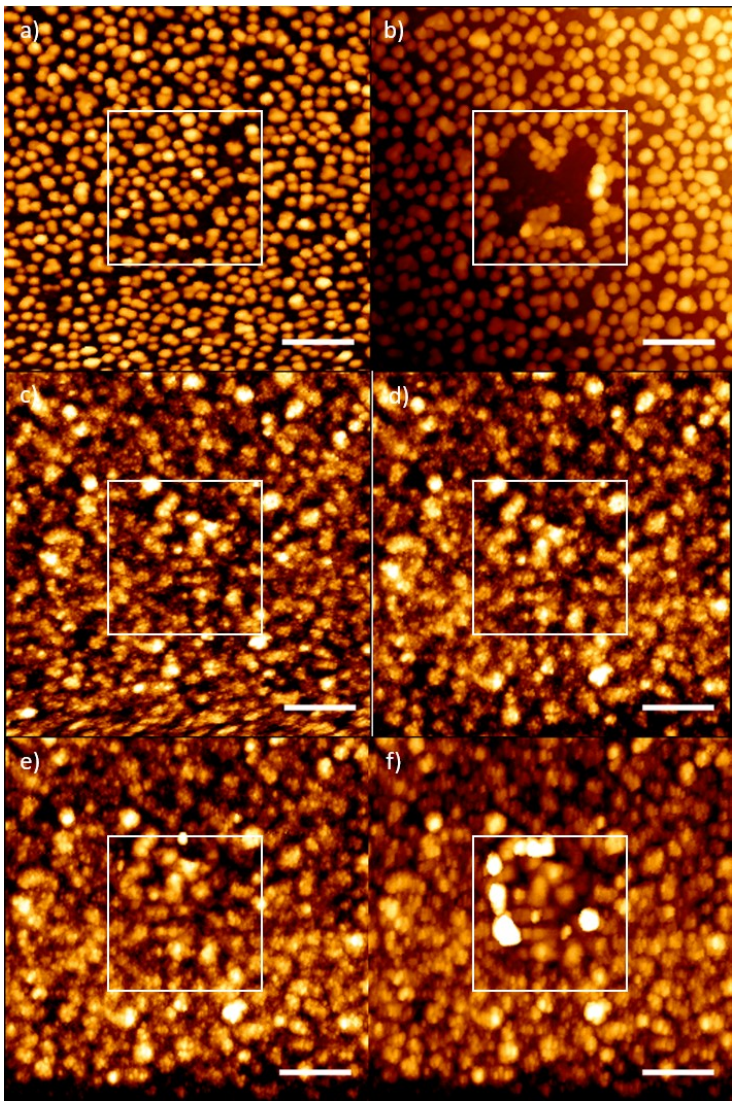

Figure 25: Test of mechanical stability of uncoated gold nanoparticles and MON performed by scanning force microscopy. (a and b) Topography images of uncoated gold nanoparticles of 28 nm in diameter immobilized on the glass before (a) and after (b) contact mode manipulation. (c–f) Immobilized, magnesium fluoride (30 nm) coated gold nanoparticles. (c) Before manipulation, (d–f) after manipulation with defined force. Applied forces: (b and d) 5 nN, (e) 20 nN, (f) 100 nN. Scale bar 200 nm. Scratched areas are marked with white squares.

The SFM scratch experiments proved, that a magnesium fluoride coating significantly increases the mechanical stability of gold nanoparticles immobilized on the glass substrate. Moreover, the presence of a magnesium fluoride layer does not decrease SERS efficiency (chapter 3.2.3); therefore, it is a very promising substrate for further investigations.

3.2.5 Adjusting MgF_2 thickness

The substrate containing gold nanoparticles in the size of 36 nm in diameter coated with 30 nm layer of magnesium fluoride turned out to be the most suitable for SERS applications. It provides a high microscopic homogeneity and a high mechanical stability, as well as, high SERS efficiency. In previous

chapters an application of gold nanoparticles in different sizes and modifications of dip-coating parameters was discussed. It was shown that coating immobilized gold nanoparticles with a 30 nm thick layer of magnesium fluoride does not result in significant decrease of SERS enhancement. In this chapter influence of thickness of magnesium fluoride layer on the SRES efficiency will be investigated.

In order to increase the thickness of the magnesium fluoride layer it was decided to multiply the dip-coating procedure according to the parameters fixed in the chapter 3.2.2 (withdrawing speed 20 cm/min, magnesium fluoride sol concentration 0.1 M). Because of the slight solubility of magnesium fluoride, calcination was required for every new dip-coating step. It was expected that every additional dip-coating step will increase the thickness of the magnesium fluoride layer about another 30 nm.[178] Figure 26 shows SEM cross section images of gold nanoparticles immobilized on the glass slides coated with a magnesium fluoride layer of 35 nm for single dip-coating (figure 26 a), 55 nm for double dip-coating (figure 26b) and 75 nm for fourfold dip-coating process (figure 26 c).

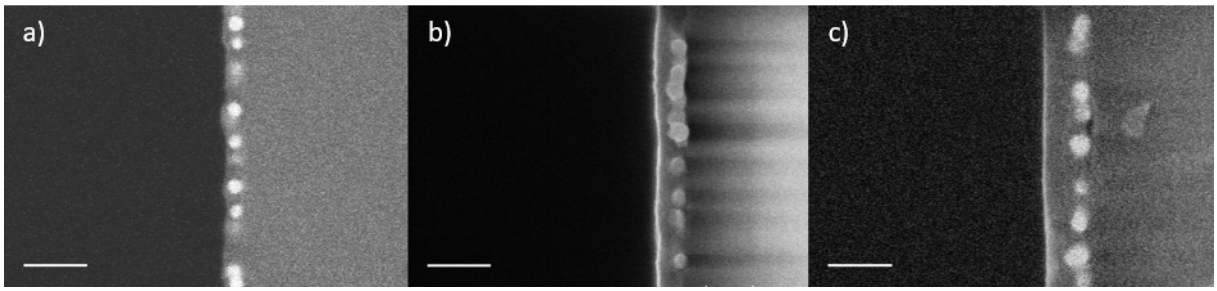

Figure 26: Cross section SEM images of gold nanoparticles immobilized on the glass substrate subjected single dip-coating (a), double dip-coating (b) and fourfold dip-coating process (c). Scale bar 100 nm

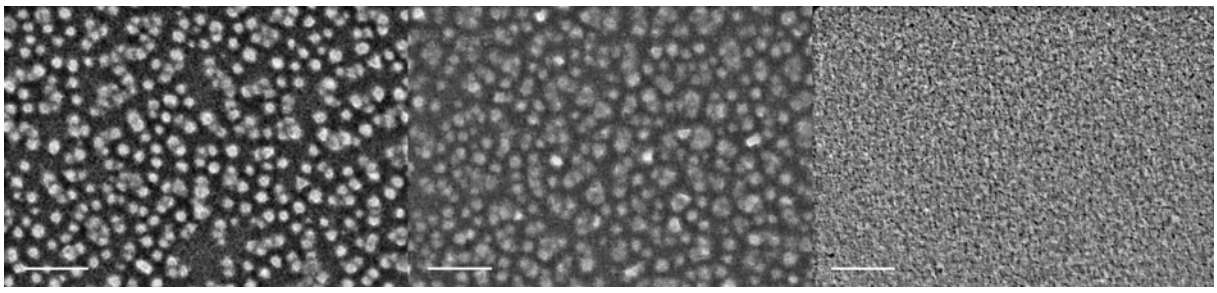

Figure 27: SEM images of gold nanoparticles immobilized on the glass slides coated with one layer of magnesium fluoride calcined one time (a) and four times at 200 °C (b), gold nanoparticles immobilized on the glass slides coated with two layers of magnesium fluoride calcined at 200 °C (c). Scale bar 200 m.

Based on ref. [178], a linear increasing of the thickness of the magnesium fluoride layer was expected. However, the system described in this work is more complex than pure glass described by Krüger.[178] The presence of gold nanoparticles immobilized on the glass using 3-aminopropyltriethoxysilane results in changes of surface roughness and adhesion. Such system is not comparable with pure glass, therefore the dip-coating process is different. It can be also speculated, that even despite calcination performed at 200 °C after each dip-coating step, during long (30s) immersion of the substrate in magnesium fluoride sol, some magnesium fluoride can be partly delaminated and/or disconnected and removed from the substrate surface. It was reported that a higher calcination temperature is more beneficial for antireflective coatings;[126] therefore, the influence of calcination temperature on MON will be investigated in the next chapter (chapter 3.2.6).

The SEM images (figure 27) of gold nanoparticles immobilized on the glass slides coated with one layer of magnesium fluoride calcined once and fourfold at 200 °C respectively, were taken in order to investigate the influence of a multiple calcination process on the samples morphology. In the figure 27 b (gold nanoparticles immobilized on the glass coated with 30 nm layer of MgF_2 calcined four times at 200 °C) gold nanoparticles are slightly less pronounced than in figure 27 a (gold nanoparticles immobilized on the glass coated with 30 nm layer of MgF_2 calcined one time at 200 °C). Significant changes in the samples morphology, e.g. aggregation of gold nanoparticles were not observed; therefore, it can be concluded, that the multiple calcination at 200 °C does not influence the samples morphology. Figure 27 c shows gold nanoparticles immobilized on the glass coated with 55 nm layer of magnesium fluoride. Increasing of magnesium fluoride layer is well pronounced and gold nanoparticles cannot be observed under the magnesium fluoride layer. The surface of magnesium fluoride appears smooth and homogeneous. Any artefacts, e.g. holes or cracks were not observed.

In order to compare SERS efficiency of the gold nanoparticles coated with magnesium fluoride layer of 35 nm, 55 nm and 75 nm, the enhancement factor for each substrate was estimated according to the procedure described in the previous chapter (3.2.3). Figure 28 display SERS spectra taken in order to estimate the enhancement factor of each substrate.

Table 4: Enhancement factors in SERS experiments of uncoated and coated gold nanoparticles subjects to different number of calcination steps at 200 °C and different number of dip-coating steps.

Sample	Dip-coating with MgF_2	Calcination at 200 °C	MgF_2 thickness	$EF_{averaged}$	EF_{max}
Uncoated Au NPs	-	1	-	$1.7x10^5$	$3.3x10^5$
Uncoated Au NPs	-	4	-	$2.0x10^5$	$3.6x10^5$
MgF_2-coated Au NPs	1	1	35	$1.5x10^5$	$2.3x10^5$
MgF_2-coated Au NPs	1	4	n. d.	$1.3x10^5$	$3.2x10^5$
MgF_2-coated Au NPs	2	2	55	$4.1x10^4$	$2.7x10^5$
MgF_2-coated Au NPs	4	4	75	$7.4x10^3$	$1.8x10^4$

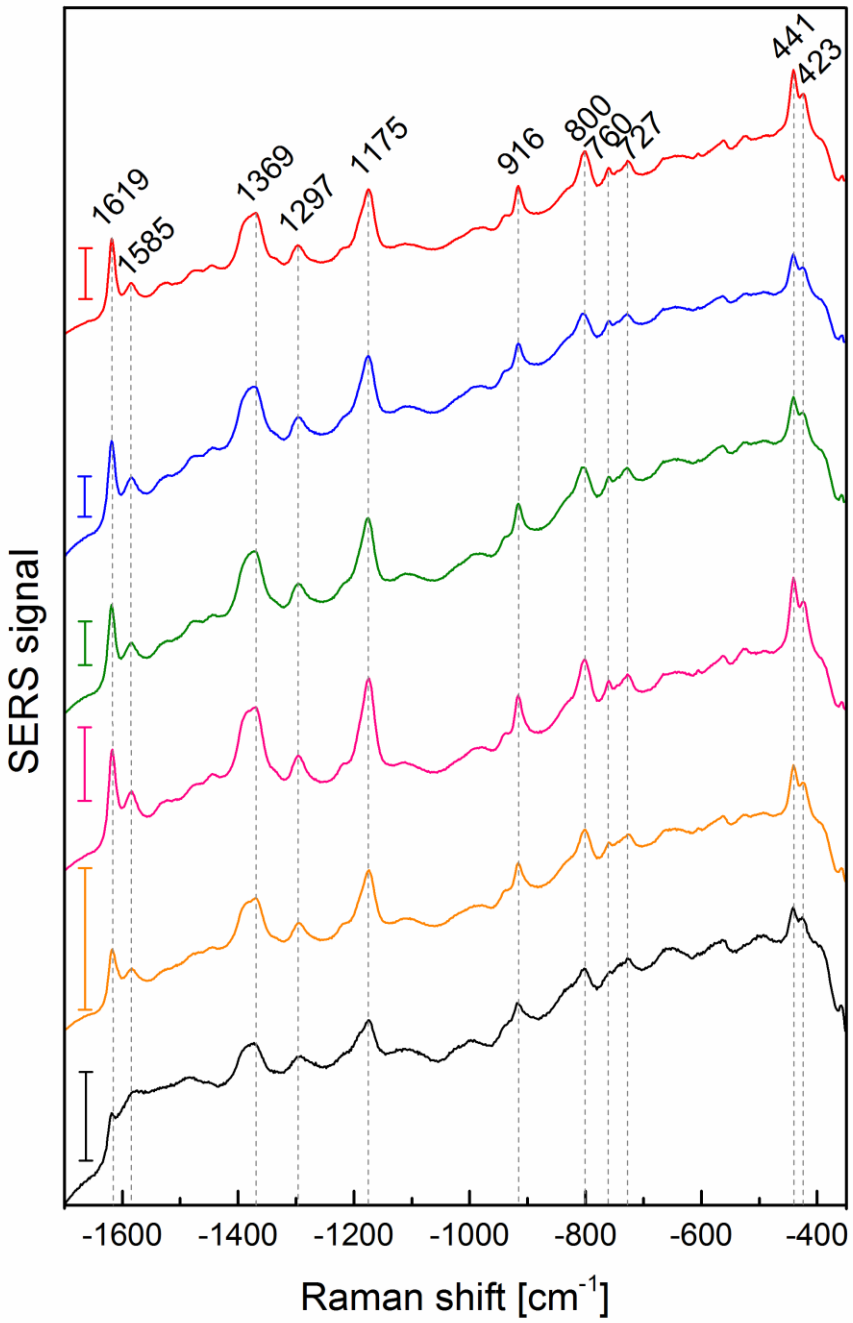

Figure 28: Surfaced enhanced Raman scattering (SERS) spectra of 1 x10^{-5} M crystal violet solution on uncoated gold nanoparticles in the size of 36 nm immobilized on the glass calcined once (red line) and four times (blue line) at 200 °C and on gold nanoparticles immobilized on the glass coated with single layer on magnesium fluoride calcined at once (green line) and four times (pink line) at 200 °C and on gold nanoparticles coated with two (orange line) and four (black line) layers of magnesium fluoride calcined at 200 °C after each single coating step. Each spectrum is an average spectrum of 50–100 individual microspectra. Excitation wavelength: 633 nm, intensity: 1.2 x 10^{5} W cm^{-2}, accumulation time: 1 s. Scale bar 3000 cps for red, blue, green, pink and orange spectra, 300 cps for black spectra

The obtained SERS spectra are displayed in figure 28. The red and blue spectra in the figure 28 are both spectra of a 1 x 10^{-5} M crystal violet solution measured on uncoated gold nanoparticles immobilized on the glass, calcined one time (red spectra) and four times at 200 °C. Those spectra show that the number of calcination steps does not have an influence qualitative nor quantitative features on the spectra (figure 2 and Table 4). The bands characteristic for crystal violet are not shifted. Relative intensities of signals presented on the red and blue spectra are equal. Similar observations were made for crystal violet spectra measured on the gold nanoparticles immobilized on the glass coated with a 30 nm layer of magnesium fluoride calcined one time (green line) and four times (pink spectrum) at 200 °C. As expected, also in this case, the presence of a magnesium fluoride layer and multiple calcination do not have an influence on the SERS spectrum. Estimated averaged enhancement factors of $1.5x10^5$ are in line with the data showed in Table 2. The spectra presented in figure 28 cannot be compared qualitatively with previously measured spectra shown in the figure 23 due to the different concentration of analyte molecules. The orange and black spectrum correspond to samples subjected to multiple dip-coating steps in order to increase the thickness of magnesium fluoride, which approximates 55 nm (orange line) and 75 nm (black line). The characteristic bands of crystal violet can be still observed on the orange spectra, however, the relative intensity of some bands has changed. The intensity of a band at 1619 cm^{-1} significantly decreased. The intensity of all crystal violet bands on the black spectra significantly decreased. Only bands at 1375 cm^{-1}, 1180 cm^{-1}, 916 cm^{-1}, 803 cm^{-1}, 439 cm^{-1} and 420 cm^{-1} are well pronounced, however, in order to observe them the scale bar in the figure 28 was decreased to 300 cps for the black spectra. The estimated enhancement factors for both samples (55 nm and 75 nm MgF_2 layer) significantly decreased in both cases. For a 55 nm thick layer of MgF_2 the estimated averaged enhancement factor approximates $4.1x10^4$ and for a 75 nm thick layer it is only $7.4x10^3$. For both samples the maximum enhancement factor is about one magnitude higher than the average value. It can be speculated that during the measurements, due to capillary forces, some crystal violet molecules were trapped within magnesium fluoride pores near the surface of the substrate and far away from the gold nanoparticles surface. It results in changes of the SERS spectra and variations of the enhancement factor caused by different concentrations of crystal violet molecules on the gold nanoparticles surface. Therefore the estimated enhancement factor can be different than the actual enhancement factor (concentration of crystal violet molecules reaching the surface of gold nanoparticles in unknown). Besides a decreasing of SERS efficiency, an increasing of the thickness of the magnesium fluoride layer leads to difficulties during SERS measurements. Focusing the excitation light and collecting the SERS of the investigated surface is one of the crucial steps for successful SERS detection. Increasing the thickness of magnesium fluoride leads to a significant decrease of the sample roughness. Therefore, during the measurements it was not possible to estimate whether the focusing on the plasmonic surface was successful or not.

It was concluded that an increasing thickness of magnesium fluoride by repeated dip-coating processes does not result in a linear increase of the thickness as expected.[178] The glass containing immobilized gold nanoparticles has a different roughness and adhesion than pure glass, therefore, during the dip-coating process it occurs differently and results in a lower thickness of the magnesium fluoride layer than expected. Increasing the magnesium fluoride thickness leads to both, a decrease in SERS efficiency and difficulties in the optical experiment.

3.2.6 Adjusting calcination temperature

The previously prepared MONs described in above chapters were calcined at a temperature of 200 °C. Such soft conditions were applied due to the presence of gold nanoparticles. A temperature of 200 °C

can be applied for metal fluorides calcination, however, calcination at 450 °C is more beneficial for antireflective coating purposes.[126] Therefore, another batch of MONs of different thicknesses of MgF_2 layers was prepared according to the procedure 4.15 and calcined at 450 °C instead of 200 °C. These samples were characterized using SEM, SFM and SERS.

The SEM images displayed in figure 29 show changes in the morphology of the samples calcined at 450 °C. In comparison with samples calcined at 200 °C (figure 27), samples calcined at 450°C exhibit more pronounced, bigger pores of magnesium fluoride and show the presence of an unidentified big structures on the surface. Figure 29 a corresponds to the gold nanoparticles immobilized on the glass, coated with one magnesium fluoride layer and calcined at 450 °C. Figure 29 b shows a sample prepared on the same way, but calcined four times at 450 °C in order to investigate the influence of a multiple calcination steps on the sample morphology. The number of already mentioned big structures increases for the samples subjected a multiple calcination. Such phenomenon was not observed for multiple calcination at 200 °C. Figure 29 c represents sample subjected double dip-coating process. In the case of this sample magnesium fluoride pores are even more pronounced, while big structures are significantly less pronounced. The formation of such structures was not observed for multiple calcination performed at 200 °C. It can be speculated that the mentioned already big structures are formed by gold nanoparticles; however, it cannot be stated based on SEM images of MgF_2-coated gold nanoparticles. Therefore, more detailed SMF investigations were performed (figure 31). Obtained SFM images will be discussed later in this chapter. The cross sectional SEM images (figure 30) were taken in order to estimate the thickness of the magnesium fluoride layer calcined at 450 °C. During the measurements it was observed, that the magnesium fluoride layer calcined at 450 °C breaks during the sample preparation procedure. In some areas of the sample the magnesium fluoride film containing gold nanoparticles was detached from the glass surface. This phenomenon was unexpected. Normally, magnesium fluoride films deposited on the glass and calcined at high temperature are mechanically more resistant than films calcined at low temperatures.[126] The presence of gold nanoparticles and APTES on the glass surface change the roughness and the adhesion of the glass substrate, what most likely results in a decrease of mechanical stability of the deposited magnesium fluoride film. Due to many layer damages, it was not possible to determine the thickness of a single magnesium fluoride layer calcined at 450 °C (figure 29 a). For the samples subjected a multiple dip-coating process the thickness of magnesium fluoride layer approximates 50 nm for double dip-coating (figure 30 b) and 70 nm for fourfold dip-coating (figure 30 c).

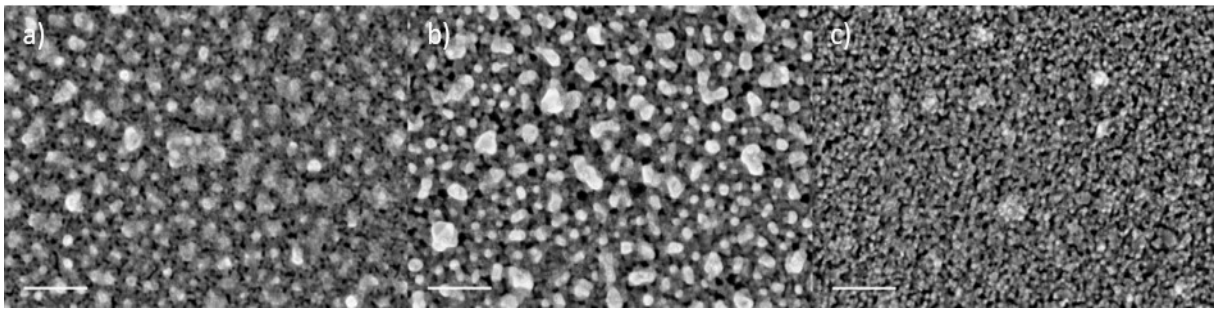

Figure 29: Gold nanoparticles in the size of 26 nm in diameter coated with one layer of magnesium fluoride calcined one (a) and four times (b) time at 450 °C, gold nanoparticles immobilized on the glass

coated with two layers of magnesium fluoride calcined at 450 °C after each dip-coating step (c). Scale bar 200 nm.

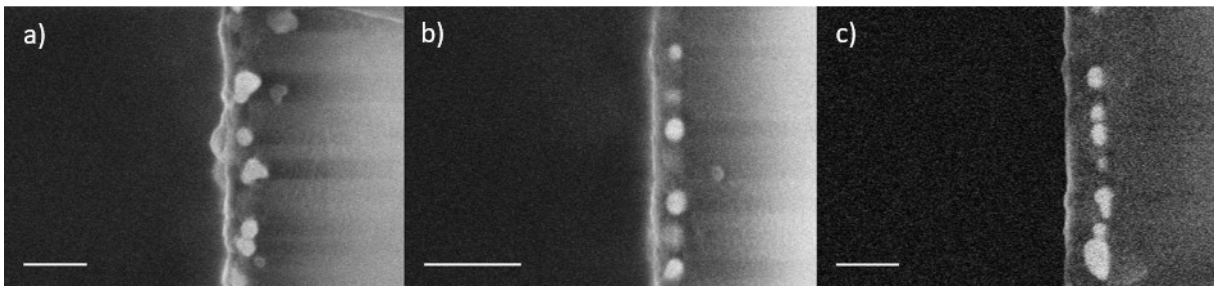

Figure 30: Cross section SEM images of gold nanoparticles in the size of 26 nm in diameter coated with one (a), two (b) and four layers of magnesium fluoride (c) calcined at 450 °C after each dip-coating step. Scale bar 100 nm.

In order to learn more about influence of calcination temperature on the samples morphology and to find out which compound forms these big structures observed on SEM images, SFM measurements of uncoated and coated samples calcined at different temperatures were taken (figure 31). Samples were prepared according to the procedure 4.15 and calcined at 200 °C (figure 31 a-b), 450 °C (figure 31 c-d) and 600 °C (figure 31 d-f) respectively.

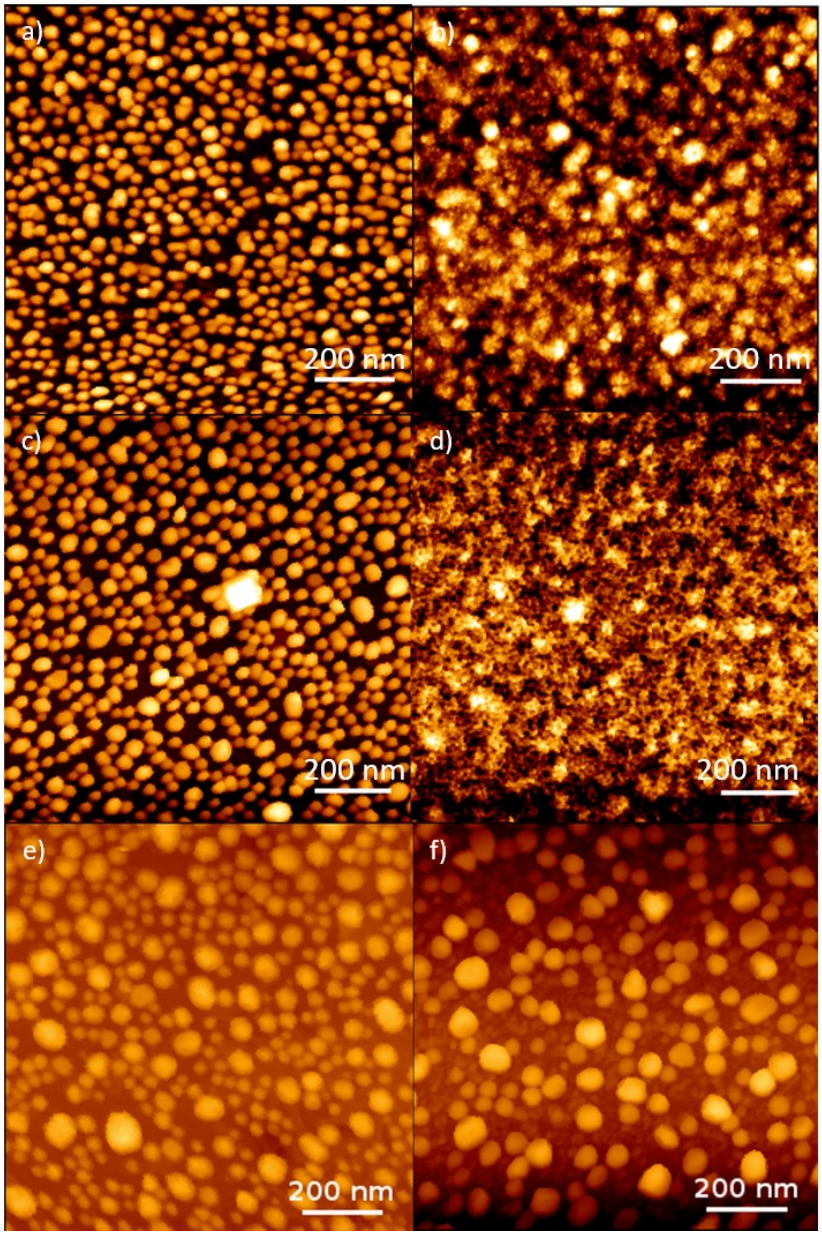

Figure 31: SFM topography images of uncoated gold nanoparticles immobilized on the glass substrate (left column) calcined at 200 °C (a), 450 °C (c), 600 ° (e) and MgF_2-coated gold nanoparticles immobilized on the glass substrate (right column) calcined at 200 °C (b), 450 °C (d), 600 ° (f). Scale bar 200 nm.

Figure 31 displays the SFM topography images of uncoated (left column) and MgF_2-coated (right column) gold nanoparticles in the size of 28 nm in diameter immobilized on the glass calcined at 200 °C (figure 31 a-b), 450 °C (figure 31 c-d), and 600 °C (figure 31 e-f). It can be observed that an increasing calcination temperature leads to significant changes in substrate morphology. After the calcination at 450 °C many medium sized structures are formed by gold uncoated nanoparticles (figure 31c). These structures are less pronounced for MgF_2-coated samples, however, they still can be observed (figure 31d). Based on SFM (figure 31) it can be speculated that these structures, observed also on SEM images, are formed rather by gold nanoparticles than magnesium fluoride. The number of big structures/aggregates increases significantly after a calcination at 600 °C, for both, coated and

uncoated gold nanoparticles. Calcination at 600 °C results in high inhomogeneity of the sample, therefore, samples calcined at 600 °C were not further investigated.

SERS measurements were performed in order to investigate the influence of the high calcination temperature on the plasmonic properties of the substrate and their SERS efficiency (figure 32). Crystal violet spectra were measured on uncoated and MgF_2-coated gold nanoparticles immobilized on the glass subjected a single and a multiple dip-coating process and calcined at 450 °C. Red and blue spectra in figure 32 were recorded in order to investigate the influence of multiple calcination at 450 °C on the SERS efficiency of uncoated gold nanoparticles. Spectra measured for the four times calcined substrate (blue line in the figure 32) exhibit shaper and more pronounced bands, than spectra measured for the single calcined substrate (red line in the figure 32). The ratio of relative intensities of crystal violet bands for the multiple calcined sample differs from the samples subjected for the single calcination. It is strongly pronounced for the bands at 1619 cm^{-1} and 1583 cm^{-1}. The averaged enhancement factor is slightly higher for the four times calcined sample (Table 5). The described differences can be caused by a different morphology of the SERS substrates (presence of different types of aggregates). Differences in morphology of single and multiple calcined samples were already shown on SFM images (figure 31). Spectra of crystal violet measured on gold nanoparticles coated with one layer of magnesium fluoride subjected single and fourfold calcination at 450 °C (green and orange lines in the figure 32), do not show any significant differences in the SERS spectra and in SERS efficiency (figure 32 and Table 5). Signal intensities and their relative ratios are equal for single and multiply calcined substrates. The estimated enhancement factors are, as expected, in the same order of magnitude as enhancement factors of uncoated samples. It means, that also in this case crystal violet molecules have almost free access to the gold nanoparticles surface. The estimated averaged enhancement factors for coated and uncoated samples subjected single and multiple calcination are only slightly lower than the maximal enhancement factors. It indicates that despite the fact that many nanoscopic aggregates were observed on the SEM and SFM images, all samples exhibit a high microscopic homogeneity.

Applying thicker layers of magnesium fluoride (55 nm and 75 nm) calcined at 450 °C result in a decrease of signal intensities and SERS efficiency. The same phenomenon was observed for samples coated with a thicker than 30 nm magnesium fluoride layer calcined at 200 °C. Also in this case some crystal violet molecules can be trapped in magnesium fluoride pores due to capillary forces, therefore they do not reach the surface of gold nanoparticles. Calcination at higher temperature leads to the formation of more dense structures of magnesium fluoride and the formation of bigger pores. The enhancement factor values reflects the formation of bigger pores for sample calcined at 450 °C. Samples covered with similar layers of magnesium fluoride calcined at 450 °C exhibit higher enhancement factor values than samples calcined at 200 °C. However, the increasing of the enhancement factor can be also caused by a different reason e.g. different aggregation states of gold nanoparticles. By comparing the location of the crystal violet bands measured on samples calcined at 200 °C and 450 °C respectively , it can be concluded that they are usually shifted about 2 to4 nm in long- or shortwaves direction. The highest observed band shift was observed for the band assigned to C-H, -CH3 and a ring C-C bending vibrations. This band was observed at 1369 cm^{-1} for a samples calcined at 200 °C and at 1378 cm^{-1} for samples calcined at 450 °C. The described differences on the spectra for samples calcined at different temperatures are caused by a different samples morphology. The increase of the pore size and the presence of the big aggregates of gold nanoparticles in samples calcined at 450 °C results in an increase of surface roughness. Therefore, focusing of excitation light on the plasmonic surface and colleting SERS was not as challenging, as for samples calcined at 200 °C.

It can be concluded that the calcination temperature has a strong influence on the substrate morphology but only little influence on SERS spectra and SERS efficiency. Calcination at 450 °C is beneficial for samples coated with approximately 70 nm magnesium fluoride layer, because the rough surface of the sample facilities focusing of excitation light on the plasmonic surface and colleting SERS.

Table 5: Enhancement factors in SERS experiments of uncoated and coated gold nanoparticles subjects different number of calcination steps at 450 °C and different number of dip-coating steps.

Sample	Dip-coating with MgF_2	Calcination at 450 °C	MgF_2 thickness	$EF_{averaged}$	EF_{max}
Uncoated Au NPs	-	1	-	$1.2x10^5$	$3.1x10^5$
Uncoated Au NPs	-	4	-	$1.6x10^5$	$3.0x10^5$
MgF_2-coated Au NPs	1	1	n. d.	$1.3x10^5$	$3.2x10^5$
MgF_2-coated Au NPs	1	4	n. d.	$1.1x10^5$	$2.9x10^5$
MgF_2-coated Au NPs	2	2	55	$7.1x10^4$	$1.3x10^5$
MgF_2-coated Au NPs	4	4	75	$1.2x10^4$	$7.6x10^4$

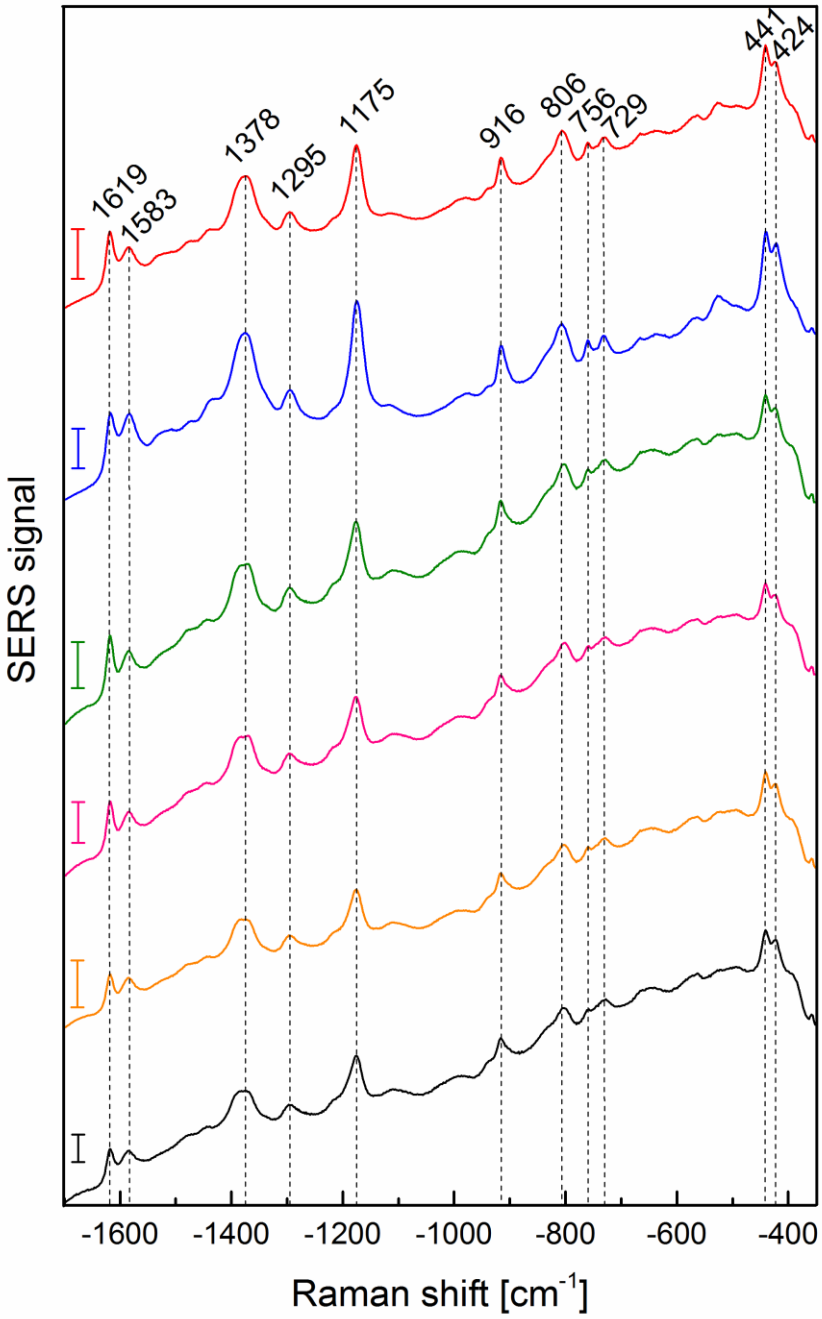

Figure 32: Surfaced enhanced Raman scattering (SERS) spectra of 1 x10^{-5} M crystal violet solution on uncoated gold nanoparticles immobilized on the glass in the size of 36 nm in diameter calcined once (red line) and four times (blue line) at 450 °C and on gold nanoparticles immobilized on the glass coated with single layer on magnesium fluoride calcined at once (green line) and four times (pink line) at 450 °C and on gold nanoparticles coated with two (orange line) and four (black line) layers of magnesium fluoride calcined at 450 °C after each single coating step. Each spectrum is an average spectrum of 50–100 individual microspectra. Excitation wavelength: 633 nm, intensity: 1.2 x 10^{5} W cm^{-2}, accumulation time: 1 s. Scale bar: 3000 cps for red, blue, green, pink and orange spectra, 300 cps for black spectra.

3.2.7 Vapor phase deposition of magnesium fluoride for MON fabrication

In the final stage of the doctoral research I was also interested in applying vapor phase deposition of magnesium fluoride in the MON fabrication. Vapor phase deposition experiments were carried out in cooperation with physical chemists. Even our cooperators had no experience in vapor deposition of magnesium fluoride on glass nor gold nanoparticles coated glass. Therefore, vapor deposition parameters known from calcium fluoride deposition on the pure glass were applied (pressure $3{,}4 \times 10^{-4}$, temperature ~390 °C, evaporation current 85 A, evaporation time 30 s, evaporation rate 20 to 30 a.u.).[179] Figure 33 shows SEM plane view (a, b) and cross section (c, d) images of obtained samples. It can be clearly seen, that the obtained surface in not homogenous; many aggregates of unknown origin are present on the surface. The cross section images suggest, that the big aggregates are formed by magnesium fluoride, while gold nanoparticles seems to be non-aggregated. Thickness of magnesium fluoride layer on the presented images varies from 65 nm to 140 nm, averaged thickness calculated based on 50 measurers in different areas approximates 70 nm.

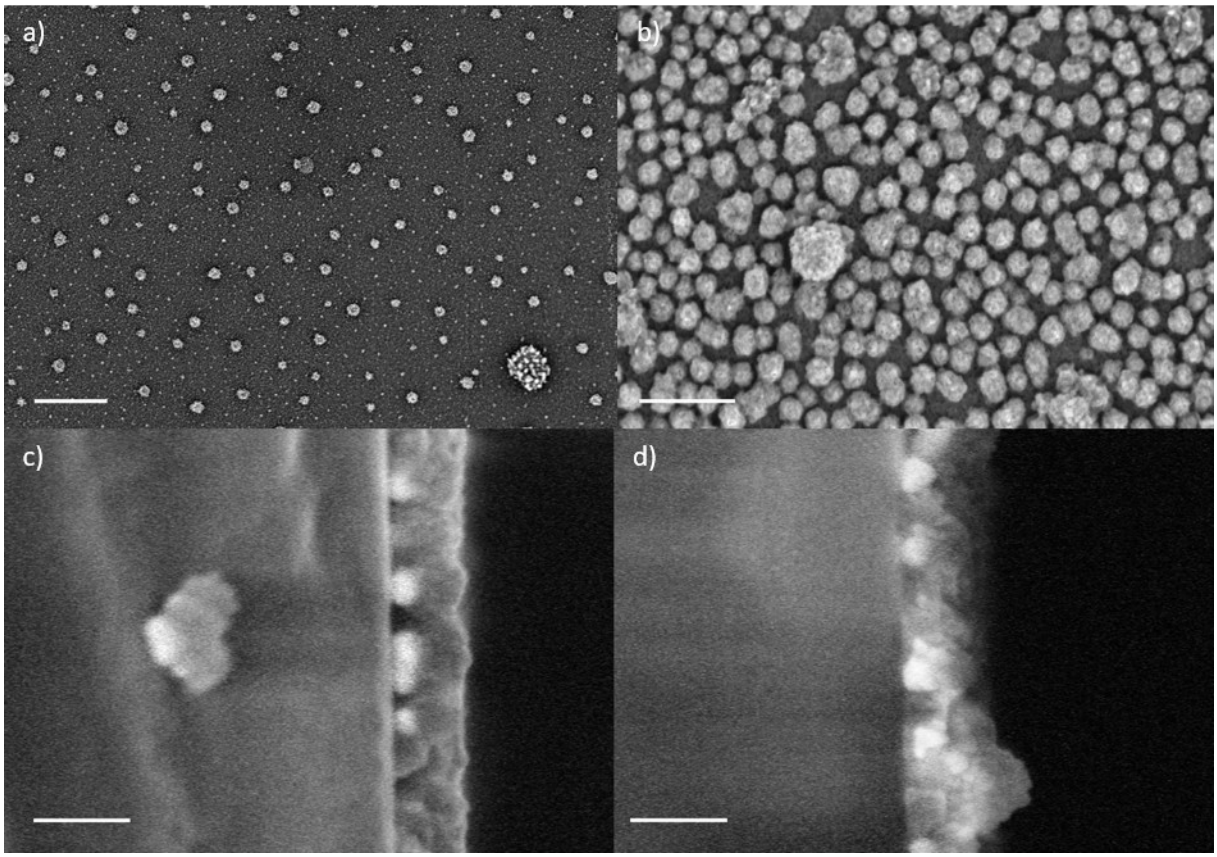

Figure 33: Plane view (a, b) and cross section (c, d) SEM images of gold nanoparticles in the size of 26 nm in diameter immobilized on the glass and coated with magnesium fluoride layer deposited from vapor phase.

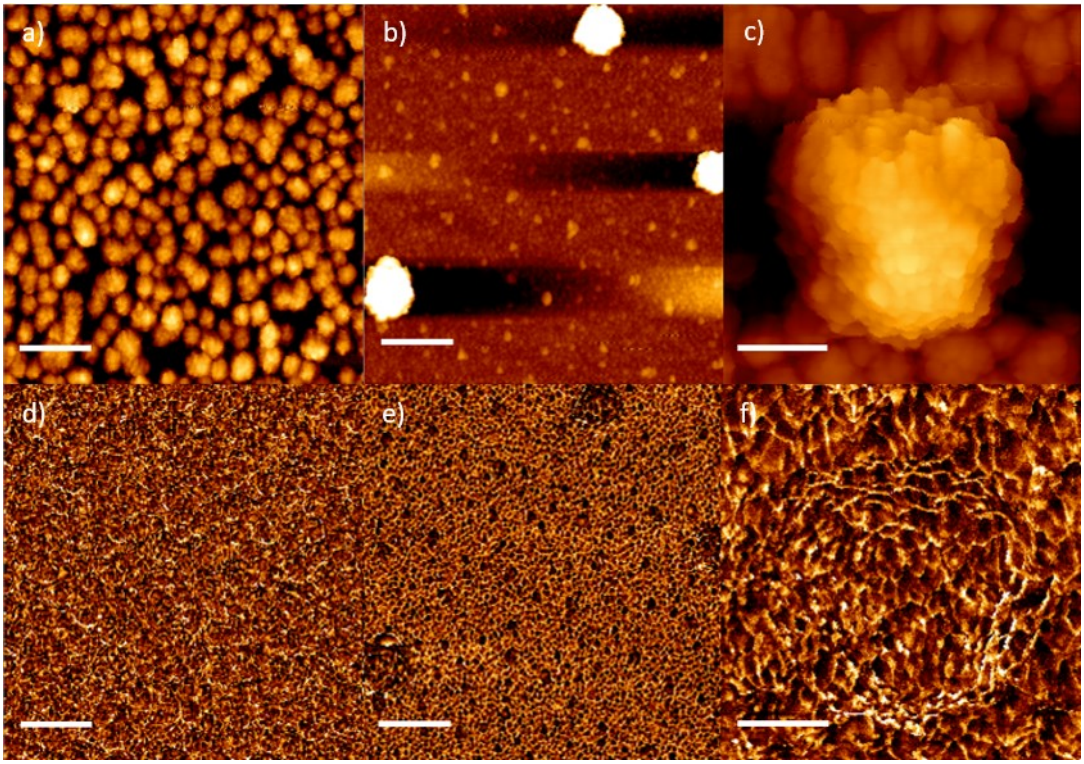

Figure 34: SFM topography (a-c) and adhesion (e-f) images of gold nanoparticles in the size of 26 nm in diameter immobilized on the glass and coated with magnesium fluoride layer deposited from vapor phase. The following pairs of images a and d, b and e, c and f, correspond to the same area of the sample. Scale bar a-b, d-e: 200 nm, c, f: 100 nm.

The same observations were made based on SFM investigations. Figure 34 a presents small sized aggregates on the sample surface, figure 34 b medium sized and figure 34 c a big sized aggregates. Adhesion images corresponding to the topography images displayed on figure 34 e-f indicate, that the surface of the whole sample is coated by magnesium fluoride. However, it cannot be assessed, which material (gold or magnesium fluoride) forms the aggregates. The origin of those aggregates is, so far, unknown. It would be interesting to investigate the influence of the conditions during evaporation on the gold nanoparticles immobilized on the glass (by caring out experiments without magnesium fluoride) and the influence of gold nanoparticles on the vapor phase deposition (vapor deposition of magnesium fluoride on the pure glass). It was already shown in the previous chapter that presence of gold nanoparticles on the surface has a significant influence on dip-coating process, therefore, it can be speculated, that it influences also vapor phase deposition process. Due to the limited time of doctoral studies and limited access to the evaporation chamber, further vapor phase deposition experiments were not conducted. However, adjusting vapor phase deposition of magnesium fluoride on glass surface coated with immobilized gold nanoparticles can be a very interesting and complex project for the future.

Even though, substrates obtained via vapor phase deposition exhibit a high non-uniformity and presence of many undefined aggregates, SERS measurements were performed. It was expected that the vapor phase deposition will provide a dense, nonporous magnesium fluoride layer, so analyte molecules used for SERS experiments should not be able to reach the gold nanoparticles surface. A 70 nm thick layer of magnesium fluoride should separate analyte molecules from the area of enhanced electromagnetic field during SERS measurements, therefore, it was expected, that the obtained sample

is not a good plasmonic substrate for SERS applications. Unexpectedly, SERS spectra of crystal violet in concentration of $1x10^{-6}$ M were successfully recorded. The calculated average enhancement factor of $1,8x10^{4}$ is comparable to the enhancement factor calculated for gold nanoparticles in the same size (26 nm in diameter) immobilized on the glass coated with a 30 nm layer of magnesium fluoride deposited via the dip-coating method (EF= $2.8x10^{4}$). According to the described in the chapter 3.2.3 methodology of SERS measurements, spectra presented in figure 35 is an averaged spectra of 4 different areas of the sample. In each of the 4 measured areas around 100 microspectra were recorded. Such a high enhancement factor indicates that the magnesium fluoride deposited from vapor phase is not a dense, bulky layer as expected. On the SEM and AFM images any holes or crakes on the magnesium fluoride surface were not observed. Therefore, it can be speculated that the obtained magnesium fluoride layer is porous. This hypothesis is supported by presence of porous-looking structures on the SEM image taken in high magnification (figure 33 b).

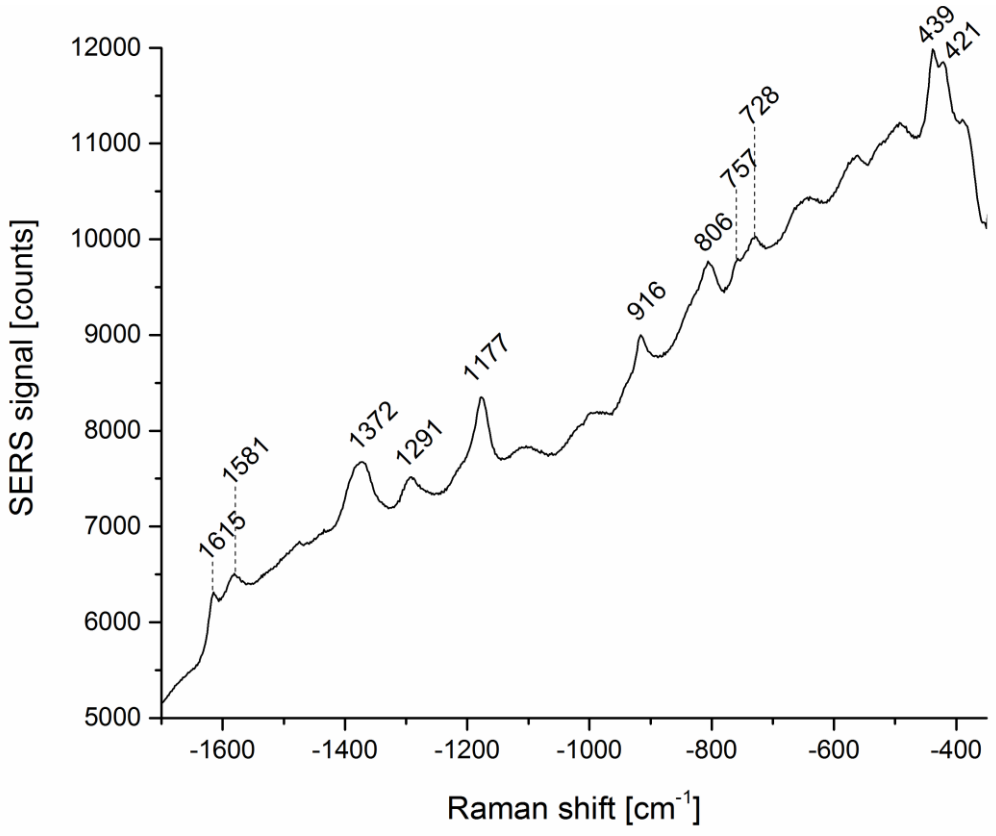

Figure 35: Surface Enhanced Raman Scattering spectra of 1 x 10^{-6} crystal violet aqueous solution measured on gold nanoparticles in the size of 26 nm immobilized on the glass surface coated with magnesium fluoride layer deposited by vapor phase deposition method. Excitation wavelength: 633 nm, intensity: 1.2 x 10^{5} W cm^{-2}, accumulation time: 1 s.

Based on presented SEM, FSM images, SERS spectra and the unexpectedly high enhancement factor, it can be concluded, that the magnesium fluoride vapor deposition process on glass surface containing immobilized gold nanoparticles requires further optimization. Different factors, e.g. presence of gold nanoparticles on the glass surface or conditions in the evaporation chamber can possibly influence the vapor deposition process. Improving parameters of the vapor phase deposition of magnesium fluoride on glass is a very complex and time consuming problem, therefore, it could not be further investigated for as a part of this doctoral thesis. This issue is an interesting topic for an ongoing project.

3.2.8 Summary

Gold nanoparticles in the size of 26 nm, 36 nm and 47 nm in diameter were immobilized on the glass surface using APTES and coated with magnesium fluoride. In order to obtain a homogenous, 30 nm thick layer of magnesium fluoride, glass slides were immersed for 30 s in a 0.1 M MgF_2 sol and drawn from the sol with the speed of 20 cm/min. SEM and SFM investigations show, that particles in all three sizes were completely covered by magnesium fluoride. MON containing gold nanoparticles in the size of 36 nm in diameter appears to be the most desirable plasmonic substrate for further applications due to its high microscopic homogeneity and high SERS efficiency. The coating with 30 nm thick magnesium fluoride significantly increases mechanical stability of the substrates and allows an almost free access of analyte molecules towards the gold nanoparticles surface. An increasing of the magnesium fluoride thickness results in a more limited access of analyte molecules towards the gold nanoparticles surface. Applying higher calcination temperatures result in changes of the samples morphology, however it does not have any significant impact on SERS spectra and SERS efficiency.

3.3. Conclusion and outlook

Two approaches for coating the plasmonic nanostructures with magnesium fluoride were proposed in this work: (i) a fabrication of core-shell nanoparticles containing plasmonic core and (ii) coating plasmonic nanostructures immobilized on the glass. Coating of the plasmonic nanostructures with magnesium fluoride described in this work was accomplished with the successful fabrication of a very promising plasmatic substrate for analytical applications. However, one of two proposed approaches, core-shell nanoparticles synthesis, turned out to be extremely challenging. Many fabrications routes proposed in this thesis based on metal@metal oxides core-shell nanoparticles synthesis were found not to be suited for metal@metal fluorides core-shell nanoparticles synthesis. Although different magnesium precursors, solvents, stabilizing agents of gold nanoparticles, as well as different reaction conditions were applied, core-shell nanoparticles formation was not proven. A successful synthesis of metal@metal fluorides core-shell nanoparticles was not achieved either for approach known to be successful for metal fluorides@metal fluoirdes core-shell nanoparticles (doped with some rare earth metals).[164] A further challenge that was met in the creation of core-shell nanoparticles was the verification of the core-shell structure formation (chapter 3.1).

The Au@MgF_2 core-shell nanoparticles formation proved to be a very challenging strategy, therefore, another strategy of MgF_2-coated plasmonic substrate fabrication, based on immobilization of gold nanoparticles on the glass and coating with magnesium fluoride via dip-coating, was proposed. The obtained porous MgF_2-over-gold nanoparticles (MON) were characterized using SEM, SFM, UV-Vis and SERS. Gold nanoparticles in different sizes were immobilized on the glass. Formation of particles multilayers was not observed, the particles tend to pack densely on the surface. Depending on the size of applied gold nanoparticles a different number of single particles, dimers, trimers or small planar aggregates were formed. For further applications, gold nanoparticles used in this work can be replaced with gold nanostructures in different sizes and shapes, as well as with different nanostructures of other plasmonic metals that can be immobilized on the glass substrate. Moreover, for the purpose of example biocompatibility or selectivity, the applied nanostructures can be functionalized.

As it was shown in the chapter 3.2.2, dip-coating with magnesium fluoride sols results in complete coverage of gold nanoparticles. Magnesium fluoride was found in between the particles as well as on their surface. The presented approach for protective coating of any kind plasmonic nanostructures can be very beneficial for different kinds of applications including spectroscopic characterization of catalytic reactions in microfluidic platforms. Dip-coating process of gold nanoparticles coated glass surfaces occurs differently than coating of the pure glass due to different properties of the coated surface. In order to provide homogenous magnesium fluoride coating time of immersion of glass slides with gold nanoparticles on the surface has to be increased. Applying magnesium fluoride as a protective layer significantly increases the mechanical stability of the analytical substrate. Due to different roughness and adhesion of glass with gold nanoparticles immobilized on the surface, increasing the thickness of magnesium fluoride is slightly more challenging than for pure glass substrate. Plasmonic nanostructures immobilized on different than glass solid substrates, examples silicon wafers, can be also coated with magnesium fluoride.

As an alternative method of magnesium fluoride coating, vapor phase deposition experiments were performed. However, according to our present knowledge, this approach requires further and complex optimization, before it can be used for coating plasmonic nanostructures for analytical applications

(chapter3.2.7). Currently, dip-coating method can be considered as the most suitable method of coating plasmonic nanostructures with magnesium fluoride for analytical applications.

Apart from the ease of the preparation procedure, the advantage of magnesium fluoride coating over coating with commonly applied metal oxides, is its wide optical window. Such a wide optical window allows for observations across the UV-Vis and NIR range. As demonstrated by the experimental determination of the local field enhancement in SERS experiments and corresponding theoretical considerations, enhancement factors that allow for analytical applications are obtained. The magnesium fluoride layer has almost no influence on the enhancement nor on the qualitative properties of the spectra, that indicate a direct interaction of the analyte molecules with the gold surfaces. The wide optical window makes MON a very promising substrate not only for SERS but also for the wide range of other optical methods. In particular, by embedding the gold nanoparticles in the magnesium fluoride layer, their plasmonic properties become more favorable for enhancement of optical processes excited in the near-infrared. Future applications will also benefit from the potential to implement additional selectivity of the protective coating due to our ability to easily control its porosity.[162]

4 Experimental section

4.1 Synthesis of gold nanoparticles

4.1.1. Synthesis of small gold nanoparticles (expected size up to 30nm)

Gold nanoparticles of the size from 20 nm to 50 nm in diameter were synthesized according to the citrate reduction procedure.[110] Before the synthesis, all the glassware was washed with aqua regia in order to remove impurities which could disturb the synthesis. All solutions were prepared using MilliQ water. Firstly 50 ml of 2.2 mM sodium citrate solution was heated till the boiling point, then 1 ml of 25 mM $HAuCl_4$ solution was injected. The solution was kept at the boiling temperature for 15 min and then cooled down to 90 °C. After 30 min, when the color turned red, 1 ml of 60 mM sodium citrate was added. After two minutes, 1 ml of 25 mM $HAuCl_4$ was injected. The number of repetitions of the two last steps allowed to control the size of the gold nanoparticles. When the process is finished (30 min after the last addition of sodium citrate and $HAuCl_{4)}$, the solution was cooled down in ice bath. All solutions were prepared using MilliQ water.

4.1.2. Synthesis of small gold nanoparticles (expected size up to 180nm)

Gold nanoparticles of the size between 50 nm and 80 nm in diameter were synthesized according to the citrate reduction procedure.[110] Before the synthesis, all the glassware was washed with aqua regia in order to remove impurities disturbing the synthesis. All solutions were prepared using MilliQ water. Firstly 50 ml of 2.2 mM sodium citrate solution was heated till the boiling point, then 1 ml of 25 mM $HAuCl_4$ solution was injected. The solution was kept at the boiling temperature for 15 min and then cooled down to 90 °C.

Then 1 ml of 25 mM $HAuCl_4$ solution was injected and reaction mixture was magnetically stirred for 30 min. This procedure was repeated twice. Afterwards 55ml of the mixture was extracted and replaced with 2 ml o 60 mM sodium citrate solution and 53 ml od MilliQ water. Depending of the desired size of gold nanoparticles the procedure was repeated a few times (every 3 injections of $HAuCl_4$ the reaction mixture was diluted).

4.2 Synthesis of Au@MgF_2 using $Mg(OAc)_2x4H_2O$ and $MgCl_2x6H_2O$ as magnesium precursors

50 mM stock solutions of magnesium acetate and magnesium chloride were prepared by dissolving respectively $Mg(OAc)_2x4H_2O$ or $MgCl_2x6H_2O$ powder in denatured ethanol. Only freshly prepared solutions were used for the core-shell nanoparticles synthesis.[140] 400 µL of 2,5 mM aqueous solution of citrate stabilized gold nanoparticles (prepared in advance according to procedure 4.1) was diluted with ethanol (Table 6 shows volume of added EtOH). After 5 min of magnetic stirring proper amounts of magnesium acetate or magnesium chloride ethanolic solution were added respectively. After another 5min ethanolic solution of HF was added to all samples. Table 6 show content of all samples prepared in this experiment.

Table 6: Composition of samples prepared according to the procedure 4.2

Sample	**2.1**	**2.2**	**2.3**	**2.4**	**2.5**	**2.6**
Au:MgF_2	*1:2*	*1:5*	*1:10*	*1:2*	*1:5*	*1:10*
AuNPs [µL]	400	400	400	400	400	400
$Mg(OAc)_2$ [µL]	40	100	200	-	-	-
$MgCl_2$ [µL]	-	-	-	40	100	200
HF/EtOH [µL]	80	200	400	80	200	400
EtOH [µL]	9480	9300	9000	9480	9300	9000

4.3 Synthesis of Au@MgF_2 using $Mg(OAc)_2x4H_2O$ and $MgCl_2x6H_2O$ as a magnesium precursors (reversed sequence of adding reagents)

50 mM stock solutions of magnesium acetate, magnesium chloride and ethanolic solution of gold nanoparticles were prepared according to the procedure 4.2. According to the Table 7 proper amount of HF was added to each sample. After 5 min of magnetic stirring 50 mM solution of magnesium acetate or magnesium chloride were added to the mixtures respectively (amounts presented in Table 7).

Table 7: Composition of samples prepared according to the procedure 4.3

Sample	**3.1**	**3.2**	**3.3**	**3.4**	**3.5**	**3.6**
Au:MgF_2	*1:2*	*1:5*	*1:10*	*1:2*	*1:5*	*1:10*
AuNPs [µL]	400	400	400	400	400	400
HF/EtOH [µL]	80	200	400	80	200	400
$Mg(OAc)_2$ [µL]	40	100	200	-	-	-
$MgCl_2$ [µL]	-	-	-	40	100	200
EtOH [µL]	9480	9300	9000	9480	9300	9000

4.4. Synthesis of Au@MgF_2 using $Mg(OEt)_2$ as a magnesium precursor

White, turbid 50 mM ethanolic solution was prepared by dissolving magnesium ethoxide powder in ethanol within 3 hours under heating to 35 ^oC. Three batches of ethanolic gold nanoparticles solution were prepared as following: 400 µL of 2,5 mM aqueous solution of citrate stabilized gold nanoparticles (prepared in advance according to procedure 4.1) was diluted with ethanol according to Table 8. Then a certain volume of 50 mM magnesium ethoxide solution (Table 8) was added and the mixture was stirred for 5 min. Next a stoichiometric amount (regarding to magnesium) of 50 mM ethanolic HF solution was added.

Table 8: Composition of samples prepared according to the procedure 4.4

Sample	**4.1**	**4.2**	**4.3**
Au:MgF_2	*1:2*	*1:5*	*1:10*
AuNPs [µL]	400	400	400
$Mg(OEt)_2$ [µL]	40	100	200
HF/EtOH [µL]	80	200	400
EtOH [µL]	9480	9300	9000

4.5. Synthesis of Au@MgF_2 using $Mg(OEt)_2$ as a magnesium precursor (reversed sequence of adding reagents)

The stock solution of magnesium ethoxide and three batches of ethanolic gold nanoparticles solution were prepared according to the procedure 4.4. A certain volume of 50 mM HF solution (Table 9) was added and each batch of AuNPs, mixture was stirred for 5 min. Then stoichiometric amount of magnesium methoxide solution was added. Samples composition presented in the Table 9.

Table 9: Composition of samples prepared according to the procedure 4.5

Sample	**5.1**	**5.2**	**5.3**
Au:MgF_2	*1:2*	*1:5*	*1:10*
AuNPs [µL]	400	400	400
HF/EtOH [µL]	80	200	400
$Mg(OEt)_2$ [µL]	40	100	200
EtOH [µL]	9480	9300	9000

4.6. Dropwise synthesis of Au@MgF_2

Stock solutions of magnesium acetate and magnesium chloride were prepared prior the synthesis according to procedure 4.2. Solutions A were prepared according to the Table 10 by mixing 400 µL of 2.5 mM of gold nanoparticles aqueous solution with required amount of 50 mM solution of magnesium acetate or chloride respectively. Solutions B were prepared according to the Table 10 by diluting 50 mM in proper amount of ethanol. Au:Mg ratio was fixed as 1:2 for samples 6.1 and 6.3, and 1:5 for samples 6.2 and 6.4. All solutions were prepared in glass viols. Solutions B were added dropwise with the speed of 40 droplets per minute to the solutions A under gentle magnetic stirring. The glass reaction vessel was placed in an ice bath.

Table 10: Composition of samples prepared according to the procedure 4.6

	Sample	**6.1**	**6.2**	**6.3**	**6.4**
	Au:MgF2	1:2	1:5	1:2	1:5
Solution A	AuNPs [µL]	400	400	400	400
	Mg(OAc)2x4H2O	40	100	-	-
	MgCl2x6H2O	-	-	40	100
Solution B	HF [µL]	80	200	80	200
	EtOH	9480	9300	9480	9300

4.7. Dropwise synthesis of Au@MgF_2 (reversed sequence of adding reagents)

Stock solutions of magnesium acetate and magnesium chloride were prepared prior the synthesis according to procedure 4.2. Solutions A were prepared according to the Table 11 by mixing 400 µL of 2.5 mM of gold nanoparticles aqueous solution, 500 µL of ethanol and required amount of 50 mM HF ethanolic solution. Solutions B were prepared according to the Table 11 by diluting 50 mM ethanolic solution of magnesium acetate and magnesium chloride respectively in required amount of ethanol. Au:Mg ratio was fixed as 1:2 for samples 7.1 and 7.3, and 1:5 for samples 7.2 and 7.4. All solutions were prepared in glass viols. Solutions A were added dropwise with the speed of 40 droplets per 1 min to the solutions B under gentle magnetic stirring. The glass reaction vessel was placed in an ice bath.

Table 11: Composition of samples prepared according to the procedure 4.7

	Sample	**7.1**	**7.2**	**7.3**	**7.4**
	Au:MgF_2	*1:2*	*1:5*	*1:2*	*1:5*
Solution A	AuNPs [µL]	400	400	400	400
	HF [µL]	80	200	80	200
	EtOH [µL]	500	500	500	500
Solution B	$Mg(OAc)_2x4H_2O$ [µL]	40	100	-	-
	$MgCl_2x6H_2O$ [µL]	-	-	40	100
	EtOH	8980	8800	8980	8800

4.8. Synthesis of Au@MgF_2 in ethylene glycol using magnesium acetate and magnesium chloride as a magnesium precursors

50 mM solutions of magnesium acetate, magnesium chloride were prepared by diluting $Mg(OAc)_2x4H_2O$ or $MgCl_2x6H_2O$ powders in ethylene glycol and intensive stirring over 1 h prior the synthesis. In six reaction vessels 400 µL of 2,5 mM aqueous solution of gold nanoparticles were mixed with certain volumes of ethylene glycol (Table 12) and stirred for 15 min. Afterwards certain volumes

of magnesium acetate or chloride were added respectively (Table 12). Next stoichiometric amount of 50 mM methanolic HF solution was added to each sample regarding to Table 12.

Table 12: Composition of samples prepared according to the procedure 4.8

Sample	**8.1**	**8.2**	**8.3**	**8.4**	**8.5**	**8.6**
Au:MgF_2	*1:2*	*1:5*	*1:10*	*1:2*	*1:5*	*1:10*
AuNPs [µL]	400	400	400	400	400	400
$Mg(OAc)_2x4H_2O$ [µL]	40	100	200	-	-	-
$MgCl_2x6H_2O$ [µL]	-	-	-	40	100	200
HF [µL]	80	200	400	80	200	400
EG [µL]	9480	9300	9000	9480	9300	9000

4.9. Synthesis of Au@MgF_2 using PVP-stabilized gold nanoparticles

2 g of Polyvinylpyrrolidone (Mw 40000) was dissolved in 50 ml of distilled water and stirred until the solution became clear and transparent (around 10 min). In six plastic tubes following solutions were prepared: 400 µL of 2,5 mM solution of sodium stabilized gold nanoparticles (synthesized before according to procedure 4.1)diluted with MQ water to the volume of 9992 µL. 8 µL of PVP aqueous solution was added to the diluted gold nanoparticles solution and stirred for 36 hours. The ratio of Au: PVP was fixed as 1:10.[170] Afterwards aqueous solution of PVP modified gold nanoparticles were centrifuged at 11000 rpm for 30 min and dispersed with ethanol to the desired volume according to the Table 13. In the next step proper volumes of 50 mM solutions of magnesium acetate or magnesium chloride were added respectively according to the Table 13. In the last step stoichiometric amount of 50 mM ethanolic solution of HF was added to each sample.

Table 13: Composition of samples prepared according to the procedure 4.9

Sample	**9.1**	**9.2**	**9.3**	**9.4**	**9.5**	**9.6**
Au:MgF_2 ratio	*1:2*	*1:5*	*1:10*	*1:2*	*1:5*	*1:10*
AuNPs [µL]	400	400	400	400	400	400
PVP [µL]	8	8	8	8	8	8
$Mg(OAc)_2x4H_2O$ [µL]	40	100	200	-	-	-
$MgCl_2x6H_2O$ [µL]	-	-	-	40	100	200
HF [µL]	80	200	400	80	200	400
EtOH [µL]	9472	9292	8992	9472	9292	8992

4.10. Synthesis of Au@MgF_2 using PVP-stabilized gold nanoparticles (reversed sequence of adding reagents)

Six batches of PVP modified gold nanoparticles were prepared from citrate stabilized gold nanoparticles and transferred to ethanol according to the procedure above (procedure 2.8.) Afterwards 50 mM ethanolic HF solution was added to each sample according to Table 14. In the last step magnesium acetate and magnesium chloride were added to each sample respectively according to the Table 14.

Table 14: Composition of samples prepared according to the procedure 4.10

Sample	**10.1**	**10.2**	**10.3**	**10.4**	**10.5**	**10.6**
Au:MgF_2	*1:2*	*1:5*	*1:10*	*1:2*	*1:5*	*1:10*
AuNPs [µL]	400	400	400	400	400	400
PVP [µL]	8	8	8	8	8	8
HF [µL]	80	200	400	80	200	400
$Mg(OAc)_2x4H_2O$ [µL]	40	100	200	-	-	-
$MgCl_2x6H_2O$ [µL]	-	-	-	40	100	200
EtOH	9472	9292	8992	9472	9292	8992

4.11. Synthesis of Au@MgF_2 using 16-MHDA-stabilized gold nanoparticles

Freshly synthesized aqueous solution of citrate stabilized gold nanoparticles (procedure 4.1) in three different sizes (30, 55 and 80 nm in diameter) were diluted with ethanol according to Table 15. Then an ethanolic solution of 16-MHDA was added to each sample and magnetically stirred for 30 min. Molar ratio of Au:16-MHDA was fixes as 3:1.[158] All samples were centrifuged at 6000 rpm for 15 min and dispersed in ethanol in order to remove organic impurities. Afterwards an ethanolic solution of magnesium acetate or magnesium chloride was added respectively. Then the ethanolic solution of HF was added (exact samples composition presents Table 15). The ratio of Au:Mg was fixed as 1:5. The mixture was purified by sedimentation in the long and narrow glass tube with a tap. Each solution was shaken, placed in there and left for 10 min. Then 1 ml fractions were collected in order to separate magnesium fluoride coated gold nanoparticles from excess of magnesium fluoride.

Table 15: Composition of samples prepared according to the procedure 4.11

Sample	**11.1**	**11.2**	**11.3**	**11.4**	**11.5**	**11.6**
Au NPs 30 nm [0,64 mM] [µL]	1562,5	1562,5	-	-	-	-
Au NPs 55 nm [0,88 mM] [µL]	-	-	1136,4	1136,4	-	-
Au NPs 80 nm [1,03 mM] [µL]	-	-	-	-	971	971
16 MHDA [µL]	190	190	190	190	190	190
$Mg(OAc)_2x4H_2O$ [µL]	100	-	100	-	100	-
$MgCl_2x6H_2O$ [µL]	-	100	-	100	-	100
HF [µL]	200	200	200	200	200	200
EtOH [µL]	8137,5	8137,5	8563,6	8563,6	8729	8729

4.12. Synthesis of Au@SrF_2 nanoparticles

Prior the synthesis 0,1028 g of strontium acetate hemihydrate was dissolved in 10 ml of denatured ethanol with addition of 100 µL TFA. 0,1333g of anhydrous strontium chloride was dissolved in 10 ml of the mixture of denatured ethanol and acetic acid in the volume ratio 3:1 and stirred for 30 min.[172] In both cases clear and transparent solutions were obtained. In each of the two glass viols 400 µL of stock solution of gold nanoparticles were diluted with ethanol according to the Table 16. Then Strontium precursors were respectively added to the diluted gold nanoparticles solutions and fluorinated afterwards by dropwise addition of HF solution. Table 16 presents detailed samples composition.

Table 16: Composition of samples prepared according to the procedure 4.12

Sample	**12.1**	**12.2**
Au:SrF_2	*1:5*	*1:5*
AuNPs [µL]	400	400
$Sr(OAc)_2x0,5\ H_2O$ [µL]	100	-
$SrCl_2$ [µL]	-	100
HF [µL]	200	200
EtOH [µL]	9300	9300

4.13. Au@ZrF_2 nanoparticles synthesis

50 mM zirconium acetate solution was prepared by dissolving zirconium acetate powder in denatured methanol.[173] In three glass viols 400 µL of 2,5 mM Au NPs aqueous solution was mixed methanol according to the Table 17 and stirred. Afterwards certain amount of zirconium acetate solution was added and stirred for 5 min. Next methanolic solution of HF was added according to the Table 17.

Table 17: Composition of samples prepared according to the procedure 4.13

Sample	**13.1**	**13.2**	**13.3**
Au:ZrF_2	1:2	1:5	1:10
AuNPs	400	400	400
$Zr(OAc)_2$	40	100	200
HF	80	200	400
MeOH	9480	9300	9000

4.14. Magnesium fluoride synthesis

Magnesium fluoride was synthesized via the fluorolytic sol–gel method.[174] Magnesium turnings (1.52 g) were dissolved in a 100 ml of dry methanol under anhydrous conditions. Then a methanolic hydrogen fluoride solution (2 eq.) was carefully added to the formed magnesium methoxylate solution under stirring. After 30 min, 10 wt% trifluoroacetic acid (TFA) was added to the obtained sol.

4.15. Porous MgF_2-over-gold nanoparticles fabrication

4.15.1. Gold nanoparticles immobilization

Microscope glass slides with a size of 76 x 24 mm and a thickness of about 1 mm were used as a substrate for MON preparation. The glass slides were cleaned with piranha solution and distilled water. The washed slides were immersed in a mixture of 3-aminopropyltriethoxysilane and water (1/4, v/v) for 30 min in a horizontal position in order to provide homogenous immobilization of gold nanoparticles on both sides of the glass. Excess of 3-aminopropyltriethoxysilane was removed by washing the glass with distilled water. Afterwards, the glass slides were dried for 10 min at room temperature and for another 10 min at 120 °C. The dried modified glass slides were immersed in a solution of gold nanoparticles for 24 h. In the last step the glass slides with immobilized gold nanoparticles were gently washed with distilled water and dried again at room temperature for 10 min and at 120 °C.

4.15.2. Dip-coating with magnesium fluoride sol

A methanolic solution of magnesium fluoride [0.1 M] was placed in a Teflon square beaker. Glass slides with immobilized gold nanoparticles on the glass surface were mounted in a sample holder, immersed in MgF_2 sol for 2 to 60 s, and removed with a speed of 20 cm/min. Afterwards they were dried in air for 10 min at room temperature and then for 10 min at 120 °C. The samples were calcined in a furnace at 200 °C, 450 °C or 600 °C respectively for 15 min.

4.16. Vapor phase deposition

Vapor phase deposition experiments were performed by Dr. K. Nörthemann at Humboldt-Universität zu Berlin, Department of Chemistry, Brook-Taylor-Str. 2, 12489 Berlin, Germany.

Glass slides containing immobilized gold nanoparticles on the surface were prepared according to the procedure 15.1. Such glass slides were carefully handled using gloves or tweezers in order to avoid greasy impurities on the surface and placed in evaporation chamber B30/III. Following parameters

were applied: pressure $3.4x10^{-4}$ mbar, temperature ~390 °C, evaporation current 85 A, evaporation time 30 s, evaporation rate 20 to 30 a.u.

4.17. Absorbance spectra measurements

UV-Vis measurements of the nanoparticle solutions and of the immobilized nanoparticles were performed using a Jasco V670 spectrophotometer in quartz cuvettes for solutions and directly on the glass substrate for uncoated and coated gold nanoparticles immobilized on the glass surface (using a holder for solid samples) in the range 300-1200 nm.

4.18. Scanning electron microscopy measurements of the glass substrates

Scanning electron microscopy (SEM) were measured by Mr. U. Gernert at the Technische Universität Berlin, Center for Electron Microscopy (ZELMI), Straße des 17.Juni 135, D-10623, Berlin, Germany.

SEM images were obtained with a Hitachi SU8030 SEM with cold field emitter. Low acceleration voltage (0.7 kV to 3 kV) and deceleration mode was used. For the cross-sectional measurements, glass slides were cut with a diamond knife, broken by hand and placed in a micro vise sample holder. Plane view measurements did not require any kind of special treatment; samples were simply fixed on the sample holder.

Measurement parameters figure 17:

a) 3.0 kV 2.5 mm x30 k LA9(U), b) 3.0 kV 2.5 mm x5 k LA9(U), c) 1 kV D 2.5 mm x20 k SE+BSE(U), d) 1kV D 2.5 mm x100 k SE+BSE(U), e) 1.0 kV D 2.5 mm x100 k SE+BSE(U), f) 1.0 kV D 2.5 mm x30.0 k SE+BSE(U), g) 1: 1.0 kV D 2.6 mm x100 k SE+BSE(U), h) 1.0 kV D 2,9 mm x100 k SE+BSE(U).

Measurement parameters figure 18:

a) 3.0 kV, 2.0 mm x200 k SE(TU), b) 3.0 kV, 2.9 mm x200 k SE(TU), c) 3.0 kV, 2.8 mm x200 k SE(TU).

Measurement parameters: figure 19:

a) 1.0 kV D 2.5 mm x50.0 k SE+BSE (U), b) 1.0 kV D 2.5 mm x200 k SE+BSE(U), c) 3.0 kV 2.9 mm x200 k SE(TU), d) 0.7 kV 2.4 mm x60.0 k SE+BSE(U), e) 0.7 kV 2.4mm x100 k SE+BSE(U), f) 3.0 kV 3.0 mm x200 k SE(TU)

Measurement parameters figure 26:

a) 3.0 kV 3.5 mm x200 k HA15(TU), b) 3.0 kV 2.5 mm x200 k SE(U), c) 3.0 kV 2.4 mm x 200 k SE(TU)

Measurement parameters: figure 27

a) 0.7 kV D2.4 mm x100 k SE+BSE(U), b) 0.7 kV D 2.5mm x100k SE+SBE(U), c) 0.7 kV D 2.7mm x100k SE+SBE(U)

Measurement parameters: figure 29

a, b, c,) 0.7 kV D 2.5 mm x100 k SE+BSE(U)

Measurement parameters: figure 30

a) 3.0 kV 2.8 mm x 200k SE(TU), b) 3.0 kV 2.3 mm x 200k SE(TU), c) 3.0 kV 2.4 mm x 200k SE(TU)

Measurement parameters: figure 33

a) 0.7 kV D3.0 mm x30.0 k SE+BSE(U), b) 0.7 kV D2.6 mm x30.0 k SE+BSE(U), c) 3.0 kV 4.7 mm x 200 k SE(TU), d) 3.0 kV 4.6 mm x200 k SE(TU)

4.19. Scanning electron microscopy measurements of samples 12 a and 13 a and EDX investigations

Scanning electron microscopy (SEM) combined with EDX investigations were performed by Dr. Steffi Rades at Federal Institute for Materials Research and Testing, Unter den Eichen 87, 12205 Berlin

Scanning electron microscope images and EDX maps/scans were obtained with a Zeiss Supra 40 with energy dispersive X-ray spectroscope Thermo Scientific UltraDry at the beam voltage 20kV on carbon foil coated copper grid.

4.20. Scanning force microscopy measurements

Scanning force microscope (SFM) images were measured by V. Reiter-Scherer at Humboldt-Universität zu Berlin, Department of Physics & IRIS Adlershof, Newtonstraße 15, 12489 Berlin, Germany.

SFM images with a with a maximum resolution of 265x256 pixels were obtained using a JPK Nanowizard 3 in combination with commercial silicon cantilevers (Olympus AC240TS) with a nominal spring constant k = 2 N/m and a nominal tip radius r = 9 nm. The SFM was operated in quantitative imaging mode (QI) measuring a force-distance curve for every pixel. From this the topography of the surface is obtained, as well as material properties such as elasticity and adhesion between tip and surface. The cantilever was moved at a constant vertical speed during a approach – retract cycle. The speed of vertical motion was kept constant for one image but varied from 23 µm/s to 75 µm/s for different images.

In order to investigate the mechanical stability of uncoated gold nanoparticles and MON, SFM scratch experiments were performed. After imaging the topography in quantitative imaging mode (Fig. 6a), a small area was scratched by imaging this area in contact mode with the feedback controlling of the SFM cantilever height reduced to a minimum. The applied force was varied between 5 nN and 100 nN. Further topography images were taken after each scratch in quantitative imaging mode.

4.21. Transmission electron microscopy measurements

Transmission electron microscopy (TEM) images of the nanoparticles were obtained with a Philips CM200 TEM on carbon-coated copper grids at 200 kV acceleration voltage.

4.22. Raman experiments

For the Raman and SERS experiments, a home-built spectrograph, equipped with a CCD-Camera and a HeNe-laser (633 nm) for excitation was used. The scattered light from the sample was collected by a 60x water immersion objective, diameter of the laser spot is 1.5 µm. The laser intensity on the sample was 1.2×10^5 W·cm^{-2}. Aqueous crystal violet solution (10^{-6} M) was used as analyte to determine SERS enhancement factors. For the measurements, a drop (15 µL) of the CV solution was placed on each substrate. A mixture of acetonitrile and toluene was used for frequency calibration of all Raman spectra.

4.23. Simulation of local fields

Simulation of local fields were performed by Dr. V. Merk at Humboldt-Universität zu Berlin, Department of Chemistry, Brook-Taylor-Str. 2, 12489 Berlin, Germany.

All 3D finite difference time domain (FDTD) simulations were performed using FDTD Solutions software (Lumerical Solutions, Inc., Canada). A plane wave was used for excitation, propagating along the negative z-axis direction with 0° polarization. The simulations were performed at two different wavelengths (633 nm and 1064 nm). All output images were normalized to the intensity of the excitation source. perfectly matched layer (PML) boundary conditions were applied. The frequency-dependent dielectric functions of gold and SiO_2 were taken from the literature[180] and the refractive index of the MgF_2 was set to 1.38. [124]

5. References

1. Brosseau, C.L., Casadio, F., Van Duyne, R.P., Revealing the invisible: Using surface-enhanced Raman spectroscopy to identify minute remnants of color in Winslow Homer's colorless skies. J Raman Spectrosc 2011, 42(6), 1305-1310.
2. Zavaleta, C.L., Smith, B.R., Walton, I., Doering, W., Davis, G., Shojaei, B., Natan, M.J., Gambhir, S.S., Multiplexed imaging of surface enhanced Raman scattering nanotags in living mice using noninvasive Raman spectroscopy. P Natl Acad Sci USA 2009, 106(32), 13511-13516.
3. Ceja-Fdez, A., Lopez-Luke, T., Torres-Castro, A., Wheeler, D.A., Zhang, J.Z., De la Rosa, E., Glucose detection using SERS with multi-branched gold nanostructures in aqueous medium. Rsc Advances 2014, 4(103), 59233-59241.
4. Lesina, A.C., Paternoster, G., Mattedi, F., Ferrario, L., Berini, P., Ramunno, L., Paris, A., Vaccari, A., Calliari, L., Modeling and Characterization of Antireflection Coatings with Embedded Silver Nanoparticles for Silicon Solar Cells. Plasmonics 2015, 10(6), 1525-1536.
5. Joseph, V., Engelbrekt, C., Zhang, J.D., Gernert, U., Ulstrup, J., Kneipp, J., Characterizing the Kinetics of Nanoparticle-Catalyzed Reactions by Surface-Enhanced Raman Scattering. Angew Chem Int Edit 2012, 51(30), 7592-7596.
6. Stewart, M.E., Anderton, C.R., Thompson, L.B., Maria, J., Gray, S.K., Rogers, J.A., Nuzzo, R.G., Nanostructured plasmonic sensors. Chem Rev 2008, 108(2), 494-521.
7. Lin, H.Y., Chen, C.T., Chen, Y.C., Detection of phosphopeptides by localized surface plasma resonance of titania-coated gold nanoparticles immobilized on glass substrates. Anal Chem 2006, 78(19), 6873-6878.
8. Driskell, J.D., Primera-Pedrozo, O.M., Dluhy, R.A., Zhao, Y.P., Tripp, R.A., Quantitative Surface-Enhanced Raman Spectroscopy Based Analysis of MicroRNA Mixtures. Appl Spectrosc 2009, 63(10), 1107-1114.
9. Sivanesan, A., Kalaivani, G., Fischer, A., Stiba, K., Leimkuhler, S., Weidinger, I.M., Complementary Surface-Enhanced Resonance Raman Spectroscopic Biodetection of Mixed Protein Solutions by Chitosan- and Silica-Coated Plasmon-Tuned Silver Nanoparticles. Analytical Chemistry 2012, 84(13), 5759-5764.
10. Xu, X.B., Li, H.F., Hasan, D., Ruoff, R.S., Wang, A.X., Fan, D.L., Near-Field Enhanced Plasmonic-Magnetic Bifunctional Nanotubes for Single Cell Bioanalysis. Advanced Functional Materials 2013, 23(35), 4332-4338.
11. Shah, N.C., Lyandres, O., Walsh, J.T., Glucksberg, M.R., Van Duyne, R.P., Lactate and sequential lactate-glucose sensing using surface-enhanced Raman spectroscopy. Anal Chem 2007, 79(18), 6927-6932.
12. Haes, A.J., Hall, W.P., Chang, L., Klein, W.L., Van Duyne, R.P., A localized surface plasmon resonance biosensor: First steps toward an assay for Alzheimer's disease. Nano Lett 2004, 4(6), 1029-1034.
13. Kneipp, K., Wang, Y., Kneipp, H., Perelman, L.T., Itzkan, I., Dasari, R., Feld, M.S., Single molecule detection using surface-enhanced Raman scattering (SERS). Phys Rev Lett 1997, 78(9), 1667-1670.
14. Peron, O., Rinnert, E., Toury, T., de la Chapelle, M.L., Compere, C., Quantitative SERS sensors for environmental analysis of naphthalene. Analyst 2011, 136(5), 1018-1022.
15. Sotiriou, G.A., Sannomiya, T., Teleki, A., Krumeich, F., Voros, J., Pratsinis, S.E., Non-Toxic Dry-Coated Nanosilver for Plasmonic Biosensors. Advanced Functional Materials 2010, 20(24), 4250-4257.
16. Raut, S.L., Rich, R., Shtoyko, T., Bora, I., Laursen, B.W., Sorensen, T.J., Borejdo, J., Gryczynski, Z., Gryczynski, I., Sandwich type plasmonic platform for MEF using silver fractals. Nanoscale 2015, 7(42), 17729-17734.
17. Ouhenia-Ouadahi, K., Yasukuni, R., Yu, P., Laurent, G., Pavageau, C., Grand, J., Guerin, J., Leaustic, A., Felidj, N., Aubard, J., Nakatani, K., Metivier, R., Photochromic-fluorescent-plasmonic nanomaterials: towards integrated three-component photoactive hybrid nanosystems. Chemical Communications 2014, 50(55), 7299-7302.

18. Hou, S., Yan, J., Hu, Z.J., Wu, X.C., Enhancing the plasmonic circular dichroism by entrapping chiral molecules at the core-shell interface of rod-shaped Au@Ag nanocrystals. Chemical Communications 2016, 52(10), 2059-2062.
19. Li, J.F., Li, S.B., Anema, J.R., Yang, Z.L., Huang, Y.F., Ding, Y., Wu, Y.F., Zhou, X.S., Wu, D.Y., Ren, B., Wang, Z.L., Tian, Z.Q., Synthesis and Characterization of Gold Nanoparticles Coated with Ultrathin and Chemically Inert Dielectric Shells for SHINERS Applications. Appl Spectrosc 2011, 65(6), 620-626.
20. Sharma, B., Frontiera, R.R., Henry, A.I., Ringe, E., Van Duyne, R.P., SERS: Materials, applications, and the future. Mater Today 2012, 15(1-2), 16-25.
21. Drescher, D., Zeise, I., Traub, H., Guttmann, P., Seifert, S., Buchner, T., Jakubowski, N., Schneider, G., Kneipp, J., In situ Characterization of SiO2 Nanoparticle Biointeractions Using BrightSilica. Adv Funct Mater 2014, 24(24), 3765-3775.
22. Nie, S., Emory, S.R., Probing Single Molecules and Single Nanoparticles by Surface-Enhanced Raman Scattering. Science 1997, 275(5303), 1102-6.
23. Rothschild, M., Bloomstein, T.M., Efremow, N., Fedynyshyn, T.H., Fritze, M., Pottebaum, I., Switkes, M., Nanopatterning with UV optical lithography. Mrs Bull 2005, 30(12), 942-946.
24. Tseng, A.A., Recent developments in nanofabrication using ion projection lithography. Small 2005, 1(6), 594-608.
25. Hinman, S.S., Chen, C.Y., Duan, J.C., Cheng, Q., Calcinated gold nanoparticle arrays for on-chip, multiplexed and matrix-free mass spectrometric analysis of peptides and small molecules. Nanoscale 2016, 8(3), 1665-1675.
26. Kha, N.M., Chen, C.H., Su, W.N., Rick, J., Hwang, B.J., Improved Raman and photoluminescence sensitivity achieved using bifunctional Ag@SiO2 nanocubes. Physical Chemistry Chemical Physics 2015, 17(33), 21226-21235.
27. Banholzer, M.J., Harris, N., Millstone, J.E., Schatz, G.C., Mirkin, C.A., Abnormally Large Plasmonic Shifts in Silica-Protected Gold Triangular Nanoprisms. Journal of Physical Chemistry C 2010, 114(16), 7521-7526.
28. Abadeer, N.S., Brennan, M.R., Wilson, W.L., Murphy, C.J., Distance and Plasmon Wavelength Dependent Fluorescence of Molecules Bound to Silica-Coated Gold Nanorods. Acs Nano 2014, 8(8), 8392-8406.
29. Lin, M., Wang, Y.Q., Sun, X.Y., Wang, W.H., Chen, L.X., "Elastic" Property of Mesoporous Silica Shell: For Dynamic Surface Enhanced Raman Scattering Ability Monitoring of Growing Noble Metal Nanostructures via a Simplified Spatially Confined Growth Method. Acs Applied Materials & Interfaces 2015, 7(14), 7516-7525.
30. Chen, H.M., Zhao, L., Chen, D.Q., Hu, W.H., Stabilization of gold nanoparticles on glass surface with polydopamine thin film for reliable LSPR sensing. Journal of Colloid and Interface Science 2015, 460, 258-263.
31. Yuan, H.K., Fales, A.M., Khoury, C.G., Liu, J., Vo-Dinh, T., Spectral characterization and intracellular detection of Surface-Enhanced Raman Scattering (SERS)-encoded plasmonic gold nanostars. Journal of Raman Spectroscopy 2013, 44(2), 234-239.
32. Sotiriou, G.A., Hirt, A.M., Lozach, P.Y., Teleki, A., Krumeich, F., Pratsinis, S.E., Hybrid, Silica-Coated, Janus-Like Plasmonic-Magnetic Nanoparticles. Chemistry of Materials 2011, 23(7), 1985-1992.
33. Wang, C.J., Ohodnicki, P.R., Su, X., Keller, M., Brown, T.D., Baltrus, J.P., Novel silica surface charge density mediated control of the optical properties of embedded optically active materials and its application for fiber optic pH sensing at elevated temperatures. Nanoscale 2015, 7(6), 2527-2535.
34. Liz-Marzan, L.M., Giersig, M., Mulvaney, P., Synthesis of nanosized gold-silica core-shell particles. Langmuir 1996, 12(18), 4329-4335.
35. Liz-Marzan, L.M., Giersig, M., Mulvaney, P., Homogeneous silica coating of vitreophobic colloids. Chem Commun 1996, (6), 731-732.
36. Wu, B.H., Liu, D.Y., Mubeen, S., Chuong, T.T., Moskovits, M., Stucky, G.D., Anisotropic Growth of TiO2 onto Gold Nanorods for Plasmon-Enhanced Hydrogen Production from Water Reduction. Journal of the American Chemical Society 2016, 138(4), 1114-1117.

37. Liz-Marzan, L.M., Mulvaney, P., The assembly of coated nanocrystal. J Phys Chem B 2003, 107(30), 7312-7326.
38. Geddes, C.D., Lakowicz, J.R., Editorial: Metal-Enhanced Fluorescence. Journal of Fluorescence 2002, 12(2), 121-129.
39. Lakowicz, J.R., Radiative decay engineering 5: metal-enhanced fluorescence and plasmon emission. Analytical Biochemistry 2005, 337(2), 171-194.
40. Sharma, B., Fernanda Cardinal, M., Kleinman, S.L., Greeneltch, N.G., Frontiera, R.R., Blaber, M.G., Schatz, G.C., Van Duyne, R.P., High-performance SERS substrates: Advances and challenges. Mrs Bull 2013, 38(8), 615-624.
41. Fleischmann, M., Hendra, P.J., McQuillan, A.J., Raman spectra of pyridine adsorbed at a silver electrode. Chemical Physics Letters 1974, 26(2), 163-166.
42. Hrelescu, C., Sau, T.K., Rogach, A.L., Jäckel, F., Feldmann, J., Single gold nanostars enhance Raman scattering. Applied Physics Letters 2009, 94(15), 153113.
43. Ciou, S.-H., Cao, Y.-W., Huang, H.-C., Su, D.-Y., Huang, C.-L., SERS Enhancement Factors Studies of Silver Nanoprism and Spherical Nanoparticle Colloids in The Presence of Bromide Ions. The Journal of Physical Chemistry C 2009, 113(22), 9520-9525.
44. McLellan, J.M., Li, Z.-Y., Siekkinen, A.R., Xia, Y., The SERS Activity of a Supported Ag Nanocube Strongly Depends on Its Orientation Relative to Laser Polarization. Nano Lett 2007, 7(4), 1013-1017.
45. Xu, P., Zhang, B., Mack, N.H., Doorn, S.K., Han, X., Wang, H.-L., Synthesis of homogeneous silver nanosheet assemblies for surface enhanced Raman scattering applications. J. Mater. Chem. 2010, 20(34), 7222-7226.
46. Akimov, A.V., Mukherjee, A., Yu, C.L., Chang, D.E., Zibrov, A.S., Hemmer, P.R., Park, H., Lukin, M.D., Generation of single optical plasmons in metallic nanowires coupled to quantum dots. Nature 2007, 450, 402.
47. Geoffrey, v.M., Andrea, C., Ji-Ho, P., Renuka, R., J., S.M., Alan, H.T., N., B.S., SERS-Coded Gold Nanorods as a Multifunctional Platform for Densely Multiplexed Near-Infrared Imaging and Photothermal Heating. Advanced Materials 2009, 21(31), 3175-3180.
48. Yan, H., Gu, C., Yang, C., Liu, J., Jin, G., Zhang, J., Hou, L., Yao, Y., Hollow core photonic crystal fiber surface enhanced Raman probe. SPIE BiOS, SPIE: 2007; Vol. 6433, p 8.
49. Wustholz, K.L., Henry, A.-I., McMahon, J.M., Freeman, R.G., Valley, N., Piotti, M.E., Natan, M.J., Schatz, G.C., Duyne, R.P.V., Structure−Activity Relationships in Gold Nanoparticle Dimers and Trimers for Surface-Enhanced Raman Spectroscopy. J Am Chem Soc 2010, 132(31), 10903-10910.
50. Joseph, V., Gensler, M., Seifert, S., Gernert, U., Rabe, J.P., Kneipp, J., Nanoscopic Properties and Application of Mix-and-Match Plasmonic Surfaces for Microscopic SERS. J Phys Chem C 2012, 116(12), 6859-6865.
51. Grabar, K.C., Freeman, R.G., Hommer, M.B., Natan, M.J., Preparation and Characterization of Au Colloid Monolayers. Anal Chem 1995, 67(4), 735-743.
52. Chumanov, G., Sokolov, K., Gregory, B.W., Cotton, T.M., Colloidal Metal-Films as a Substrate for Surface-Enhanced Spectroscopy. J Phys Chem-Us 1995, 99(23), 9466-9471.
53. Chaudhuri, R.G., Paria, S., Core/Shell Nanoparticles: Classes, Properties, Synthesis Mechanisms, Characterization, and Applications. Chem Rev 2012, 112(4), 2373-2433.
54. Wang, A.X., Kong, X.M., Review of Recent Progress of Plasmonic Materials and Nano-Structures for Surface-Enhanced Raman Scattering. Materials 2015, 8(6), 3024-3052.
55. Doering, W.E., Nie, S., Spectroscopic Tags Using Dye-Embedded Nanoparticles and Surface-Enhanced Raman Scattering. Anal Chem 2003, 75(22), 6171-6176.
56. Evanoff, D.D., Chumanov, G., Synthesis and optical properties of silver nanoparticles and arrays. Chemphyschem 2005, 6(7), 1221-1231.
57. Freeman, R.G., Grabar, K.C., Allison, K.J., Bright, R.M., Davis, J.A., Guthrie, A.P., Hommer, M.B., Jackson, M.A., Smith, P.C., Walter, D.G., Natan, M.J., Self-Assembled Metal Colloid Monolayers: An Approach to SERS Substrates. Science 1995, 267(5204), 1629-32.
58. Su, K.H., Wei, Q.H., Zhang, X., Mock, J.J., Smith, D.R., Schultz, S., Interparticle coupling effects on plasmon resonances of nanogold particles. Nano Lett 2003, 3(8), 1087-1090.

59. Chumanov, G., Sokolov, K., Cotton, T.M., Unusual extinction spectra of nanometer-sized silver particles arranged in two-dimensional arrays. J Phys Chem-Us 1996, 100(13), 5166-5168.
60. Freeman, R.G., Grabar, K.C., Allison, K.J., Bright, R.M., Davis, J.A., Guthrie, A.P., Hommer, M.B., Jackson, M.A., Smith, P.C., Walter, D.G., Natan, M.J., Self-Assembled Metal Colloid Monolayers - an Approach to Sers Substrates. Science 1995, 267(5204), 1629-1632.
61. Thio, T., Ghaemi, H.F., Lezec, H.J., Wolff, P.A., Ebbesen, T.W., Surface-plasmon-enhanced transmission through hole arrays in Cr films. J Opt Soc Am B 1999, 16(10), 1743-1748.
62. Goss, C.A., Charych, D.H., Majda, M., Application of (3-Mercaptopropyl)Trimethoxysilane as a Molecular Adhesive in the Fabrication of Vapor-Deposited Gold Electrodes on Glass Substrates. Anal Chem 1991, 63(1), 85-88.
63. Yee, J.K., Parry, D.B., Caldwell, K.D., Harris, J.M., Modification of Quartz Surfaces Via Thiol Disulfide Interchange. Langmuir 1991, 7(2), 307-313.
64. Carolyn F. Hoener, K.A.A., Allen J. Bard, Alan Campion, Marye Anne Fox, Thomas E. Mallouk, Stephen E. Webber, and J. M. White, Demonstration of a Shell-Core Structure in Layered CdSe-ZnSe Small Particles by X-ray Photoelectron and Auger Spectroscopies. J. Phys. Chem. 1992, 96, 3812-3811.
65. Honma, I., Sano, T., Komiyama, H., Surface-Enhanced Raman-Scattering (Sers) for Semiconductor Microcrystallites Observed in Ag-Cds Hybrid Particles. J Phys Chem-Us 1993, 97(25), 6692-6695.
66. Zhou, H.S., Sasahara, H., Honma, I., Komiyama, H., Haus, J.W., Coated Semiconductor Nanoparticles - the Cds/Pbs Systems Photoluminescence Properties. Chem Mater 1994, 6(9), 1534-1541.
67. Henglein, A., Small-Particle Research - Physicochemical Properties of Extremely Small Colloidal Metal and Semiconductor Particles. Chem Rev 1989, 89(8), 1861-1873.
68. Hyeong-Chan Youn, S.B., Janos H. Fendler, Dihexadecyl Phosphate, Vesicle-Stabilized and In Situ Generated Mixed CdS and ZnS Semiconductor Particles. Preparation and Utilization for Photosensitized Charge Separation and Hydrogen Generation J. Phys. Chem 1988, 92(22), 6320–6327.
69. Lubomir Spanhel, H.W., Arnim Henglein, Photochemistry of semiconductor colloids. 22. Electron ejection from illuminated cadmium sulfide into attached titanium and zinc oxide particles. J. Am. Chem. Soc 1987, 109(22), 6632–6635.
70. Spanhel, L., Weller, H., Henglein, A., Photochemistry of Semiconductor Colloids. 22. Electron Injection from Illuminated CdS into Attached TiO2 and ZnO Particles. J Am Chem Soc 1987, 109(22), 6632-6635.
71. Youn, H.C., Baral, S., Fendler, J.H., Dihexadecyl phosphate, vesicle-stabilized and in situ generated mixed cadmium sulfide and zinc sulfide semiconductor particles: preparation and utilization for photosensitized charge separation and hydrogen generation. The Journal of Physical Chemistry 1988, 92(22), 6320-6327.
72. Feng, L.L., Wu, X.C., Ren, L.R., Xiang, Y.J., He, W.W., Zhang, K., Zhou, W.Y., Xie, S.S., Well-Controlled Synthesis of Au@Pt Nanostructures by Gold-Nanorod-Seeded Growth. Chem-Eur J 2008, 14(31), 9764-9771.
73. Aherne, D., Gara, M., Kelly, J.M., Gun'ko, Y.K., From Ag Nanoprisms to Triangular AuAg Nanoboxes. Adv Funct Mater 2010, 20(8), 1329-1338.
74. Xue, C., Chen, X., Hurst, S.J., Mirkin, C.A., Self-assembled monolayer mediated silica coating of silver triangular nanoprisms. Adv Mater 2007, 19(22), 4071-+.
75. Gou, L.F., Murphy, C.J., Solution-phase synthesis of Cu2O nanocubes. Nano Lett 2003, 3(2), 231-234.
76. Bardhan, R., Mukherjee, S., Mirin, N.A., Levit, S.D., Nordlander, P., Halas, N.J., Nanosphere-in-a-Nanoshell: A Simple Nanomatryushka. J Phys Chem C 2010, 114(16), 7378-7383.
77. Chen, L.Y., Peng, Y., Wang, H., Gua, Z.Z., Duana, C.Y., Synthesis of Au@ZIF-8 single- or multi-core-shell structures for photocatalysis. Chem Commun 2014, 50(63), 8651-8654.
78. Nandiyanto, A.B.D., Ogi, T., Okuyama, K., Control of the Shell Structural Properties and Cavity Diameter of Hollow Magnesium Fluoride Particles. Acs Appl Mater Inter 2014, 6(6), 4418-4427.

79. Imhof, A., Preparation and characterization of titania-coated polystyrene spheres and hollow titania shells. Langmuir 2001, 17(12), 3579-3585.
80. Fu, W.Y., Yang, H.B., Chang, L.X., Li, M.H., Bala, H., Yu, Q.J., Zou, G.T., Preparation and characteristics of core-shell structure nickel/silica nanoparticles. Colloid Surface A 2005, 262(1-3), 71-75.
81. Wang, G.H., Harrison, A., Preparation of iron particles coated with silica. J Colloid Interf Sci 1999, 217(1), 203-207.
82. Zhang, X.F., Dong, X.L., Huang, H., Lv, B., Zhu, X.G., Lei, J.P., Ma, S., Liu, W., Zhang, Z.D., Synthesis, structure and magnetic properties of SiO2-coated Fe nanocapsules. Mat Sci Eng a-Struct 2007, 454, 211-215.
83. Mazaleyrat, F., Ammar, M., LoBue, M., Bonnet, J.P., Audebert, P., Wang, G.Y., Champion, Y., Hytch, M., Snoeck, E., Silica coated nanoparticles: Synthesis, magnetic properties and spin structure. J Alloy Compd 2009, 483(1-2), 473-478.
84. Lu, X.G., Liang, G.Y., Sun, Z.B., Zhang, W., Ferromagnetic Co/SiO2 core/shell structured nanoparticles prepared by a novel aqueous solution method. Mat Sci Eng B-Solid 2005, 117(2), 147-152.
85. Carnes, C.L., Klabunde, K.J., Unique chemical reactivities of nanocrystalline metal oxides toward hydrogen sulfide. Chem Mater 2002, 14(4), 1806-1811.
86. Decker, S., Klabunde, K.J., Enhancing effect of Fe2O3 on the ability of nanocrystalline calcium oxide to adsorb SO2. J Am Chem Soc 1996, 118(49), 12465-12466.
87. Sneh, O., Clark-Phelps, R.B., Londergan, A.R., Winkler, J., Seidel, T.E., Thin film atomic layer deposition equipment for semiconductor processing. Thin Solid Films 2002, 402(1-2), 248-261.
88. Wang, Y.Y., Cai, K.F., Yao, X., Facile synthesis of PbTe nanoparticles and thin films in alkaline aqueous solution at room temperature. J Solid State Chem 2009, 182(12), 3383-3386.
89. Yoo, S.H., Liu, L., Park, S., Nanoparticle films as a conducting layer for anodic aluminum oxide template-assisted nanorod synthesis. J Colloid Interf Sci 2009, 339(1), 183-186.
90. Subramanian, R., Denney, P.E., Singh, J., Otooni, M., A novel technique for synthesis of silver nanoparticles by laser-liquid interaction. J Mater Sci 1998, 33(13), 3471-3477.
91. Kumar, P., Kumar, R., Kanjilal, D., Knobel, M., Thakur, P., Chae, K.H., Ion beam synthesis of Ni nanoparticles embedded in quartz. J Vac Sci Technol B 2008, 26(4), L36-L40.
92. Hong, L., Vilar, R.M., Wang, Y.M., Laser beam processing of a SiC particulate reinforced 6061 aluminium metal matrix composite. J Mater Sci 1997, 32(20), 5545-5550.
93. Dodd, A.C., A comparison of mechanochemical methods for the synthesis of nanoparticulate nickel oxide. Powder Technol 2009, 196(1), 30-35.
94. Deng, W.J., Xia, W., Li, C., Tang, Y., Formation of ultra-fine grained materials by machining and the characteristics of the deformation fields. J Mater Process Tech 2009, 209(9), 4521-4526.
95. Salari, M., Khoie, S.M.M., Marashi, P., Renee, M., Synthesis of TiO2 nanoparticles via a novel mechanochemical method. J Alloy Compd 2009, 469(1-2), 386-390.
96. Ocana, M., Hsu, W.P., Matijevic, E., Preparation and Properties of Uniform-Coated Colloidal Particles .6. Titania on Zinc-Oxide. Langmuir 1991, 7(12), 2911-2916.
97. Li, T., Moon, J., Morrone, A.A., Mecholsky, J.J., Talham, D.R., Adair, J.H., Preparation of Ag/SiO2 nanosize composites by a reverse micelle and sol-gel technique. Langmuir 1999, 15(13), 4328-4334.
98. Chen, Y.C., Zhou, S.X., Yang, H.H., Wu, L.M., Interaction and microstructure of polyurethane/silica hybrid films prepared by sol-gel process. J Sol-Gel Sci Techn 2006, 37(1), 39-47.
99. Hota, G., Idage, S.B., Khilar, K.C., Characterization of nano-sized CdS-Ag2S core-shell nanoparticles using XPS technique. Colloid Surface A 2007, 293(1-3), 5-12.
100. Hota, G., Jain, S., Khilar, K.C., Synthesis of CdS-Ag2S core-shell composite nanoparticles using AOT n-heptane water microemulsions. Colloid Surface A 2004, 232(2-3), 119-127.
101. Han, M.Y., Huang, W., Chew, C.H., Gan, L.M., Zhang, X.J., Ji, W., Large nonlinear absorption in coated Ag2S/CdS nanoparticles by inverse microemulsion. J Phys Chem B 1998, 102(11), 1884-1887.
102. Dresco, P.A., Zaitsev, V.S., Gambino, R.J., Chu, B., Preparation and properties of magnetite and polymer magnetite nanoparticles. Langmuir 1999, 15(6), 1945-1951.

103. Zou, H., Wu, S.S., Shen, J., Polymer/silica nanocomposites: Preparation, characterization, properties, and applications. Chem Rev 2008, 108(9), 3893-3957.
104. Okaniwa, M., Okaniwa, M., Synthesis of poly (tetrafluoroethylene)/poly(butadiene) core-shell particles and their graft copolymerization. J Appl Polym Sci 1998, 68(2), 185-190.
105. Shenoy, D.B., Antipov, A.A., Sukhorukov, G.B., Mohwald, H., Layer-by-layer engineering of biocompatible, decomposable core-shell structures. Biomacromolecules 2003, 4(2), 265-272.
106. Srivastava, S., Kotov, N.A., Composite Layer-by-Layer (LBL) Assembly with Inorganic Nanoparticles and Nanowires. Accounts Chem Res 2008, 41(12), 1831-1841.
107. Schlesinger, H.I., Brown, H.C., Abraham, B., Bond, A.C., Davidson, N., Finholt, A.E., Gilbreath, J.R., Hoekstra, H., Horvitz, L., Hyde, E.K., Katz, J.J., Knight, J., Lad, R.A., Mayfield, D.L., Rapp, L., Ritter, D.M., Schwartz, A.M., Sheft, I., Tuck, L.D., Walker, A.O., New Developments in the Chemistry of Diborane and the Borohydrides .1. General Summary. J Am Chem Soc 1953, 75(1), 186-190.
108. Chen, J.P., Lim, L.L., Key factors in chemical reduction by hydrazine for recovery of precious metals. Chemosphere 2002, 49(4), 363-370.
109. Turkevich, J., Stevenson, P.C., Hillier, J., A Study of the Nucleation and Growth Processes in the Synthesis of Colloidal Gold. Discuss Faraday Soc 1951, (11), 55-&.
110. Bastus, N.G., Comenge, J., Puntes, V., Kinetically Controlled Seeded Growth Synthesis of Citrate-Stabilized Gold Nanoparticles of up to 200 nm: Size Focusing versus Ostwald Ripening. Langmuir 2011, 27(17), 11098-11105.
111. Ji, X.H., Song, X.N., Li, J., Bai, Y.B., Yang, W.S., Peng, X.G., Size control of gold nanocrystals in citrate reduction: The third role of citrate. J Am Chem Soc 2007, 129(45), 13939-13948.
112. Ji, Y.T., Yang, S.C., Guo, S.W., Song, X.P., Ding, B.J., Yang, Z.M., Bimetallic Ag/Au nanoparticles: A low temperature ripening strategy in aqueous solution. Colloid Surface A 2010, 372(1-3), 204-209.
113. Lee, C.C., Chen, D.H., Large-scale synthesis of Ni-Ag core-shell nanoparticles with magnetic, optical and anti-oxidation properties. Nanotechnology 2006, 17(13), 3094-3099.
114. Park, J.I., Cheon, J., Synthesis of "solid solution" and "core-shell" type cobalt-platinum magnetic nanoparticles via transmetalation reactions. J Am Chem Soc 2001, 123(24), 5743-5746.
115. Lee, W.R., Kim, M.G., Choi, J.R., Park, J.I., Ko, S.J., Oh, S.J., Cheon, J., Redox-transmetalation process as a generalized synthetic strategy for core-shell magnetic nanoparticles. J Am Chem Soc 2005, 127(46), 16090-16097.
116. Kim, H., Achermann, M., Balet, L.P., Hollingsworth, J.A., Klimov, V.I., Synthesis and characterization of Co/CdSe core/shell nanocomposites: Bifunctional magnetic-optical nanocrystals. J Am Chem Soc 2005, 127(2), 544-546.
117. Wang, L.Y., Luo, J., Fan, Q., Suzuki, M., Suzuki, I.S., Engelhard, M.H., Lin, Y.H., Kim, N., Wang, J.Q., Zhong, C.J., Monodispersed core-shell Fe3O4@Au nanoparticles. J Phys Chem B 2005, 109(46), 21593-21601.
118. Salavati-Niasari, M., Davar, F., Mir, N., Synthesis and characterization of metallic copper nanoparticles via thermal decomposition. Polyhedron 2008, 27(17), 3514-3518.
119. Salavati-Niasari, M., Davar, F., Synthesis of copper and copper(I) oxide nanoparticles by thermal decomposition of a new precursor. Mater Lett 2009, 63(3-4), 441-443.
120. Korshunov, A., Heyrovsky, M., Electrochemical behavior of copper metal core/oxide shell ultra-fine particles on mercury electrodes in aqueous dispersions. J Electroanal Chem 2009, 629(1-2), 23-29.
121. Fu, Y.Q., Shearwood, C., Characterization of nanocrystalline TiNi powder. Scripta Mater 2004, 50(3), 319-323.
122. Dong, S.S., Hou, P., Yang, H.B., Zou, G.T., Synthesis of intermetallic NiAl by SHS reaction using coarse-grained nickel and ultrafine-grained aluminum produced by wire electrical explosion. Intermetallics 2002, 10(3), 217-223.
123. Wang, Q., Yang, H.B., Shi, J.L., Zou, G.T., Preparation and characterization of nanocrystalline powders of Cu-Zn alloy by wire electrical explosion method. Mat Sci Eng a-Struct 2001, 307(1-2), 190-194.

124. Noack, J., Fritz, C., Flugel, C., Hemmann, F., Glasel, H.J., Kahle, O., Dreyer, C., Bauer, M., Kemnitz, E., Metal fluoride-based transparent nanocomposites with low refractive indices. Dalton T 2013, 42(16), 5706-5710.
125. Bernsmeier, D., Polte, J., Ortel, E., Krahl, T., Kemnitz, E., Kraehnert, R., Antireflective Coatings with Adjustable Refractive Index and Porosity Synthesized by Micelle-Templated Deposition of MgF2 Sol Particles. Acs Appl Mater Inter 2014, 6(22), 19559-19565.
126. Noack, J., Scheurell, K., Kemnitz, E., Garcia-Juan, P., Rau, H., Lacroix, M., Eicher, J., Lintner, B., Sontheimer, T., Hofmann, T., Hegmann, J., Jahn, R., Lobmann, P., MgF2 antireflective coatings by sol-gel processing: film preparation and thermal densification. J Mater Chem 2012, 22(35), 18535-18541.
127. Fujihara, S., Naito, H., Kimura, T., Visible photoluminescence of ZnO nanoparticles dispersed in highly transparent MgF2 thin-films via sol-gel process. Thin Solid Films 2001, 389(1-2), 227-232.
128. Fujihara, S., Ono, S., Kishiki, Y., Tada, M., Kimura, T., Sol-gel synthesis of inorganic complex fluorides using trifluoroacetic acid. J Fluorine Chem 2000, 105(1), 65-70.
129. Fujihara, S., Tada, M., Kimura, T., Preparation and characterization of MgF2 thin film by a trifluoroacetic acid method. Thin Solid Films 1997, 304(1-2), 252-255.
130. Nandiyanto, A.B.D., Iskandar, F., Ogi, T., Okuyama, K., Nanometer to Submicrometer Magnesium Fluoride Particles with Controllable Morphology. Langmuir 2010, 26(14), 12260-12266.
131. Waltz, F., Swider, M.A., Hoyer, P., Hassel, T., Erne, M., Mohwald, K., Adlung, M., Feldhoff, A., Wickleder, C., Bach, F.W., Behrens, P., Synthesis of highly stable magnesium fluoride suspensions and their application in the corrosion protection of a Magnesium alloy. J Mater Sci 2012, 47(1), 176-183.
132. Scheurell, K., Noack, J., Konig, R., Hegmann, J., Jahn, R., Hofmann, T., Lobmann, P., Lintner, B., Garcia-Juan, P., Eicher, J., Kemnitz, E., Optimisation of a sol-gel synthesis route for the preparation of MgF2 particles for a large scale coating process. Dalton T 2015, 44(45), 19501-19508.
133. Hench, L.L., West, J.K., The sol-gel process. Chem Rev 1990, 90(1), 33-72.
134. Niederberger, M., Nonaqueous Sol–Gel Routes to Metal Oxide Nanoparticles. Accounts of Chemical Research 2007, 40(9), 793-800.
135. Oskam, G., Metal oxide nanoparticles: synthesis, characterization and application. J Sol Gel Sci Technol 2006, 37(3), 161-164.
136. Wuttke, S., Coman, S.M., Krohnert, J., Jentoft, F.C., Kemnitz, E., Sol-gel prepared nanoscopic metal fluorides - a new class of tunable acid-base catalysts. Catal Today 2010, 152(1-4), 2-10.
137. Kemnitz, E., Gross, U., Rudiger, S., Shekar, C.S., Amorphous metal fluorides with extraordinary high surface areas. Angewandte Chemie (International ed. in English) 2003, 42(35), 4251-4.
138. Kemnitz, E., Gross, U., Rudiger, S., Shekar, C.S., Amorphous metal fluorides with extraordinary high surface areas. Angew Chem Int Edit 2003, 42(35), 4251-4254.
139. Rudiger, S., Kemnitz, E., The fluorolytic sol-gel route to metal fluorides-a versatile process opening a variety of application fields. Dalton T 2008, (9), 1117-1127.
140. Scheurell, K., König, R., Troyanov, S.I., Kemnitz, E., Structural chemistry of magnesium acetates. Z. Anorg. Allg. Chem. 2012, 638(9), 1265-1273.
141. Murata, T., Ishizawa, H., Motoyama, I., Tanaka, A., Investigations of MgF2 Optical Thin Films Prepared from Autoclaved Sol. J Sol Gel Sci Technol 2004, 32(1), 161-165.
142. Stefan, W., M., C.S., Gudrun, S., Holm, K., Alexandré, V., Maro, D., M., S.S.L., Erhard, K., Novel Sol–Gel Synthesis of Acidic MgF2−x(OH)x Materials. Chemistry – A European Journal 2008, 14(36), 11488-11499.
143. Rehmer, A., Scheurell, K., Kemnitz, E., Formation of nanoscopic CaF2via a fluorolytic sol-gel process for antireflective coatings. J. Mater. Chem. C 2015, 3(8), 1716-1723.
144. Krahl, T., Bro, Scheurell, K., Lintner, B., Kemnitz, E., Novel aspects in the chemistry of the non-aqueous fluorolytic sol-gel synthesis of nanoscaled homodisperse MgF2 sols for antireflective coatings. J. Mater. Chem. C 2016, 4(7), 1454-1466.
145. Wuttke, S., Coman, S.M., Kröhnert, J., Jentoft, F.C., Kemnitz, E., Sol–gel prepared nanoscopic metal fluorides – a new class of tunable acid–base catalysts. Catal Today 2010, 152(1), 2-10.
146. Erhard, K., Stefan, W., M., C.S., Tailor-Made MgF2-Based Catalysts by Sol–Gel Synthesis. European Journal of Inorganic Chemistry 2011, 2011(31), 4773-4794.

147. Kemnitz, E., Nanoscale metal fluorides: a new class of heterogeneous catalysts. Catalysis Science & Technology 2015, 5(2), 786-806.
148. Hegmann, J., Löbmann, P., Sol–gel preparation of TiO2 and MgF2 multilayers. J Sol Gel Sci Technol 2013, 67(3), 436-441.
149. Krüger, H., Kemnitz, E., Hertwig, A., Beck, U., Transparent MgF2-films by sol–gel coating: Synthesis and optical properties. Thin Solid Films 2008, 516(12), 4175-4177.
150. Palashov, O.V., Khazanov, E.A., Mukhin, I.B., Mironov, I.A., Smirnov, A.N., Dukel'skii, K.V., Pavel, P.F., Vyacheslav, V.O., Tasoltan, T.B., Comparison of the optical parameters of a CaF 2 single crystal and optical ceramics. Quantum Electronics 2007, 37(1), 27.
151. Ritter, B., Krahl, T., Rurack, K., Kemnitz, E., Nanoscale CaF2 doped with Eu3+ and Tb3+ through fluorolytic sol-gel synthesis. J. Mater. Chem. C 2014, 2(40), 8607-8613.
152. Scheurell, K., Kemnitz, E., Garcia-Juan, P., Eicher, J., Lintner, B., Hegmann, J., Jahn, R., Hofmann, T., Lobmann, P., Porous MgF2 antireflective lambda/4 films prepared by sol-gel processing: comparison of synthesis approaches. J Sol-Gel Sci Techn 2015, 76(1), 82-89.
153. Brinker, C.J., Frye, G.C., Hurd, A.J., Ashley, C.S., Fundamentals of sol-gel dip coating. Thin Solid Films 1991, 201(1), 97-108.
154. Landau, L., Levich, B., Acta Phys.-Chim. Sin. 1942, 42-54.
155. Frens, G., Controlled Nucleation for Regulation of Particle-Size in Monodisperse Gold Suspensions. Nature-Phys Sci 1973, 241(105), 20-22.
156. Daniel, M.C., Astruc, D., Gold Nanoparticles: Assembly, Supramolecular Chemistry, Quantum-Size-Related Properties, and Applications Toward Biology, Catalysis, and Nanotechnology. Chem Rev 2004, 104(1), 293-346.
157. Graf, C., Vossen, D.L.J., Imhof, A., van Blaaderen, A., A general method to coat colloidal particles with silica. Langmuir 2003, 19(17), 6693-6700.
158. Lin, Y.C., Yu, B.Y., Lin, W.C., Lee, S.H., Kuo, C.H., Shyue, J.J., Tailoring the surface potential of gold nanoparticles with self-assembled monolayers with mixed functional groups. J Colloid Interf Sci 2009, 340(1), 126-130.
159. Noack, J., Emmerling, F., Kirmse, H., Kemnitz, E., Sols of nanosized magnesium fluoride: formation and stabilisation of nanoparticles. J. Mater. Chem. 2011, 21(38), 15015-15021.
160. Sonavane, G., Tomoda, K., Makino, K., Biodistribution of colloidal gold nanoparticles after intravenous administration: Effect of particle size. Colloids and Surfaces B: Biointerfaces 2008, 66(2), 274-280.
161. Wuttke, S., Scholz, G., Rüdiger, S., Kemnitz, E., Variation of sol-gel synthesis parameters and their consequence for the surface area and structure of magnesium fluoride. J. Mater. Chem. 2007, 17(47), 4980-4988.
162. Scheurell, K., Kemnitz, E., Garcia-Juan, P., Eicher, J., Lintner, B., Hegmann, J., Jahn, R., Hofmann, T., Löbmann, P., Porous MgF2 antireflective λ/4 films prepared by sol–gel processing: comparison of synthesis approaches. J Sol Gel Sci Technol 2015, 76(1), 82-89.
163. Karg, M. Fluorolytische Sol-Gel-Synthese von Magnesiumfluorid. Humboldt-Universität zu Berlin, Mathematisch-Naturwissenschaftliche Fakultät, 2015.
164. Ritter, B., Haida, P., Krahl, T., Scholz, G., Kemnitz, E., Core-shell metal fluoride nanoparticles: Via fluorolytic sol-gel synthesis-a fast and efficient construction kit. J. Mater. Chem. C 2017, 5(22), 5444-5450.
165. Kelly, K.L., Coronado, E., Zhao, L.L., Schatz, G.C., The Optical Properties of Metal Nanoparticles: The Influence of Size, Shape, and Dielectric Environment. The Journal of Physical Chemistry B 2003, 107(3), 668-677.
166. Lee, K.-S., El-Sayed, M.A., Gold and Silver Nanoparticles in Sensing and Imaging: Sensitivity of Plasmon Response to Size, Shape, and Metal Composition. The Journal of Physical Chemistry B 2006, 110(39), 19220-19225.
167. Lin, S.Y., Tsai, Y.T., Chen, C.C., Lin, C.M., Chen, C.H., Two-step functionalization of neutral and positively charged thiols onto citrate-stabilized Au nanoparticles. J Phys Chem B 2004, 108(7), 2134-2139.

168. Chou, K.S., Lin, M.Y., Wu, H.H., Studies on the removal of 2-propanol by Ag@Fe2O3 core-shell structured catalyst. J Taiwan Inst Chem E 2013, 44(2), 228-232.
169. Yang, X.H., Fu, H.T., Wong, K., Jiang, X.C., Yu, A.B., Hybrid Ag@ TiO2 core-shell nanostructures with highly enhanced photocatalytic performance. Nanotechnology 2013, 24(41).
170. Huang, Y.F., Ma, K.H., Kang, K.B., Zhao, M., Zhang, Z.L., Liu, Y.X., Wen, T., Wang, Q., Qiu, W.Y., Qiu, D., Core-shell plasmonic nanostructures to fine-tune long "Au nanoparticle-fluorophore" distance and radiative dynamics. Colloid Surface A 2013, 421, 101-108.
171. Goebl, J., Joo, J.B., Dahl, M., Yin, Y.D., Synthesis of tailored Au@TiO2 core-shell nanoparticles for photocatalytic reforming of ethanol. Catal Today 2014, 225, 90-95.
172. Schmidt, L., Emmerling, F., Kirmse, H., Kemnitz, E., Sol-gel synthesis and characterisation of nanoscopic strontium fluoride. Rsc Adv 2014, 4(1), 32-38.
173. Schmidt, L.
174. Krishna Murthy, J., Groß, U., Rüdiger, S., Kemnitz, E., Winfield, J.M., Sol–gel-fluorination synthesis of amorphous magnesium fluoride. J Solid State Chem 2006, 179(3), 739-746.
175. Pfreundschuh, M., Martinez-Martin, D., Mulvihill, E., Wegmann, S., Muller, D.J., Multiparametric high-resolution imaging of native proteins by force-distance curve–based AFM. Nature Protocols 2014, 9, 1113.
176. Joseph, V., Matschulat, A., Polte, J., Rolf, S., Emmerling, F., Kneipp, J., SERS enhancement of gold nanospheres of defined size. J Raman Spectrosc 2011, 42(9), 1736-1742.
177. Kudelski, A., Raman studies of rhodamine 6G and crystal violet sub-monolayers on electrochemically roughened silver substrates: Do dye molecules adsorb preferentially on highly SERS-active sites? Chemical Physics Letters 2005, 414(4), 271-275.
178. Krüger, H. Niedertemperatur Sol-Gel Verfahren für optische Schichtsysteme auf Basis von Magnesiumfluorid und Titandioxid. Humboldt-Universität zu Berlin, Mathematisch-Naturwissenschaftliche Fakultät I, 2009.
179. Nörthemann, K.
180. Johnson, R.A., Relationship between 2-Body Interatomic Potentials in a Lattice Model and Elastic-Constants. Phys Rev B 1972, 6(6), 2094-&.

6. List of abbreviations

16MHDA	16-Mercaptohexadecanoic acid
APTES	3-Aminopropyltriethoxysilane
DLS	Dynamic Light Scattering
EDX	Energy Dispersive X-ray Spectroscopy
FDTD	Finite-Difference Time Domain
LSPR	Localized Surface Plasmon Resonance
MON	Porous Magnesium fluoride-Over gold Nanoparticles
NPs	Nanoparticles
NMR	Nuclear Magnetic Resonance Spectroscopy
PML	Perfectly Matched Layer
PVP	Polyvinylpyrrolidone
RMS roughness	Root Mean Square roughness
SEM	Scanning Electron Microscopy
SERS	Surface Enhanced Raman Scattering
SFM	Scanning Force Microscopy
TEM	Transmission Electron Microscopy
TFA	Trifluoroacetic Acid
TMOS	Tetraethyl Orthosilicate
XPS	X-ray Photoelectron Spectroscopy